A NOVEL APPROACH TO PERIPHERAL NERVE ACTIVATION USING LOW FREQUENCY ALTERNATING CURRENTS

A Thesis

Submitted to the Faculty

of

Purdue University

by

Awadh Mubarak M Al Hawwash

In Partial Fulfillment of the

Requirements for the Degree

of

Master of Science in Biomedical Engineering

August 2020

Purdue University

Indianapolis, Indiana

THE PURDUE UNIVERSITY GRADUATE SCHOOL
STATEMENT OF COMMITTEE APPROVAL

Dr. Ken Yoshida, Chair

Department of Biomedical Engineering

Dr. Edward J. Berbari

Department of Biomedical Engineering

Dr. John H. Schild

Department of Biomedical Engineering

Approved by:

Dr. Julie Ji

Head of the Graduate Program

And my success can only come from Allah. In Him I trust, and unto Him I return.

-Quran: Hud [11:88]

Dedicated to my wonderful wife and daughter Sumou

ACKNOWLEDGMENTS

I would like to first acknowledge and express my sincere gratitude to Dr. Ken Yoshida for welcoming me into the Bioelectronics Lab team and giving me the opportunity to expand and strengthen my skills under his supervision. I thank him for his continuous valuable guidance, patience, assistance, motivation, and immense knowledge. It has been my honor to work with him through this research journey and I will always be grateful for his support.

I wish to show my gratitude to Ivette Van Dyke for her continuous support during this journey. I am indebted to her for her patience with my unstoppable questions, and I really appreciate the collaboration we've had. I will always be grateful for her guidance and efforts.

My gratitude is also extended to my former colleagues Lindsay Richardson who was the first person to walk me through the lab and Shozaf Zaidi. I am grateful for their valuable advice and support.

My sincere gratitude is also extended to the Bioelectronics Lab members for their efforts and friendly support during the experiments: Christian Vetter, Ryne Horn, Onna Doering, Nathaniel Lazorchak, Christopher Hoffman, and Macallister Smolik.

I also owe my sincere thanks to Sultan Almunif and Rashed Almousa for their valuable advice, guidance, comments and suggestions through this journey.

I am grateful to my parents and family for their continuous support and prayers.

I would like also to acknowledge King Saud University in Riyadh, Saudi Arabia for the scholarship.

TABLE OF CONTENTS

Page

LIST OF TABLES

LIST OF FIGURES

Figure Page

Figure Page

Figure Page

LIST OF ABBREVIATIONS

AC	Alternating Current
ANS	Autonomic Nervous System
CAP	Compound Action Potential
CNS	Central Nervous System
DC	Direct Current
ECG	Electrocardiogram
EMG	Electromyogram
ENG	Electroneurogram
FFT	Fast Fourier Transform
H-reflex	Hoffmann reflex
HB-reflex	Hering-Breuer reflex
KHFAC	Kilohertz Frequency Alternating Current
LFAC	Low Frequency Alternating Current
PNS	Peripheral Nervous System
PSD	Power Spectrum Density
RPES	Rectangular Pulse Electrical Stimulation
SNS	Somatic Nervous System
SWT	Stationary Wavelet Transform
VCCS	Voltage Controlled Current Source
iSWT	inverse Stationary Wavelet Transform
tDCS	transcranial Direct Current Stimulation

ABSTRACT

Awadh Mubarak M Al Hawwash M.S, Purdue University, August 2020. A Novel Approach to Peripheral Nerve Activation Using Low Frequency Alternating Currents. Major Professor: Ken Yoshida.

The standard electrical stimulation waveform used for electrical activation of nerve is a rectangular pulse or a charge balanced rectangular pulse, where the pulse width is typically in the range of $\sim$100 μsec through $\sim$1000 μsec. In this work, we explore the effects of a continuous sinusoidal waveform with a frequency ranging from 5 through 20 Hz, which was named the Low Frequency Alternating Current (LFAC) waveform. The LFAC waveform was explored in the Bioelectronics Laboratory as a novel means to evoke nerve block. However, in an attempt to evoke complete nerve block on a somatic motor nerve, increasing the amplitude of the LFAC waveform unexpectedly produced nerve activation, and elicited a strong non-fatiguing muscle contraction in the anesthetized rabbit model (*unpublished observation*). The present thesis aimed to further explore the phenomenon to measure the effect of LFAC waveform frequency and amplitude on nerve activation.

In freshly excised canine cervical vagus nerve (n=3), it was found that the LFAC waveform at 5, 10, and 20 Hz produced burst modulated activity. Compound action potentials (CAP) synchronous to the stimuli was absent from the electroneurogram (ENG) recordings. When applied *in-vivo*, LFAC was capable of activating the cervical vagus nerve fibers in anaesthetized swine (n=5) and induced the Hering-Breuer reflex. Additionally, when applied *in-vivo* to anesthetized Sprague Dawley rats (n=4), the LFAC waveform was able to activate the left sciatic nerve fibers and induced muscle contractions.

The results demonstrate that LFAC activation was stochastic, and asynchronous to the stimuli unlike conventional pulse stimulation where nerve and muscle response simultaneously and synchronously to stimulus. The activation thresholds were found to be frequency dependent. As the waveform frequency increases the required current amplitude decreases. These experiments also implied that the LFAC phenomenon was most likely to be fiber type-size dependent but that more sophisticated exploration should be addressed before reaching clinical applications. In all settings, the LFAC amplitude was within the water window preventing irreversible electrochemical reactions and damages to the cuff electrodes or nerve tissues. This thesis also reconfirms the preliminary LFAC activation discovery and explores multiple methods to evaluate the experimental observations, which suggest the feasibility of the LFAC waveform at 5, 10, and 20 Hz to activate autonomic and somatic nerve fibers. LFAC appears to be a promising new technique to activate peripheral nerve fibers.

1. INTRODUCTION

This introductory chapter covers a review of the peripheral nervous system structure and a history of the stimulation methods and modes of activating nerve fibers. The aim of this chapter is to introduce the thesis hypothesis and to provide the historical relevance leading to the experimental validation studies.

1.1 Overview of the Peripheral Nervous System

The human nervous system cooperates with other organ systems to reach the ultimate homeostasis conditions and produces the appropriate behavioral responses. The five senses: vision, taste, touch, smell and hearing are integrated in a complex network with other internal senses, such as hunger, pain, and pressure in order to produce the appropriate decisions and actions. The human nervous system is the soul of all the communications inside the human body, and that explains the complexity of its network. Scientists have been studying the human nervous system for centuries, some dated to the time of ancient Egyptian, and others consider that as part of the evolution of neuroscience in 1859 [1].

Neurons are the basic building structure units of the nervous system; which are specialized cells that are capable of transmitting signals known as excitable cells. The nervous system consists mainly of two parts: the Central Nerves System (CNS) and the Peripheral Nervous System (PNS) [2]. The CNS consists of the brain, and the spinal cord, which control mostly all the human body functions, decisions, and actions as well as defines the humankind mental behaviors. On the other hand, the PNS is the communication pathway that links the CNS to the body organs. The PNS is further classified into Autonomic Nervous System (ANS), and Somatic Nervous System (SNS). The overall mechanism of this communication further classifies the

PNS fibers into: sensory afferent fibers that carry signals toward the CNS (sensory components), and motor efferent fibers that carry signals from the CNS toward the effector organs (motor components). This classification can also be seen in term of voluntary and involuntary responses. For example, in term of efferent fibers, the SNS links the voluntary skeletal muscles responses and movements to the CNS with conscious control whereas the smooth, and cardiac muscles and their reflexes are involuntarily linked to CNS by the ANS. In term of afferent fibers, the exteroreceptors such as the eyes and cochlea, send their signals through SNS while interoreceptors, such as pH sensors use ANS for their communication [2].

The importance of the ANS functions to reach the homeostatic mechanisms is expanded to control most of the internal organs and reflexes. Thus, the ANS is divided into two main pathways, or divisions: sympathetic, and parasympathetic. This classification arises from the communication pathway and structure of those neurons and how they are interconnected between the CNS and target tissues. Anatomically, the somatic path from the spinal cord to the target organs consists of a one long neuron whereas the autonomic path takes two neurons to reach the target organs; which are preganglionic and postganglionic neurons, that meet in an autonomic ganglion [2].

The sympathetic pathway is directly involved in controlling and regulating the metabolic resources and energy release whenever it is necessary to take actions of emergency, such as increasing the heart rate during physical exercises or stimulating the secretion of insulin whenever it is needed. It is also known as the "fight or flight" response. However, the parasympathetic inhibits those changes by reducing the heart rate at rest and the insulin secretion once glucose level has reached homeostasis. This pathway is known to control the "rest and digest" state [2].

Nerve fibers classification is further carried to distinguish them based on their physical features and conduction properties. Figure 1.1 shows the major classification of the PNS axons based on their conduction velocity, diameter, and myelination [3]. For motor neurons, the anatomical structure is divided into two main fibers: myelinated and unmyelinated nerve fibers. The myelinated nerve fibers have sheaths

Axon	Conduction velocity (m/s)	Diameter (μm)	Myelination
Squid giant axon	25	500	No
Human			
Motor axons			
Aα type	80–120	13–20	Yes
Aγ type	4–24	5–8	Yes
Sensory axons			
Aα type	80–120	13–20	Yes
Aβ type	35–75	6–12	Yes
Aδ type	3–35	1–5	Thin
C type	0.5–2.0	0.2–1.5	No
Autonomic			
preganglionic B type	3–15	1–5	Yes
postganglionic C type	0.5–2.0	0.2–1.5	No

Figure. 1.1. Classification of the axons based on their conduction velocity, diameter, and myelination [3] Reproduced with permission of the Licensor through PLSclear (LN: 39162),NEUROSCIENCE 6TH EDITION, Oxford Publishing Limited, 2018

that wrap their axons, made up of Schwann cells. These sheaths cover the axons in a discontinues form that makes gaps along the myelin known as Nodes of Ranvier. This myelination plays an important role in increasing the conduction velocity of the action potential. Unlike the myelinated nerve fibers, the unmyelinated fibers lack those sheaths, resulting in a lower conduction velocity due to the leak of ionic current [3].

1.1.1 Action Potential Generation and Propagation

The ability of communication within the nervous system and all other parts of the body is through sending and receiving information. Despite all of the classification of neurons, they are excitable cells which have the capability of transmitting and receiving electrical signals along their bodies by changing their resting membrane potential. The action potential is the fundamental signal that arises from altering

the resting potential of a cell and carries information from one cell to another. From an intercellular level prospective, the resting membrane potential of a neuron can be measured by the technique called "voltage clamp", and studies have shown that for motor neurons, the resting membrane potential is typically ranged from -40 to -90 mV [4–6]. Altering the resting membrane potential (negative level) to reach a certain threshold by injecting an electrical current results in a significant and quick depolarization of the membrane (positive level) which is known as the action potential. The ability of the cell to fire the action potential depends on how strong the injected current, or stimuli is, to change the membrane potential and reach the threshold.

More than seventy years ago, Hodgkin and Huxley successfully modeled and recorded the action potential from the squid giant axon [7]. They studied the mechanism of the action potential firing and propagation, which led to the development of their mathematical model that describes the action potential, and its associated ionic currents' changes [4, 6]. Movements of ions across the cell membrane produces the potential difference, which is analogies to the movement of electrical charges in a conductive medium. The ionic current flow mostly consists of sodium (Na^+), potassium (K^+), calcium (Ca^{2+}), chloride (Cl^-), and proton (H^+) ions. Hodgkin, and Huxley, before the discovery of the ion channels, indicated that there are three gating variables or particles "m, h, and n" that have an underlying control over the process of the ions' movement and action potential generation. For Na^+ ions, the m gating variable is the activation particle to allow Na^+ movements, and h gating variable as the inactivation particle. Unlike the Na^+, K^+ ions movements have only one activation gating variable n. These gating variables describe the probability of opening (activating) and closing (inactivating) the ion channels as function of time and voltage dependents [2, 4].

The ionic currents is driven by the potential difference across the membrane as the electrical force and concentration gradient. With the ion concentration being different between the two sides of the membrane, $[Na^+]$ is higher outside cell membrane and the $[K^+]$ is higher inside than outside the cell. The dynamic of the action potential generation starts when the voltage-gate channels open allowing Na^+ to flow inside the

cell, producing the depolarization of the cell membrane. This change in membrane potential derives the K^+ voltage-gated channels to open allowing for the outward flow of K^+ ions. Thus, in order to trigger the action potential generation, an electrical or chemical stimulus is required to initiate a change in the membrane potential to reach the threshold. If the stimuli strength is not high and fast enough, subthreshold, to cause the depolarization, a graded or an electrotonic potential occurs due to local depolarization of the membrane [2]. Additionally, based on the stimuli information, it could be either an excitatory or inhibitory. The excitatory stimulus would enhance the Na^+ inflow to favor membrane potential to reach the threshold, leading to the action potential generation, whereas inhibitory stimulus would favor the outflow of K^+, causing the membrane potential to move away from the threshold [2]. Once the action potential is triggered, the membrane potential will change rabidly propagating through the axon.

Anatomically, a motor neuron consists of three main parts: the dendrites, soma, and axon [2]. The electrochemical signal is received from the dendrites into the soma, either excitatory or inhibitory, then changes the resting membrane potential to reach the threshold to fire an action potential. If the action potential is fired, it propagates along the axon to reach the target tissue, such as muscles, or synapse to another neuron. At the binding site of the end-terminal, presynaptic cells release neurotransmitters, which have a variety of specific mechanisms based on the target receptors and the nerve types [2,3]. Furthermore, the conduction velocity of the action potential depends on the axon type, and its physical characteristics, as mentioned in figure 1.1 above. The electrical characteristics of the axon significantly impact or influence the propagation of the action potential due to the cable properties [2].

The cable properties include membrane resistance; which defines the ability of the ions to move across the membrane, cytoplasmic resistance, which describes the ions' ability to flow within the axoplasm, and membrane capacitance which defines the membrane ability to store ionic charges [2, 8]. From these cable properties, the time course of the action potential propagation varies from one nerve fiber to another in

time and space, which explains the conduction velocity along the axon. The current distribution along the axon is also depending on the location of those ion gated channels. For the myelinated axons, the Na^+ and K^+ channels reside at the nodes of Ranvier, which results in less current being lost during the propagation. Since the myelin provides higher resistance by insulating the axon, as well as discharging from the axon capacitance is less, the conduction velocity is higher with myelinated nerve fibers [2].

1.2 History of Peripheral Nervous System Stimulation

The differences in nerve fibers functionality, action potential velocity, structure, chemistry, and biophysics have led to different therapy approaches in cases of nerve injuries, and diseases. The previous review of PNS covered the basic underlying classifications and structures that suggest considering nerves as large wires. In fact, neurons are found in nerve bundles that contain large number of axons, and they branch to different target organs. The electrical stimulation of nerve bundles produced the Compound Action Potential (CAP) as a result of the recruitment of all the action potential within a bundle [9]. It can be seen as the summation of all the action potentials from the resided neurons. Thus, the CAP is usually extracellularly stimulated and used as a diagnostic parameter in many nerve injuries situations.

Since the evolution of neuromodulation, either in electrical or pharmaceutical therapy, the neurology field has become more advanced and equipped with painless and suitable therapy methods. The term neuromodulation in fact refers to the alteration of the nerve activity either transcutaneously or subcutaneously, and it has been widely utilized in several clinical applications, such as the deep brain stimulation, lower back pain and neuroprosthetic devices [10]. With this technology, physicians are able to interfere with the nerves signaling pathway that produce pain, reflex, instability of movement, and other forms of neural injuries and inhibit or enhance those signals to produce the adequate responses. Thus, stimulation and recording of the nerve

activity, in form of CAP, or evoked bioelectrical signals, such as EMG, or ENG is an essential step for a successful treatment. In this section, a review of the stimulation modes and waveforms that have been used in the PNS is presented specifically to the extent of this thesis.

1.2.1 Standard Electrical Activation

In order to achieve nerve activation, the nerve has to be triggered to change its membrane potential. Historically, conventional rectangular pulses are applied with a short pulse width (duration) and a high current intensity (amplitude). This stimulation method has been used for a long time in several applications to treat or restore the functionality of injured or disabled nervous system. The underlying theory of this Rectangular Pulses Electrical Stimulation (RPES) is controlled by several principles and concepts, such as the charge injection balance, electrodes activation function, strength-duration curve, electrode types and materials, homogeneity of the target tissue medium and other electrochemical and bioelectromagnetism principles [10–15].

For the RPES, an ionic current is injected into a biological tissue and requires the adoption of specific parameters such as charge balance to avoid any tissue damaging. The waveform of the rectangular pulse can be monophasic, or biphasic based on the stimulation application. The amount of charges being delivered is depending on the stimulation type (constant voltage or current), pulses magnitude (amplitude), duration, and number of pulses [16]. Studies have shown that based on the application of the RPES the waveform can be modified to achieve the threshold of nerve activation. Figure 1.2 shows the common pulse waveforms and their parameters [17].

The monophasic cathodal (negative polarity) stimulation (figure 1.2a) is usually preferred in PNS over the anodal (positive polarity) stimulation in order to change the membrane potential at a lower threshold especially when charge balance is not required in stimulating a large area of tissue. On the other hand, the biphasic stimu-

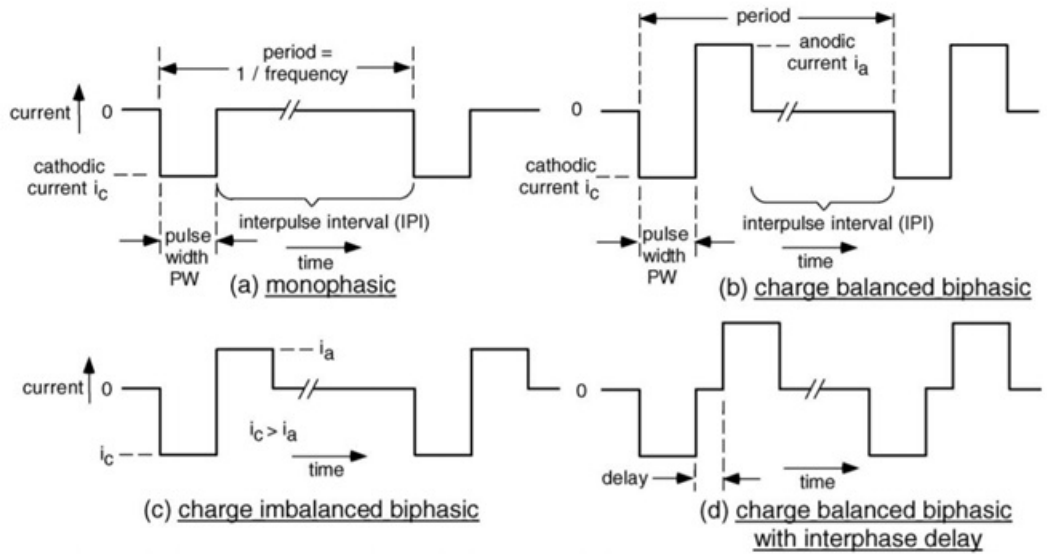

Figure. 1.2. Common pulse waveform types used in the electrical rectangular pulse stimulation [17]. Reprinted from Electrical stimulation of excitable tissue: design of efficacious and safe protocols, 141/2, Daniel R. Merrill, Marom Bikson, John G.R. Jefferys, 171-198., Copyright (2005), with permission from Elsevier 4855551279644

lation (figure 1.2b) provides a high precision of charge balance, and a safe stimulation in term of preventing electrical field damages as well as more control over the current rather than the voltage [16, 17]. The charge-imbalanced biphasic pulse (figure 1.2c) provides imbalanced charges over the two stimulating phases; where the anodal phase has less reversed charges than the cathodal phase. This imbalanced charges alters the evoked potential magnitude to prevent electrode corrosion, and plays an important role in the Faradaic reactions that take place on the activation sites [17]. The biphasic stimulation with interphase delay (figure 1.2d) has been shown to provide sufficient stimulation but with electrode corrosion due to the longer period of the irreversible Faradaic reactions [17].

The spatial properties of the electrodes in the vicinity of nerve bundle control the thresholds to selectively activate a group of nerve fiber without the neighboring ones. Based on several studies, the pulse duration, amplitude, waveform, nerve size, and the

distance between the electrode and the nerve fiber define the selective nerve activation thresholds [17–19]. The pulse stimulation influences large nerve fibers to depolarize before small fibers [20]. This means, the threshold to activate larger-myelinated nerve fibers is lower than small-size fibers thresholds [18, 20, 21]. The mechanism of selectively activating nerve fibers due to pulse stimulation is in direct dependency of the change in m, h, and n gating variables. Since those changes are randomized, the activation of nerve fibers occurs synchronously with the stimuli producing CAP. The differentiation in nerve size and electrodes distances introduces the current-to-diameter, and current-to-distance relationships that alters the excitation thresholds.

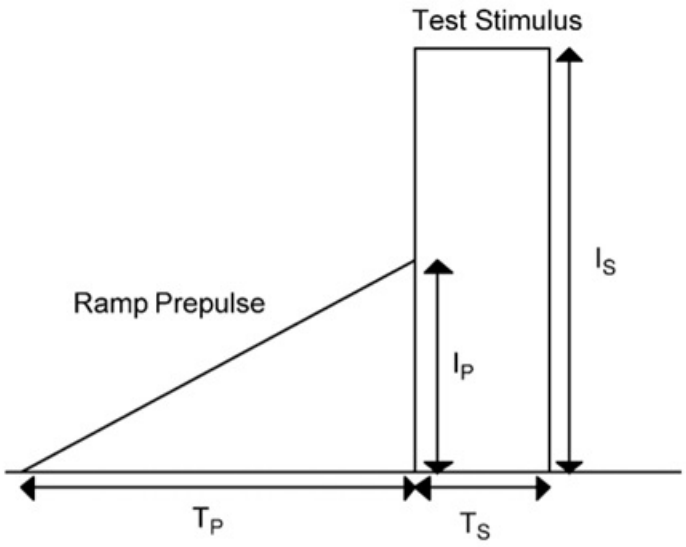

Figure. 1.3. An example of the ramp prepulse waveform used for selective activation [11]. Reprinted from Orderly activation of human motor neurons using electrical ramp prepulses, 116/3, Kristian Hennings, Lars Arendt-Nielsen ,Ole K. Andersen, 597-604., Copyright (2005), with permission from Elsevier 4855550695031

For PNS stimulation and especially motor neurons, several types of pulse waveforms have been evolved to minimize the tissue and electrodes damages and selectively activate the desired nerve fibers. Subthreshold prepulses, and ramp prepulses stimulation using a gradually or an instantaneous increasing waveform before the rectangular

stimuli have been used in research to selectively activate and block specific nerve fiber activity [11, 18, 19, 22, 23]. Figure 1.3 shows an example of the ramp prepulse waveform used in a noninvasive study to change the recruitment order of motor nerve fibers activation, and study the nerve accommodation to the ramp prepulse [11]. Furthermore, another simulation study shows that using exponentially rising waveform selectively would activate small nerve fiber first, then, as the intensity increases, large fiber get activated [24]. Another study demonstrates that quasi-trapezoidal current pulses applied with tripolar cuff electrode can selectively block the generation of action potential based on the applied intensity [21].

With the ability to selectively activate nerve fiber using different pulse-based waveforms, the phenomenon known as neural accommodation arises to interfere with the activation threshold. This accommodation is explained by Hodgkin and Huxley in term of the ionic channels conductance ability to maintain subthreshold [6]. They attributed that to the increase in the degree of inactivation and the K^+ conductance when applying slowly rising current [6]. Bostock defined the accommodation as processes that influence an increase or a decrease in the excitability threshold due to slow or sustained depolarization of the subthreshold [25]. Several studies investigated the accommodation mechanism to determine its dependency on the ionic channels in parallel with the nerve excitability changes [25–27]. For pre-depolarized axons in human and animal, the accommodation happened more rapidly due to the inactivation of Na^+ channels; whereas in normal axons, the accommodation was adopted more frequently due to the slow activation of K^+ conductance [25, 27, 28].

In contrast with the accommodation, a persistent Na^+ current injection has been simulated hypothesizing the breakdown of the accommodation processes [29]. This study demonstrated, *in silico*, that increasing the number of Na^+ channels would allow for persistent Na^+ current flow, resulting in a firing of action potential at a lower threshold [29]. The study hypothesis assumes a large diameter nerve fiber that contains more Na^+ channels, in sensory or motor nerve fibers. According to those studies, it can be seen that once a cathodic current is applied with a rising intensity slowly,

all the gating variables are changing simultaneously, but the inactivation processes become more dominant and rapid repolarization occurs, preventing depolarization from reaching the activation threshold even at higher intensity [25, 27, 29, 30]. In term of the ion channels, the K^+ gating variable n, and the inactivation Na^+ gating variable h overcome the activation Na^+ gating variable m over the time course of the applied current [25,27,29,30]. Furthermore, the influence of hyperpolarization on the accommodation was found to play an important role in selection of the appropriate stimulation waveform [25, 30].

This accommodation process might be accompanied with the negative accommodation, which indicates the change in threshold to be increased more than the initial activation threshold following a period of time [25–27]. In either case of the accommodation, the dynamic of the activation threshold change is explained by the stimulation waveform and the voltage-gated ion channels ability to adapt and change its thresholds. This phenomenon also emphasizes the threshold-tracking techniques, such as superexcitability and refractoriness measurements, and using of trains of impulses to investigating the characteristics of axonal responses in clinical applications [28].

Although the RPES is an efficient method to induce nerve activation and muscle contraction, there are some limitations associated with the activation mechanism and fibers recruitment order [11]. During RPES, nerve activation occurs synchronously to the stimuli and all muscles fibers activate at the same time in response to the stimuli. For motor nerve fibers, this mode of activation is known as the reverse recruitment mode where larger axons activate with lower threshold before small nerve fibers [11]. In the size principle, small axons fibers activate first followed by larger nerve fibers, however this RPES causes larger nerves to induce larger force resulting in muscle fatigue due to the reverse recruitment order [11, 31]. Another limitation of RPES is its associated artifact that is unavoidable during ENG recording. The induced electrical potential also interferes with the biopotential field produced by the nerve, which would alter the accuracy of the ENG measurements [17, 32].

1.2.2 Direct Current (DC) Activation

Unlike the conventional rectangular pulse activation, the DC activation is rarely used in PNS stimulation. However, DC activation is reported to be used in the form of transcranial direct current stimulation (tDCS) for chronic brain and spinal treatments [33]. The rareness of using DC activation in PNS modulation is due to its electrical unbalanced charge properties for long period of time. In two studies, the unbalance of charge injection, either cathodic or anodic polarity, causes nonspecific inflammatory changes and myelin and axon degeneration [34, 35]. Those studies demonstrate that pulse stimulation is safer than DC stimulation. On the other hand, a recent study shows that DC stimulation can be coupled with alternating pulses to achieve direct ionic flow in the chinchillas of the vestibular part of the inner ear [36]. The study suggests using a switching network that involves mechanical valves and square pulses control implemented through microcatheter salt bridge electrodes, which would dramatically overcome the unbalance charge issue [36].

1.2.3 Chemical Activation

Movement of ions across the neuron membrane is the key point in maintaining the resting membrane potential and firing action potentials, which indeed is an electrochemical process. The chemical environment around the nerve is an essential factor that can enhance or inhibit the membrane potential changes. The role of the chemical agents used in pharmacological treatments of nerve disorders are targeting specific protein structure of those ionic channels to alter their mechanisms. Anesthesia is a common example of the chemical alteration of nerve environment; where specific chemical agents are used to block the transmission of the action potential to the target organs, resulting in temporal loss of pain or sensation or unconsciousness [37]. The basic underlying concept is directly related to the Nernst equation; which relates the resting membrane potential to the specific ion concentration inside and outside the cell, temperature, ideal gas constant, and Faraday's constant [37]. Thus, the

concentrations of K^+ and Na^+ ions relevant to the cell membrane are the essential components for chemical alternation.

In terms of nerve activation and excitation, several chemical agents have been proven to evoke action potential generation and propagation [38–41]. A study using organic and inorganic agents, as chemical stimuli, shows a variation in the excitation of the peripheral trigeminal nerve (the long ciliary nerves of the frog) when varying the concentration of those agents [41]. The study used ammonium hydroxide as an inorganic chemical agent, amyl acetate and beta-phenyl-ethyl alcohol as the organic agents [41]. The action potential firing rate following the administration of those agents demonstrated that higher concentration of organic agents declined the firing rate while the opposite was observed with the inorganic agent [41]. The study also relates the chemical excitation's rate to the CAP conduction velocity which predicted the presence of afferent A and C fibers [41].

Furthermore, potassium chloride and lactic acid were pronounced to induce the afferent sympathetic nerve extinction at the left ventricular wall in animal studies [38, 39]. Several concentrations of potassium chloride were dissolved in physiological saline, administrated to mechanosensitive receptor site resulted in an immediate activation of those nerve fibers [39]. The study highlights the minimum concentration to activate myelinated A-delta fibers and unmyelinated C fibers to be 100 μg/ml following 1-7 seconds of administration [39]. The same research group also demonstrated that lactic acid and hydrochloric acid have a role on nerve fibers' activation [38]. In contrast with the potassium chloride, the minimum concentrations of those acids depend on the nerve type and the pH value of the solutions. Table 1.1, shows the minimum acids' concentrations and their corresponding pH values required to activate myelinated and unmyelinated nerve fibers [38].

From those studies, the chemical activation mechanism is revealed to induce the CAP firing asynchronously in comparison with the synchronous electrical pulse stimulation. Once the chemical nerve activation is reached, the CAP propagates with different velocity depending on the fiber type; however, the firing rate increases from

Table 1.1.
Minimum acidic concentrations required to reach chemical activation of afferent sympathetic nerve fibers [38]

Acids	**Myelinated Fibers**		**Unmyelinated Fibers**	
	Concentrations μg/ml	**pH**	**Concentrations μg/ml**	**pH**
Lactic	375-750	3.11-2.86	7.5-75	4.58-3.55
Hydrochloric	18.2-36.5	3.85-3.20	0.365-3.65	5.60-4.53

the site of activation irregularly mimicking the natural activation during myocardial ischemia [38, 39]. The accumulation of natural acids and the increase of potassium ions are examples of the intrinsic nerve environmental changes that alter the resting membrane potential, which led to the activation of nerve fibers. This process also occurred in a stochastic manner rather than deterministic. The electrical pulse stimulation evokes the action potential at a known time and frequency, but the chemical activation alters the nerve environment properties with a latency and irregularity of the action potential generation. As the above studies show, the concentration of the chemical agents play a significant role in inducing the potential generation, but the time and frequency of the induced CAP were independent [38–41].

1.3 Sinusoidal Alternating Current Stimulation

The efficiency of electrical stimulation waveforms made a significant role in the field of neuromodulation. Recently, the discovery of Low Frequency Alternating Current Block (LFACb) in the Bioelectronic laboratory bridges the gap between the high alternating current (AC) frequency block and DC block [42–45]. This phenomenon is unique and a promising technique for a safe, reversible block that can be highly

utilized in several clinical applications [42, 43]. Furthermore, LFACb initiates the discovery of the LFAC activation, which could be a change in history for muscle and nerve activation. The use of sinusoidal AC stimulation has emerged in the field of functional electrical stimulation recently, but the history of attempting to block the nerve activity using AC goes back to 1940 [46–50]. The following three sections discuss few controversial studies that have demonstrated the possibility of enhancing and inhibiting selective nerve activities with different nerve fibers.

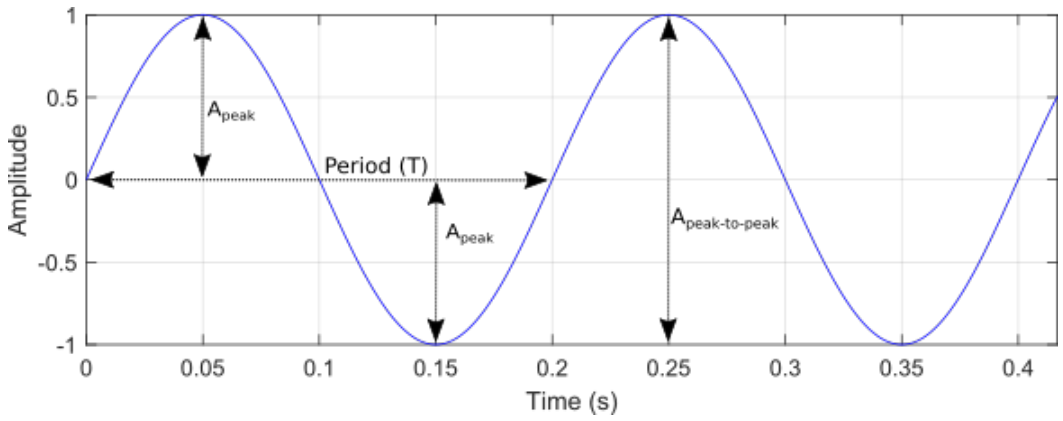

Figure. 1.4. An example of 5 Hz AC sinusoidal waveform parameters. The amplitude measures the magnitude of current in ampere A_p or A_{pp}. The period is the time the wave takes to complete one full cycle which is inversely proportional to wave frequency

Frequency and amplitude are two main parameters that governor the AC influence on the nerve activity. The frequency of the sine wave is inversely proportional to its period (f=1/T), which defines how many cycles of oscillation occur per second. The amplitude is a measure of the amount of current delivered during stimulation. The peak (I_p) amplitude is a measure of the maximum current value delivered during half cycle of the waveform regardless of the polarity. During AC stimulation, the peak value represents the functional stimuli-strength that derives depolarization or hyperpolarization of the membrane. On the other hand, the peak-to-peak value (I_{pp}) represents the total magnitude of the positive and negative peaks.

1.3.1 High Frequency Sinusoidal Alternating Current Block

The use of high frequency alternating current to block nerve activity in the motor PNS has been demonstrated in several studies [46, 49, 50]. In neuromodulation, interfering with the signal pathway between the CNS and end of organs can improve the selectivity of blocking signals responsible for neurological disorders. Using AC to block nerve activity is considered more reliable method than other pharmacological blocking techniques. The main features of using AC block in the PNS have been proven to produce a reversible and quick slow or block of the CAP, and can be selective based on nerve fibers [49].

Using a sinusoidal AC waveform at frequencies ranging from 3 to 5 kHz has been shown to produce 100% block of nerve activity in the frog sciatic nerve [49]. The study highlights that efficiency and reversibility of the block when using the appropriate methodology of delivering the blocking AC waveform in terms of voltage and current control. In term of efficiency, the muscles twitching was gradually blocked when using 3-5 kHz AC at 0.5-2 mA_{pp} [49]. Furthermore, another simulation study hypothesizes that the membrane tonic depolarization might be the cause of this block [49]. Another study also demonstrated the selectivity of the AC block using 130 Hz [50]. This study shows that the rabbit sural-gastrocnemius reflex was reversibly blocked at a threshold between 500 to 900 μA_{pp} and suggested to be due to block of C fibers around the blocking electrodes [50].

A more recent review on the Kilohertz Frequency Alternating Current (kHFAC) block has highlighted some experimental evaluation on this method for preclinical applications [51]. The study includes a detailed review of the kHFAC block in terms of reversibility, partial block, electrode design, fiber type and size, species and nerve diameter [51]. Based on this review, the "onset response", which is described as the transient activation of the nerve due to the application of kHFAC, impacts the blocking mechanism [51]. The impact time of this response varies based on the applied amplitude, but it is always followed by a conduction block. Furthermore, from those

experimental findings, the kHFAC waveform might cause nerve or tissue damages due to the very high fluctuating of the electrical field [51].

1.3.2 Low Frequency Alternating Current Block (LFACb)

The sinusoidal LFACb is the most recent method discovered in our lab that has shown promise as a reversible nerve conduction block in the PNS [42, 43, 45]. The application of this method is in line with those utilizing high frequency stimulation block, but with much less injected current and lower frequency. The LFAC block was observed with L. terestris Earthworms giant nerves, and *ex-vivo* canine cervical vagus nerves [42]. From that study, the action potentials showed a slowing of their conduction velocities that led to a complete or partial cease of conduction [42]. This study also demonstrated the LFAC blocking mechanism within a simulation model that relates the inactivation process to the Na^+ gating variable and the spatial distribution of the membrane potential [42].

The recent *in-vivo* study (*unpublished work*) on cervical vagus nerve in rats has shown a clear reversible block of the evoked bradycardia and hypotension when applying LFAC waveform at 1 Hz with an amplitude less than 0.2 mA_p [42, 52, 53]. A more recent *in-vivo* study also demonstrated LFAC ability to block Hering-Breuer (HB) reflex in anaesthetized swine [52–54]. The results showed a clear slowing in the induced compound nerve action potential (CNAP) velocity of the cervical vagus nerve when applying 1 Hz LFAC with the intensity less than 1.0 mA_p [52, 54]. The breathing rate during the induced HB-reflex dropped substantially and the normal breathing was recovered by applying LFAC waveform [52, 54]. In contrast with the high frequency AC block, LFACb is well below that risk factor of causing tissue or nerve damage and considered a promising technique for clinical applications.

1.3.3 Attempts on Sinusoidal Alternating Current Activation

The use of the sinusoidal AC for motor PNS fibers activation has not been investigated yet, but a form of this technique has been utilized as a diagnostic tool to evaluate the sensory nerve function [47, 48, 55]. Although the kHFAC block shows the onset activation, there is no experimental evidence that the kHFAC waveform results in sustained activation. The diagnostic device used in market, Neurometer, is a transcutaneous stimulator that is designed and approved to selectively evoke the activation of sensory nerves based on three frequencies [55]. This device is capable of producing a sinusoidal AC at frequencies 2000, 250, and 5 Hz and a current intensity ranging from 0.01 to 9.99 mA_p [55]. It is mostly used during nerve conduction studies to assist identifying nerve fibers based on their functional characteristics and conduction velocity [55].

A study utilizing the Neurometer has shown a degree of selectively activating the afferent unmyelinated C fibers, large-small diameter myelinated A-beta and A-delta fibers based on the applied frequency in dorsal root ganglion (DRG) of rat models [48]. This study shows, with the use of patch-clamp recordings and antidromic action potential recording, that the sinusoidal AC is the main cause of inducing the antidromic action potential selectively [48]. The minimal current amplitude was varying among the frequencies, but the study indicates that 2000 Hz waveform selectively activates A-beta fibers, 250 Hz activates A-delta fibers, and 5 Hz activates C fibers [48]. Those findings from the cellular level recordings were also compared with the transcutaneous responses, which shows a variation on the minimum current amplitude required to cause the activation [48].

In contrast, a simulation study utilizing Neurometer argues that the selective activation of C, A-delta, and A-beta fibers may not be possible using those frequencies [47]. Both of those studies are in agreement that 2000 Hz can selectively activate A-beta fibers, and 5 Hz can activate C fibers. However, 250 Hz induced the activation in both A-beta and A-delta fibers. The action potential firing rate was one of the

parameters analyzed in both studies at each applied AC frequency [47, 48]. Interestingly, the action potential firing frequency did not reach the applied AC frequency at any current amplitude. This observation is seen from both studies, which would require further investigations on the efficiency of such selective activation.

1.4 Thesis Hypothesis and Aims

The hypothesis of this thesis stems from the discovery of LFAC activation in the Bioelectronics Laboratory. During the attempt to block the conducted sciatic nerve activity in a rabbit experiment (*unpublished work*), long lasting, non-fatigable twitches were observed during the steady application of LFAC blocking waveform. The twitches were related to the sinusoidal waveform cycles that suggests a role of the LFAC waveform frequency and fiber type difference in electing either block or activation. These preliminary data suggested the possibility to activate motor nerve fibers using Low Frequency Alternating Current activation method (LFACa). Based on that work, it is hypothesized that there is a possibility to evoke the peripheral nerve activity using LFAC (<100 Hz), and that activation is unique and may be in the right order of activating nerve fibers. The observed muscle contraction was significant with a large amount of force that did not cause muscle fatigue. This phenomenon arouses several questions to be investigated as the aims of this thesis.

The hypothetical mechanism of LFAC activation is also driven from the current findings of LFACb and its associated simulation models [42, 43]. It is predicted that the LFAC waveform cycles influence the membrane potential change leading to a complete or partial block of the conducted action potential. Similar to block, the LFAC activation mechanism is hypothesized to be affected by the waveform cycles and electrode-contact geometry. The pure sinusoidal current waveform has a symmetrical charge balance that naturally maintains zero-net charge injection and suggests a safe approach to prevent tissue injuries. A single sinusoidal cycle is predicted to produce two bursts of activity rather than a single CAP. This prediction is directly related to

the waveform frequency and might be nerve fibers type-size dependent. The LFAC activation observed in the rabbit experiment suggested that the activation was in the normal order with small fibers getting activated first at lower current intensity. This is different than the standard pulse activation and any other methods of selective activation. The pulse stimulation activates all fibers at the same time or activates large fibers first that does not allow for the selectivity of small nerve fibers. Thus, exploring the LFAC activation in different animal settings would characterize the waveform cycles influence and provide experimental verification of those predictions in terms of feasibility, scalability and threshold findings.

1.4.1 Thesis Aim 1

Provide Experimental Evidence of the Possibility of Activating Peripheral Nerve Fibers Using the LFAC Waveform

Ex-vivo experiments were conducted on excised canine cervical vagus nerves (Chapter 2) to investigate the nerve excitation during LFAC activation at 5, 10, and 20 Hz. From those experiments, several post processing methods were developed to evaluate the nerve activity induced by LFAC waveform. The *in-vivo* investigations (Chapter 3) of LFAC activation were accomplished on (1) the cervical vagus nerve in anaesthetized swine, and (2) the sciatic nerve in anaesthetized rats. From these studies, evidence of LFAC activation was established to report the feasibility and scalability of the LFAC activation between autonomic and somatic nerve bundles using neural based reflexes as biomarkers.

1.4.2 Thesis Aim 2

Determine Whether There is a Frequency Dependence for LFAC Activation in Peripheral Nerves

The LFAC activation, as stated above, is a unique method that requires sophisticated characterization of its underlying mechanism. Thus, for this thesis aim, it is

more informative to establish and determine the threshold of activation as a function of the applied LFAC frequency. In parallel with Aim 1, the frequency-amplitude thresholds could be fiber type dependent that would allow for further investigation between autonomic and somatic nerve fibers. Indeed, the activation threshold determination would promote the expansion to characterize the frequency dependent window between LFAC block and activation.

2. EX-VIVO VISUALIZATION OF LFAC NERVE ACTIVATION

The review of the standard pulse activation in Chapter 1 highlights the neurophysiological theory in terms of the underlying mechanism and considerations during the electrical nerve stimulation and recording of nerve activities. In this chapter, we explore methods to measure the neural activity induced by LFAC waveform. Also, an experimental protocol for the LFAC activation method is established and discussed in terms of the nerve activity induced by the LFAC and implications of extracellular stimulation.

2.1 Introduction

Activation of peripheral nerves has been utilized in the field of neuromodulation and bioelectronics for centuries. Since the time of Galvani, the excitability of the peripheral nerves has been demonstrated to improve the clinical applications of electrical stimulation [16]. With the most recent advances in designing implantable neural prostheses, electrical activation of the peripheral nervous system (PNS) plays major roles in improving the efficiency and selectivity of nerve fibers activation. Although the standard pulse stimulation has been approved in several clinical applications, the improvement of a selective stimulation method of nerve fibers remains slow in progress and expensive in research settings. Research studies focusing on the selectivity of nerve stimulation and recording can be classified based on their purpose as either (1) stimulation waveform studies or (2) electrode studies.

The electrode studies have been investigating the influence of electrodes' characteristics on the recording of the electroneurogram (ENG) signals. Electrodes' type, size, geometry, material, and their electrical conductivity properties play significant

roles on the validity and selectivity of transducing neural activity. The intercellular stimulation and recording provide the optimal understanding of the nerve activity, but they require specific tools and techniques that might not be suitable in all neural prosthesis implantation. However, the extracellular recording and stimulation of peripheral nerve fibers provide a substantial amount of information that has significantly improved the field of neuromodulation. It provides reachability to a large population of nerve calibers as well as characterizing the nerves' bundles tissue properties such as permittivity, conductivity, and capacitive [15]. The current use of cuff electrodes for either stimulation or recording has been demonstrated to provide a certain degree of fiber recruitment for activation and easiness for correct positioning over nerve bundles [56]. Beside the advantages of cuff electrodes in implementation and possible selectivity during stimulation, they provide a noise rejection in recording nerve activity [15]. Thus, the geometry and configuration of such recording electrodes can enhance the ionic biopotential field to be transduced from the electrode-tissue interface with minimum noise before amplification.

The electrical stimulation of the peripheral nerves provides an onset trigger for the nerve fibers to activate. In terms of selectivity, several studies have utilized different waveforms to achieve the proper selective activation of nerve fibers [9,17,18, 21,24]. The most common aspect between those studies is the use of pulse stimulation, or a modified version of it, as described in Chapter 1, which can be controlled by pulse duration and amplitude to reach the threshold or subthreshold requirements to evoke the CNAP. One of the limitations of pulse stimulation is its associated artifact that is unavoidable during recording. The injected electrical current voltage during stimulation produces an electrical field that overlaps with the biopotential field produced by the nerve [32]. Additionally, based on the waveform of the pulse stimulation, the net charge imbalance has a severe impact on the nerve tissue and the electrodes [17]. The impact of these limitations alters the recorded nerve activity and requires further analysis to precisely obtain and analyze the electrophysiological response of nerve fibers.

Utilizing the Low Frequency Alternating Current (LFAC) waveform in blocking mammalian peripheral nerve activity has been shown in [42, 43, 52–54]. The previous observations from the rabbit experiment (*unpublished data*) suggested the possibility of using LFAC to activate the peripheral nerve fibers. The nerve activity recordings from that experiment showed unusual behavior of the nerve responses and require further investigations. To examine this hypothesis, we combine the long historical theories of the electrical stimulation and the principles of extracellular recordings to study the nerve activation behavior using LFAC waveform. However, the fundamental stimulus-triggered average tool to measure the CNAP activity is no longer available with LFAC waveform. Thus, the objectives of this study are (1) to explore the LFAC activation phenomenon using LFAC waveform (5, 10, and 20 Hz) in *ex-vivo* settings using excised canine vagus nerves. (2) To find alternative analysis methods to measure the neural activity induced by LFAC waveform.

2.2 Methods

2.2.1 Nerve Tissue Preparation

The experiments of this study were conducted on freshly excised canine vagus nerves (n=3) harvested 10-15 mins after the euthanasia of the animal. The nerves were kept in a cold Krebs solution while aerating for 20 to 30 minutes. The Krebs solution was prepared using: Sodium chloride (NaCl=7.00 g), sodium bicarbonate ($NaHCO_3$=1.26 g), potassium chloride (KCl=1.72 g), magnesium chloride hexahydrate ($MgCl_2.6H_2O$=0.27 g), sodium dihydrogen phosphate monohydrate ($NaH_2PO_4.H_2O$ =0.17 g), calcium chloride dihydrate ($CaCl_2.2H_2O$=0.23 g), glucose (2.0 g), and 1.0 liter of distilled water.The nerve tissue was extended and pinned with hypodermic needles at both ends on a dissection tray as shown in figure 2.1 at room temperature (26-28 C°). Krebs solution was applied to the nerve to ensure it did not dry out during the experiment. Furthermore, the Krebs solution allowed for conductivity of the electrodes.

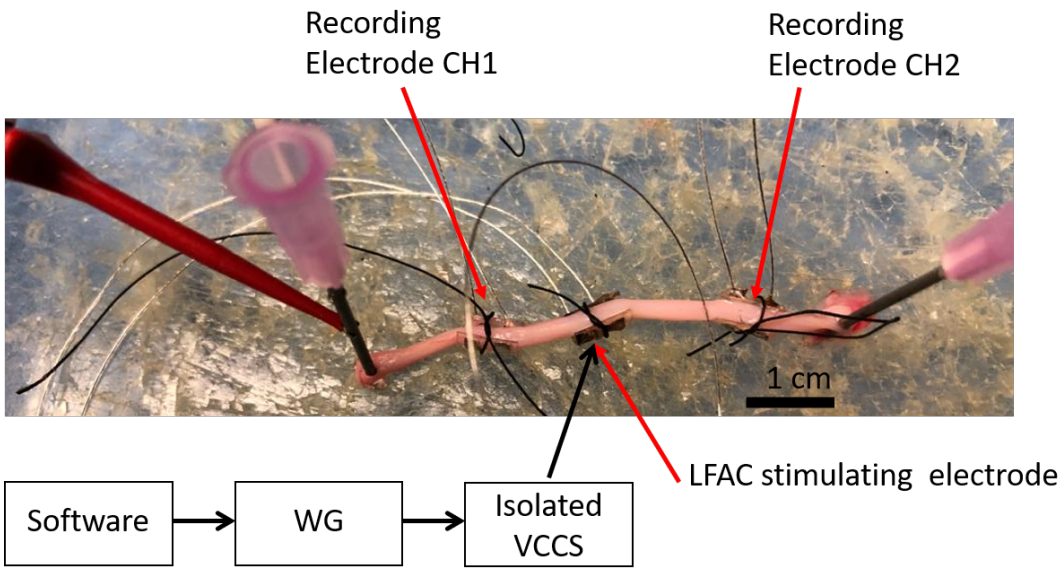

Figure. 2.1. Electrodes setup of the canine vagus nerves experiment. Below the image, the generation of the LFAC waveform pathway is shown.The waveform and stimulus timing were controlled using LabVIEW® application to programmatically control a Digilent Analog Discovery 2 Waveform Generator (WG). The waveform was passed through a custom built isolated voltage controlled current source (VCCS) which sourced the current to the LFAC electrodes, and relayed the voltage drop across the electrodes back through an isolation amplifier to the recording bench

2.2.2 Experimental Setup and Electrode Configuration

Three bipolar custom-made cuff electrodes with platinum contacts, 1.8-2.0 mm inner diameter, were placed under the nerve as shown in figure 2.1. The stimulation electrode was placed between the two recording electrodes to deliver the pulse stimulation as well as the LFAC waveform. To verify the nerve was active -able to generate CAP, a rectangular pulse stimulation (50-100 μsec duration, and 0.5-1.3 mA_p amplitude) was used to evoke the CAP at the beginning of the experiment (DS3 Isolated Current Stimulator, Digitimer, UK). The stimulator was triggered using the analog discovery 2 (Digilent, USA) waveform generator, controlled by a tuning application written in LabVIEW® (K. Yoshida, 2019). Both channels of the nerve activity were

passed through a differential amplifier with an exchangeable gain of 2500x-10,000x, and high pass filter at 300 Hz (CyberAmp 320, Axon Instruments). The LFAC waveform was generated and tuned using the analog discovery 2 and aided through a custom-made isolated voltage controlled current source unit before connecting to the tissue. The LFAC waveform and both ENG channels were recorded digitally (NI USB-6212, National Interments) at a sampling rate of 48 kHz using Mr. Kick (Knud Larsen, Aalborg University, Denmark).

2.2.3 Activation Protocol

To evaluate the LFAC activation, the experiment was broken down into two main stages. In stage 1, experiments were conducted within 40 min after the animal was euthanised. We refer to this stage as 'Fresh'. Two hours were allowed to pass following the Stage 1 procedures before repeating the experiment in Stage 2, which we refer as '2Hr-Post'. Within this period we expect the nerve's excitability to diminish, and serve as the negative control for the study. Since the nerve tissues were excised, the nerve surrounding conditions differed from the physiological environment in terms of pH, temperature, level of oxygen, and exposure to different air components. As a result, the excitability of the nerve fibers decays with time [57]. Taking that into our advantage, this experimental paradigm would assess observing the effect of the LFAC waveform on the active nerve tissue during the first stage while observing the passive activity of the nerve tissue in the second stage. In addition, the noise from the surrounding equipment was evaluated by recording a brief baseline before applying the LFAC.

Stage 1

Pulse stimulation was delivered to the nerve through the middle electrode to ensure that the nerve was able to produce CAP and conducting prior to the LFAC application. If a CAP was clearly visible on the oscilloscope (HMO1002, Rohde and

Schwarz), the stimulation electrode was disconnected from the stimulator and connected to the VCCS isolator unit for the delivery of the LFAC waveform. The LFAC waveform was applied at three different frequencies: 5, 10, and 20 Hz, with a gradual increasing of the amplitude. Each frequency was applied individually, and allowed few seconds of recording between each amplitude increment. To avoid reaching the water window and causing irreversible hydrolysis reactions, the amplitude was limited to be less than 2 mA_p. The water window was defined as the minimum potential difference at the nerve-electrode interface to breakdown water into oxygen and hydrogen known as electrolysis of water [15, 58]. If this reaction occurs, the electrodes are no longer operating in the linear region and might cause damages to the nerve tissue and electrode contacts. For the used platinum-electrodes contacts the water window was about 2.2 V_p and was monitored throughout the experiments.

Stage 2

Two hours following stage 1 completion, the nerve was stimulated again with a pulse stimulation to verify its inability to produce the CAP. Once that was verified, the same procedure of applying the LFAC was repeated.

2.2.4 Signal Processing

Historically, when using pulse stimulation, the fundamental stimulus-triggered average tool is used to evaluate the neural activity by identifying the CAP and measuring its velocity with respect to the stimulus which always occurs synchronously. That method not only unmasks the CAP but also clear the random noise that might interfere with the signal. However, in these LFAC-based experiments, there is no stimulus artifacts to keep track of the location of those activity. Alternatively, we explore some signal processing techniques that might reveal the evoked neural activity by LFAC waveform.

The acquired ENG signals from both channels were processed digitally using a custom MATLAB script (Version: R2018b, The MathWorks). Since there were two sets of data for each frequency, the analysis was processed with respect to each frequency. For most of the analysis, the continuous recordings were divided into segments based on the applied LFAC amplitude and analyzed individually.

Basic Filtering Process

Using a digital Butterworth bandpass filter (4^{th} order, high pass: 300 Hz and low pass: 6 kHz) the continuous ENG recordings were filtered and showed burst modulation when the nerve was fresh.

Averaging Algorithm

The raw ENG signals include the LFAC waveform, which could be filtered using the digital bandpass filter; however, the digital filter characteristics undesirably alter the signal phase and may include random fluctuations. Although the applied frequency of the LFAC is known, the amplitude of the delivered current is depending on the instantaneous electrodes' complex impedance. Thus, using a nonlinear model, with Levenberg-Marquardt method and standard deviations (K. Yoshida, 1999), the embedded sine-wave could be estimated and subtracted from the ENG signal. This algorithm was used in order to eliminate the filtering effect on the ENG recordings. Following the subtraction, the ENG was phased locked with the applied LFAC cycles and averaged in one period window with respect to each applied frequency. This step allowed to identify and observe any synchronized spikes or CAP to the LFAC cycles.

Furthermore, the rectified version of the ENG recording was calculated to show the LFAC peaks influence on the ENG. This step allowed to observe the variance locations with respect to the LFAC cycle and how that might correlate with the overall activity. The moving average of this averaging algorithm results was used to observe the ENG change as a function of the LFAC waveform parameters.

Power Spectrum Density (PSD)

To evaluate the LFAC activation and the induced nerve activity on the ENG, the power spectral density was estimated in MATLAB using Welch's segment averaging estimator with respect to a Hamming window and the sampling rate. The PSD distribution of the ENG allowed to separate the spectral contents of the ENG and revealed the nerve activity at multiple LFAC amplitudes if any existed. It also provided a means to observe the noise level comparing to the LFAC waveform contents.

2.3 Results

The nerve activity evoked by the LFAC was found to be in a different fashion than the standard pulse stimulation. Although there was not an observed indication of the activation during the experiment, the post processing of the recorded ENG revealed the nerve activity changed during LFAC stimulation stage 1, when the nerve was fresh. Figure 2.2A shows 7-second combined recordings of the ENG and the corresponding 5Hz LFAC waveform (baseline, 0.1, 0.5, 1.0, and 1.2 mA_p) in both stages of one of the experiments. To observe the change on the ENG at different amplitudes, the lower panels of figure 2.2 (B and C) show a 2-second windows of the ENG and the corresponding 5Hz LFAC waveform during both stages of the experiment at amplitudes of 0.1 and 1.2 mA_p. Increasing the amplitude of the 5Hz LFAC to 1.2 mA_p as shown in figure 2.3 evoked a clear burst modulation on the ENG that was not observe during the lower LFAC amplitudes of 0.1 mA_p as shown in figure 2.4. Those activities are more likely to be superposition waveform of several spontaneous nerve activity.

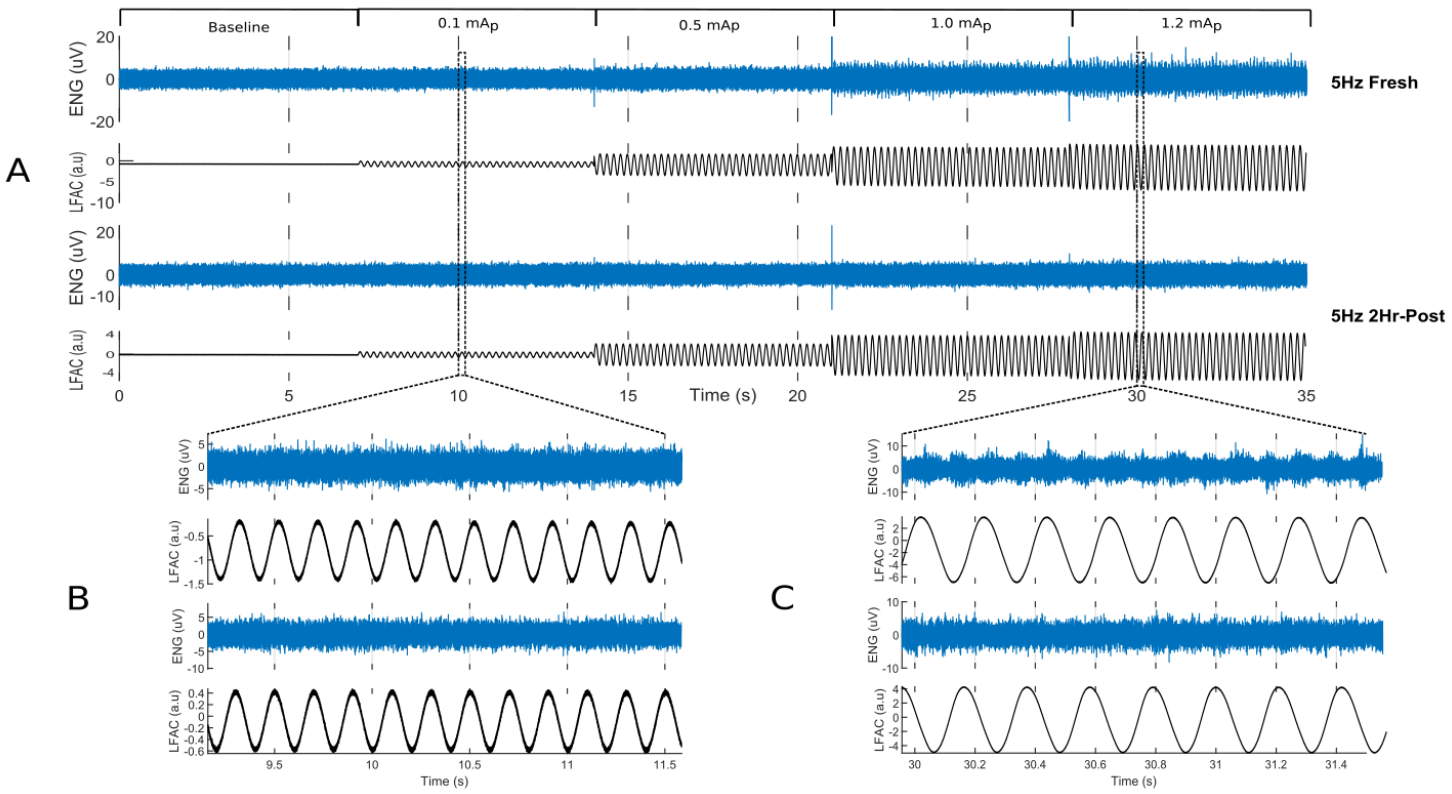

Figure. 2.2. A result example of the ENG signal and the corresponding **5Hz** LFAC waveform when the nerve tissue was fresh (top two traces of each panel) and 2Hr-post (bottom two traces) at different amplitudes. A: a 7-second combined segments of each applied LFAC amplitude. B: a 2-second window when no activation was observed at **0.1 mA**$_p$. C: a 2-seconds window when the activation was observed at **1.2 mA**$_p$

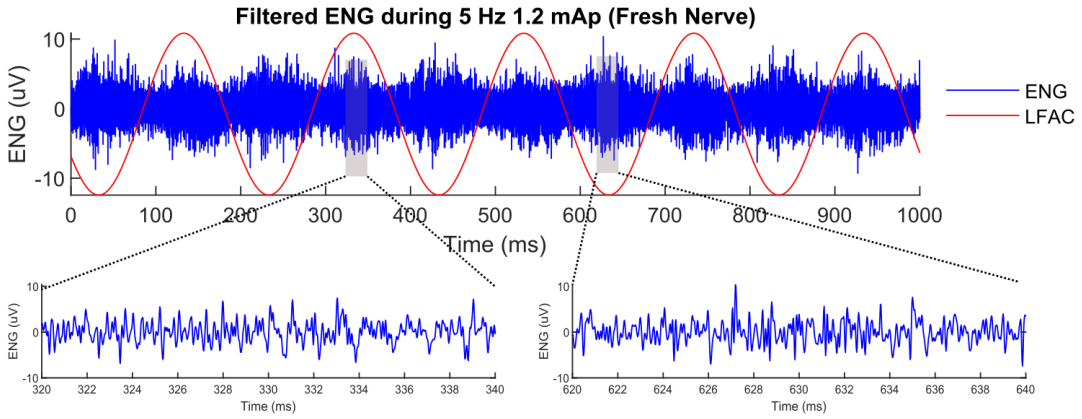

Figure. 2.3. Milliseconds scale of the filtered ENG during the LFAC activation of **a fresh** nerve (stage 1) at **5 Hz 1.2 mA**$_p$

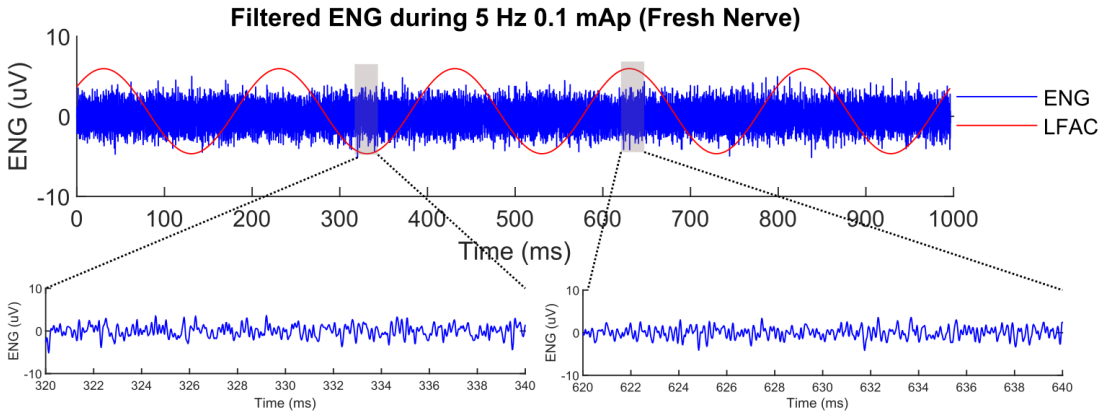

Figure. 2.4. Milliseconds scale of the filtered ENG during the LFAC activation of **a fresh** nerve (stage 1) at **5 Hz 0.1 mA**$_p$

During the second stage of the experiment, at 5 Hz 1.2 mA$_p$ LFAC waveform, the burst modulation disappeared as shown in figure 2.5. Similarly, When applying 0.1 mA$_p$, 5Hz LFAC waveform, figure 2.6, the ENG did not show any change in either cases. This is also in agreement with the baseline recording. The absence of the burst modulation during the second stage suggests that the modulation on the ENG was due to the nerve activity induced by the LFAC and was not a response from the nerve tissue to the LFAC waveform.

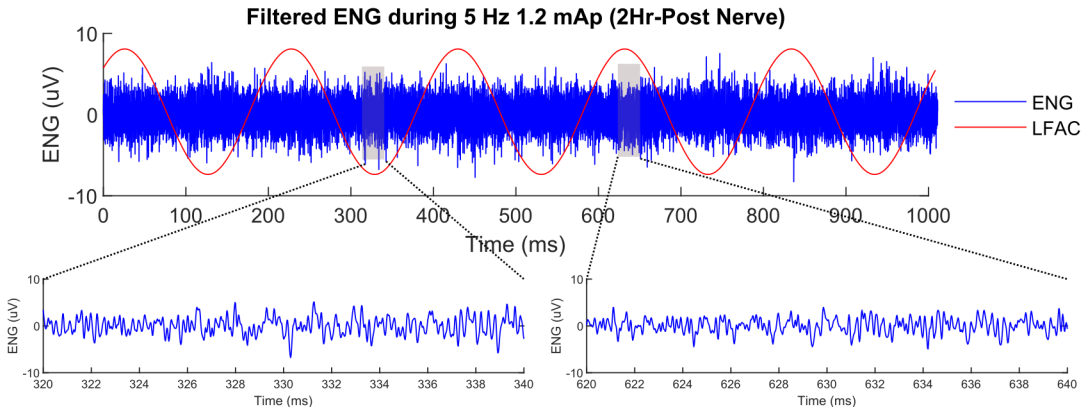

Figure. 2.5. Milliseconds scale of the filtered ENG during the LFAC activation of **2Hr-Post** nerve (stage 2) at **5 Hz 1.2 mA**$_p$

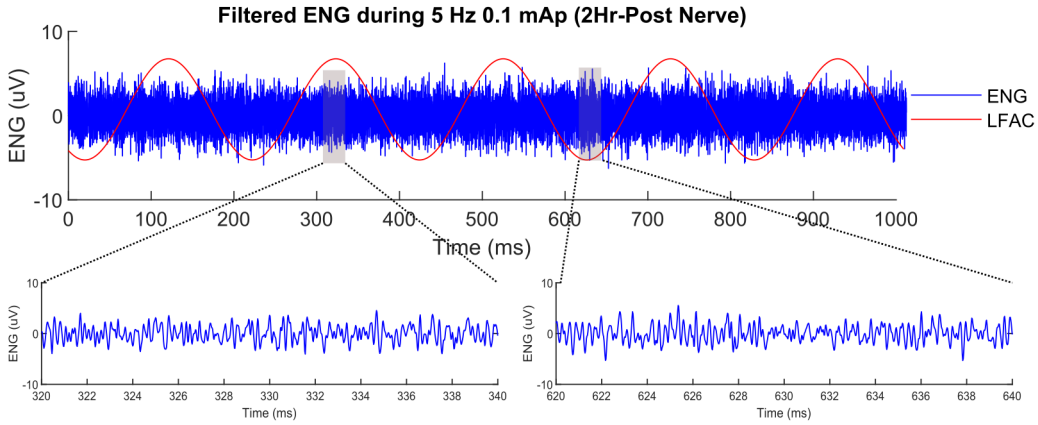

Figure. 2.6. Milliseconds scale of the filtered ENG during the LFAC activation of **2Hr-Post** nerve (stage 2) at **5 Hz 0.1 mA**$_p$

Subtracting the fitted sine wave from the raw ENG manifests the LFAC phase-correlated activity as burst modulation during stage 1 (figure 2.7A and B); however, during stage 2, the subtraction of the sine wave showed no change on the ENG (figure 2.8A and B). Following the subtraction, the ENG signal was traced back to the estimated sine wave, segmented into one period windows, and then averaged. The results showed a clear burst modulation with respect to the LFAC cycles as shown in figure 2.7D during stage 1 and the absence of those activity during stage 2 as shown

in figure 2.8D. Since the CAP is a zero-mean, averaging several spontaneous activity resulted in a significant reduction in the modulation amplitude, which suggests that the LFAC waveform elects unsynchronized nerve activity. Additionally, figure 2.7C and figure 2.8C show the rectification of the burst modulation, when present, after eliminating the sine wave from the ENG. This rectified version of the ENG signal suggested that the burst modulation was mostly influenced by the LFAC cycle only in the fresh nerve, producing two bursts of activity for each cycle.

By averaging those rectified activities as shown in figure 2.7F and figure 2.8F, the results show a correlation between the LFAC peaks and the amount of nerve activity when the nerve was fresh, with no remarkable activities on the 2Hr-Post nerve. For further investigation to reveal any synchronized activity with the LFAC cycles, the rectified version of the burst modulation in panel D of figure 2.7 and 2.8 were produced in panel E of each figure. The differences between those averaged and rectified versions of the modulation are shown in panel G of figure 2.7 and 2.8. The moving average revealed slight change between the averaging results. The rectification implies that the activation to be with respect to the LFAC cycle peaks as there are two bursts modulation for each LFAC cycle. Averaging those modulations shows a dispersion in the magnitude that explains the randomness of the nerve activity.

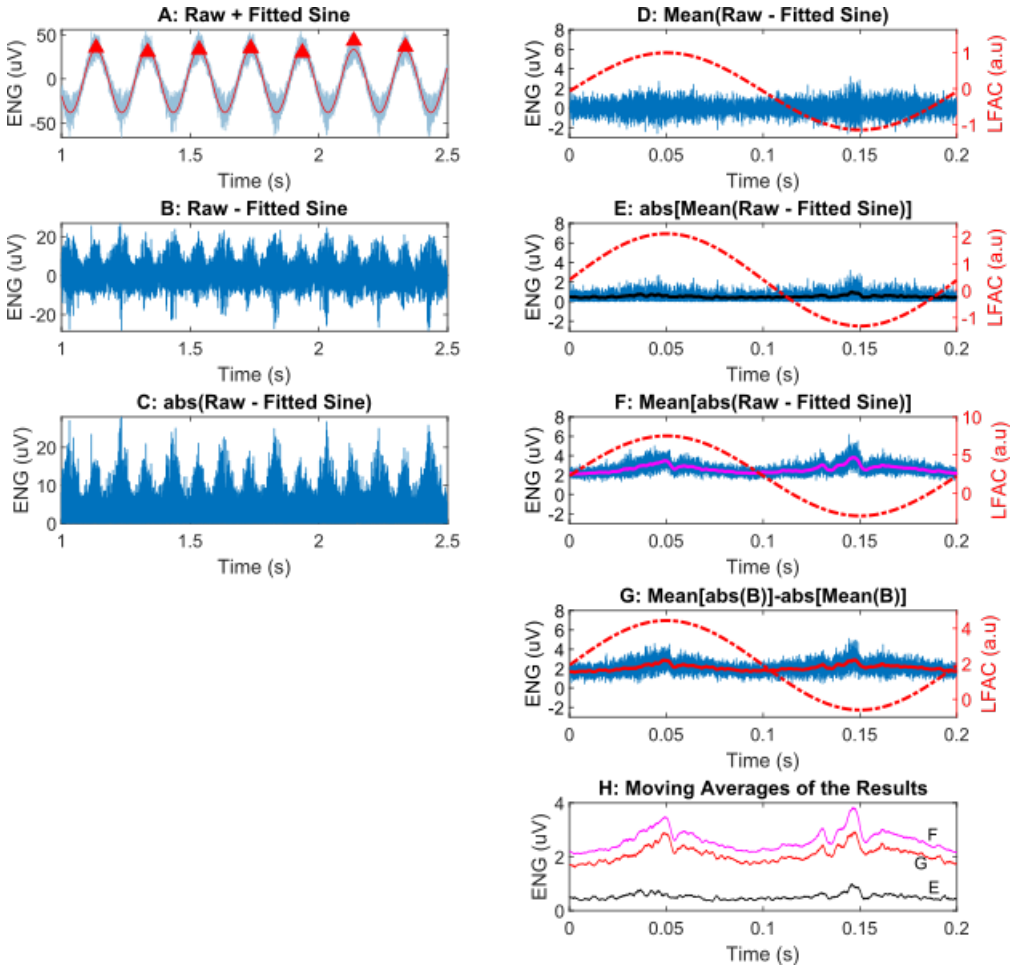

Figure. 2.7. The averaging algorithm results during LFAC activation of **a fresh** nerve (stage 1) at **5 Hz 1.2 mA**$_p$. A: 1.5-second of the raw ENG and fitted sine wave. B: burst modulation resulting from subtracting the sine wave from the raw ENG. C: a rectified version of the burst modulation. D: averaging the modulation against one LFAC cycle. E: the rectified version of the average in D. F: averaging the rectified modulation in C. G: the difference between F and E. H: the moving average of E, F, and G. The red LFAC waveform is an arbitrary unit to show the phase relationship

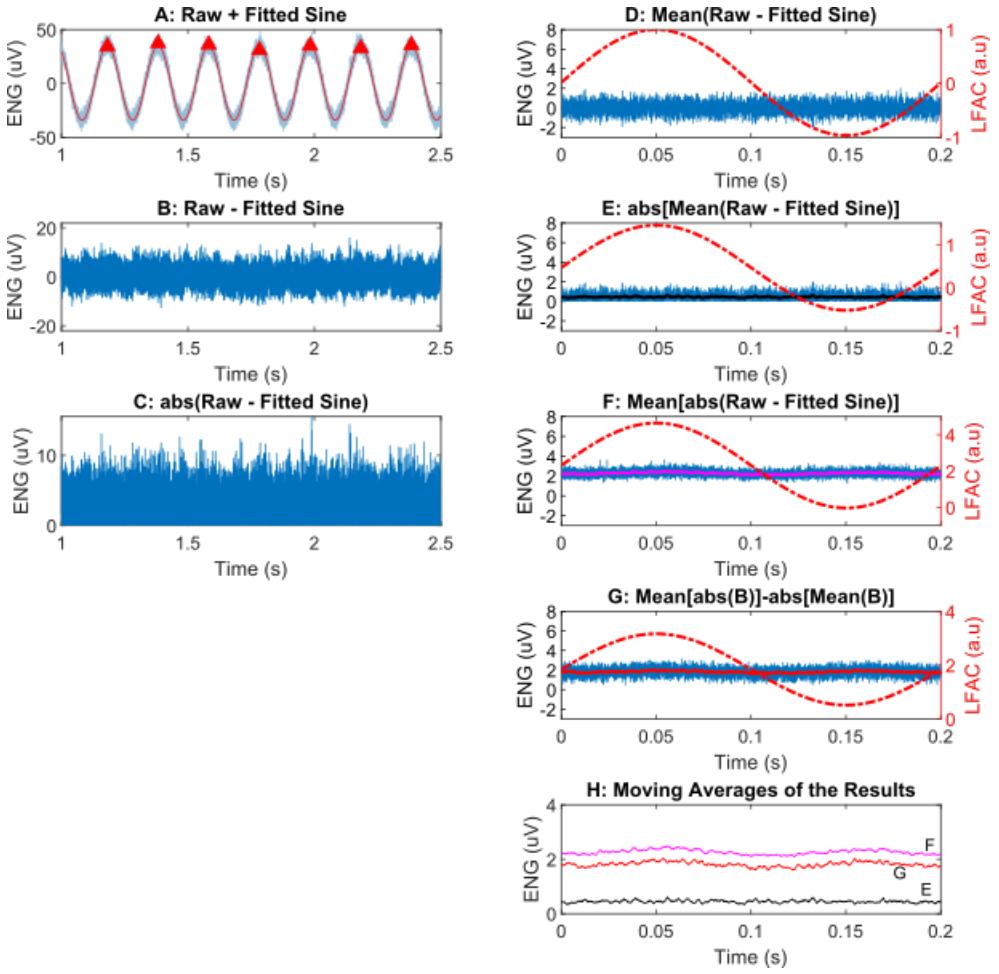

Figure. 2.8. The averaging algorithm results during LFAC activation of **2Hr-Post** nerve (stage 2) at **5 Hz 1.2 mA**$_p$. Refer to figure 2.7 for description

The PSD distribution of the ENG in figure 2.9 shows a slight deviation as the 5 Hz LFAC amplitude increases. The large peaks at 5 Hz correspond to the applied LFAC waveform, as seen in lower panel of figure 2.9, and the deviation started in the range between 1 kHz to 10 kHz which was more likely corresponding to the neural activity band [15]. The baseline recording and the lower amplitudes (0.1 and 0.5 mA_p) superimposed each other, which show the absence of the neural components in that band. Moreover, while activating the 2Hr-Post nerve, there was not any neural activity observed regardless of the applied LFAC amplitude. Although the in-band noise appeared to be significantly interfering with the raw signals at the lower frequency range, the ENG band shows a clear increase in the PSD during the application of 1.0 and 1.2 mA_p 5Hz LFAC.

Similar to the process of 5 Hz LFAC activation, the 10 and 20 Hz LFAC application caused the nerve fibers to activate as the burst modulation indicates in figure 2.10 with amplitudes: baseline, 0.1, 0.5, 0.8, and 1.0 mA_p and figure 2.11 with amplitudes: baseline, 0.1, 0.2, 0.3, 0.4, 0.5, and 0.6 mA_p. The minimum amplitude to cause the nerve modulation was 50% less than 5 Hz. At 10 Hz, 0.5 ± 0.06 mA_p, and at 20 Hz, 0.3 ± 0.06 mA_p the LFAC evoked the nerve modulation during the first stage, and further increment of the amplitude caused the modulation to be higher in magnitude. Comparing the results of both stages, the 2Hr-Post nerve fibers were not influenced by the 10 Hz LFAC waveform. However, the 20 Hz LFAC caused the 2Hr-Post nerve to response irregularly to the LFAC waveform. This onset behavior was observed to be random and not correlated with LFAC peaks, which might be nerve activity induced by the LFAC due to the recruitment of different nerve fibers that were not completely declined.

The averaging algorithm also revealed the nerve burst modulation when applying 10 and 20 Hz LFAC waveforms. As shown in figure 2.12 for 10 Hz and figure 2.14 for 20 Hz, the subtraction of the sine wave and the rectification clarified the modulation apparency, which suggests the activation the fresh nerve fibers. On the other hand, the 2Hr-Post nerve activation using 10 Hz reveal no change over the LFAC cycles

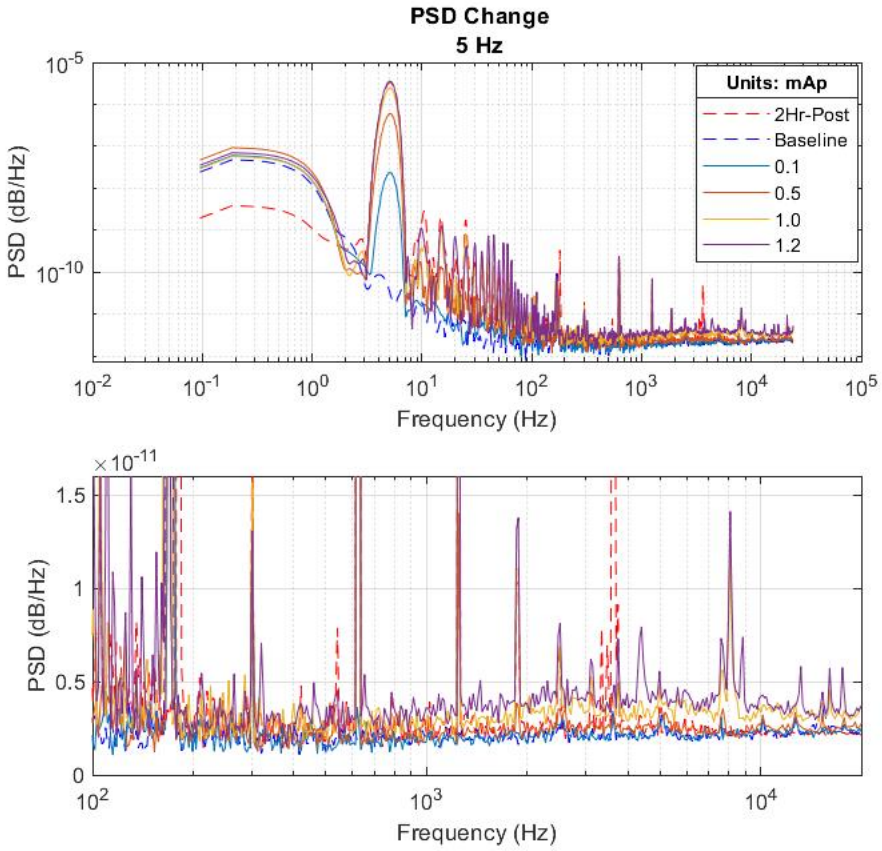

Figure. 2.9. The PSD results during the application of **5 Hz** LFAC waveform. Upper panel shows the full frequency range of the PSDs as the LFAC amplitude increases. The 2Hr-Post nerve PSD result was at 5 Hz, 1.2 mA_p with the absence of neural activity change. The lower panel shows a zoomed in version in semi-log x-axis scale

even at higher amplitudes as shown in figure 2.13. The 20 Hz activation of the 2Hr-Post nerve was able to generate very random activity as shown in figure 2.15. The averaging method reveled that common noise related to the LFAC, but the magnitude was very low comparing to the fresh nerve fibers. Even without applying any filter, the averaged ENG in figure 2.12 and 2.14, display the burst nerve modulation in correlation with the LFAC cycles. In addition, the rectification and averaging of the ENG show a conformation of the variance of nerve activity with respect to the LFAC cycles.

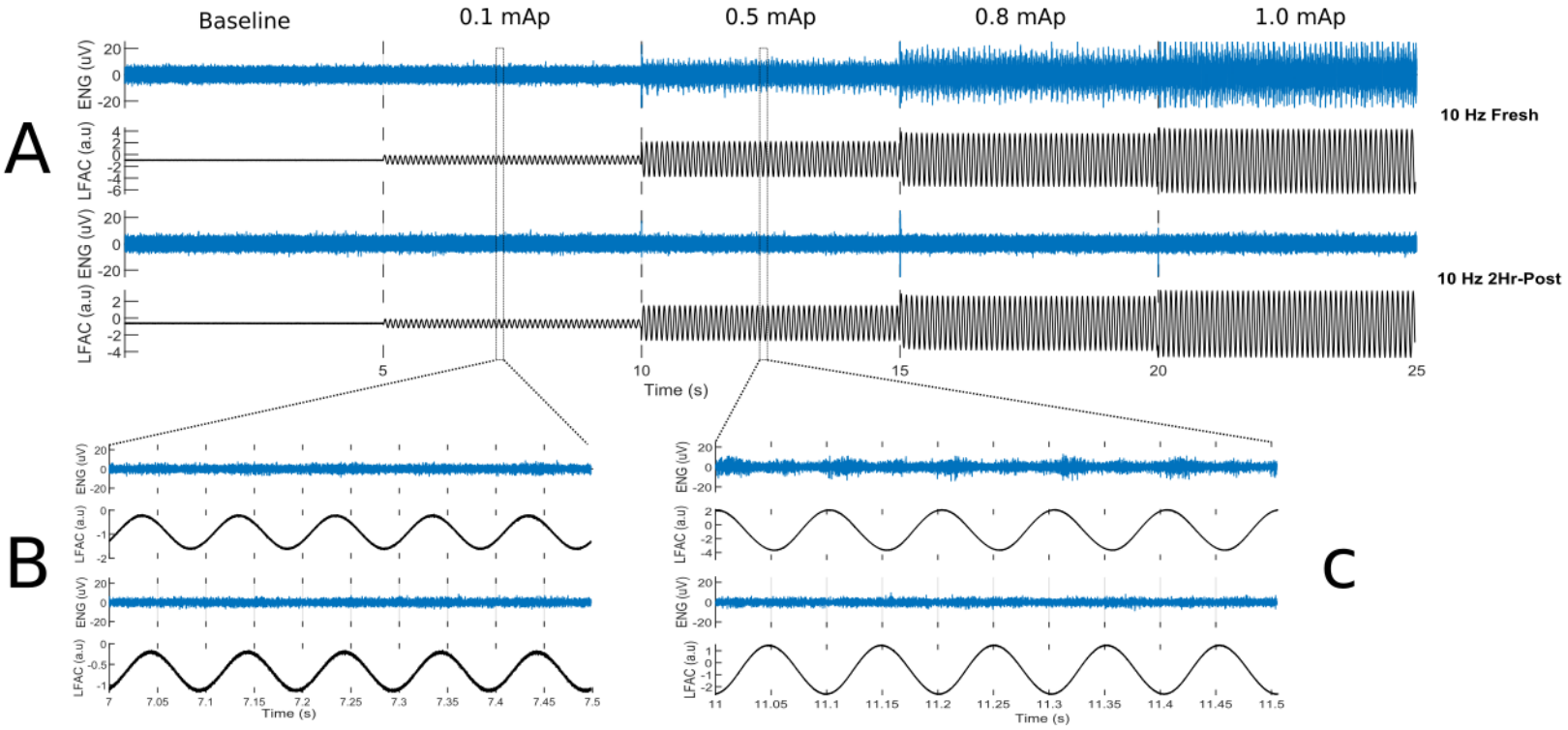

Figure. 2.10. A: continues recording of the ENG signal and the corresponding **10 Hz** LFAC waveform when the nerve tissue was fresh (top two traces of each panel) and 2Hr-Post (bottom two traces of each panel). B: a 0.5-second window when no activation was observed at **0.1 mA**$_p$. C: a 0.5-second window when the activation was observed at **0.5 mA**$_p$

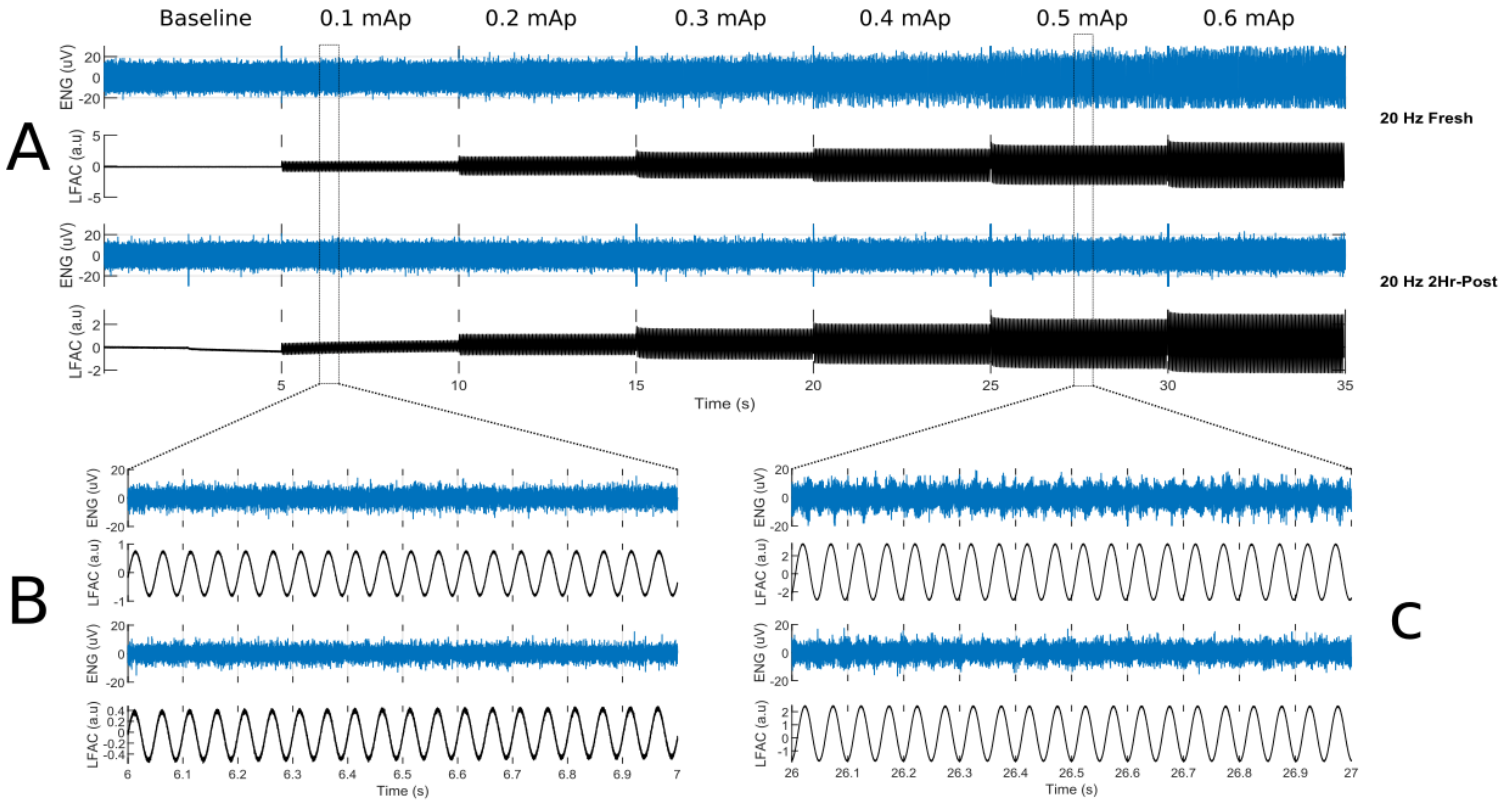

Figure. 2.11. A: continues recording of the ENG signal and the corresponding **20 Hz** LFAC waveform when the nerve tissue was fresh (top two traces of each panel) and 2Hr-Post (bottom two traces of each panel). B: one-second window when no activation was observed at $\mathbf{0.1\ mA}_p$. C: one-second window when the activation was observed at $\mathbf{0.5\ mA}_p$

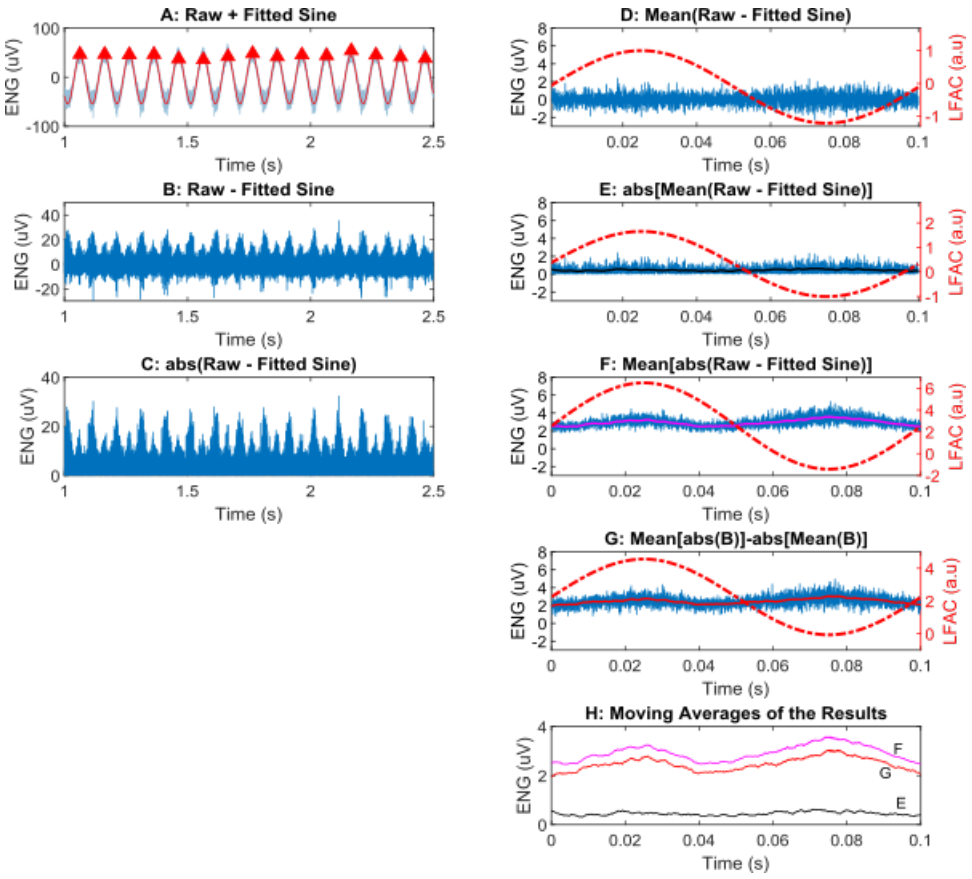

Figure. 2.12. The averaging algorithm results during LFAC activation of **a fresh** nerve (stage 1) at **10 Hz 0.5 mA**$_p$. Refer to figure 2.7 for description

The PSD analysis of the ENG while applying 10 Hz LFAC waveform followed the same trend as the 5 Hz LFAC analysis. However, the frequency components of the induced nerve activity, during stage 1, started to shift to the lower bandwidth between 100 Hz and 10 kHz as shown in figure 2.16. The deviation of the PSD with respect to the applied LFAC amplitude is clearly shown in the lower panel of figure 2.16, which follows the larger peak that corresponds to the 10 Hz LFAC. The baseline and 2Hr-Post nerve ENGs displayed no change over the frequency band from 100 Hz to 10 kHz in comparison with stage 1 results.

On the other hand, the 20 Hz LFAC activation showed a deviation in the ENG during stage 1 and stage 2, as the PSD shows in figure 2.17 and 2.18. The variation in

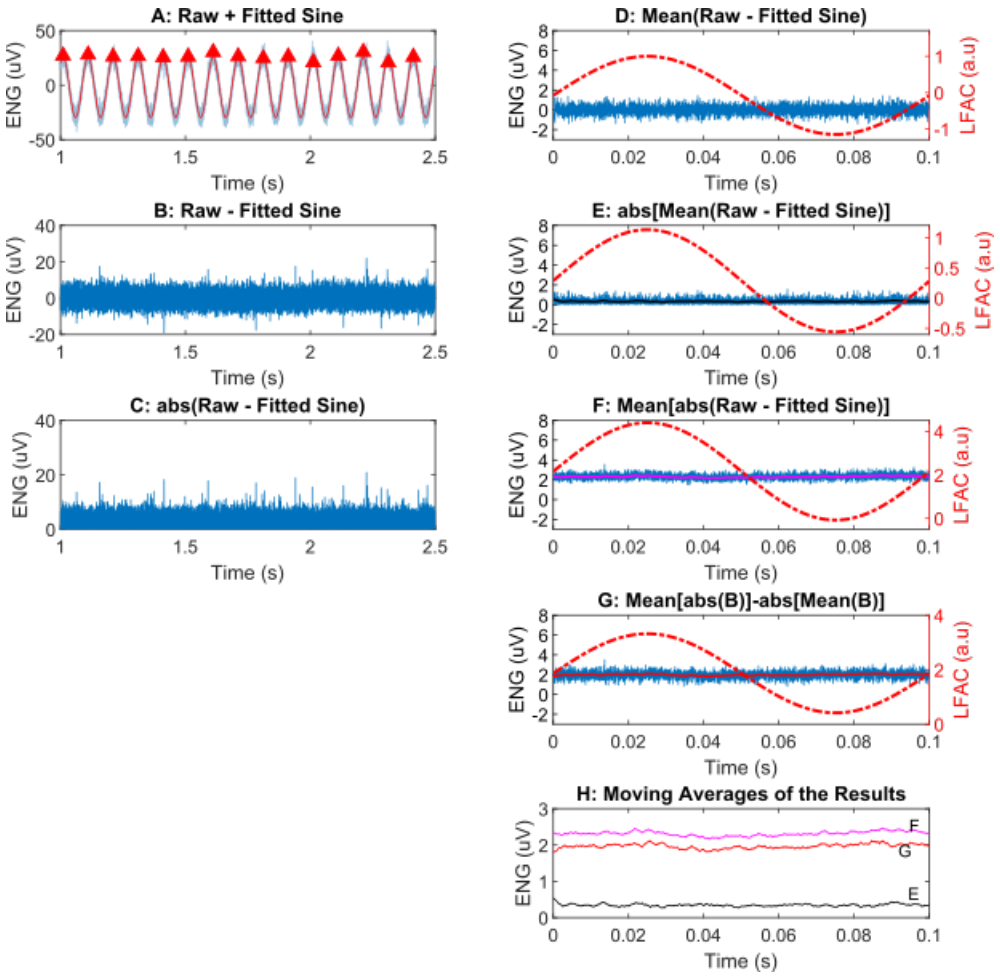

Figure. 2.13. The averaging algorithm results during LFAC activation of **a 2Hr-Post** nerve (stage 2) at **10 Hz 0.5 mA**$_p$. Refer to figure 2.7 for description

the PSD appeared in a form of wider peak over the bandwidth from 100 Hz to 1 kHz. During stage 1, as shown in figure 2.17, the ENG deflections corresponding to the nerve activity have shifted more to the lower frequencies band and the PSD magnitude changed as the LFAC amplitude increases. During stage 2, as shown in figure 2.18, the deviation in the nerve activity PSD is presented at the same bandwidth, which could be corresponding to the irregular nerve modulation.

From these findings of the nerve modulation induced by the LFAC, the minimum threshold was characterized by frequency dependence. Figure 2.19 shows the mini-

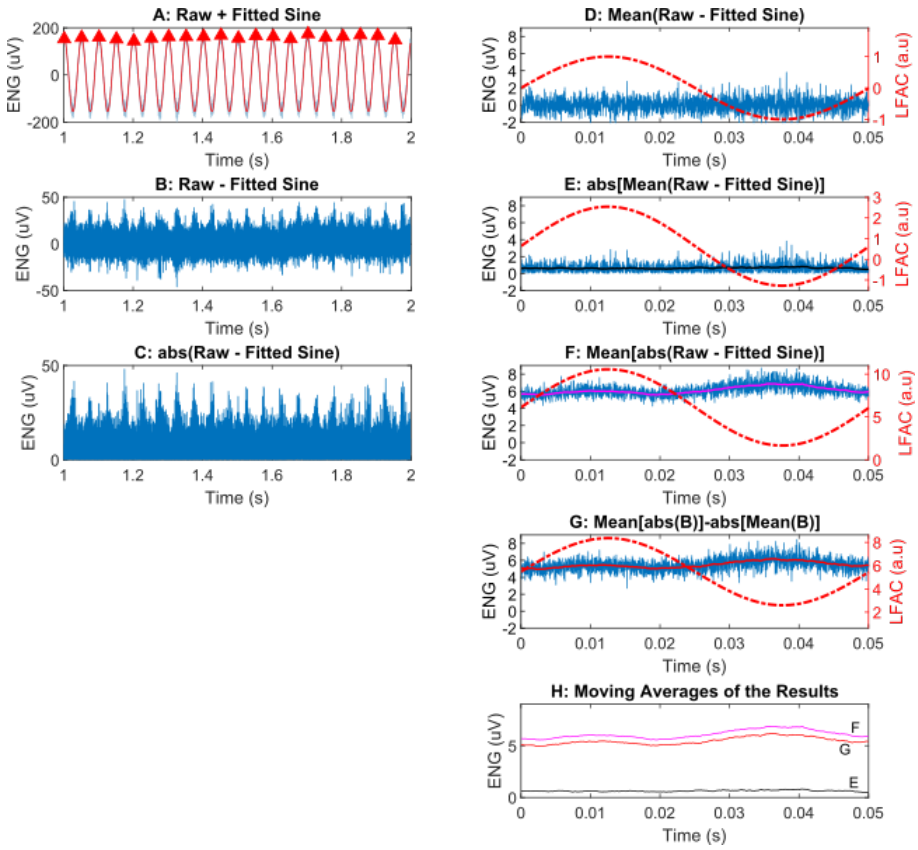

Figure. 2.14. The averaging algorithm results during LFAC activation of **a fresh** nerve (stage 1) at **20 Hz 0.3 mA**$_p$. Refer to figure 2.7 for description

mum threshold for LFAC waveform amplitude as a function of frequency for each of the experiments. At 5 Hz, the nerve activity modulation started to appear on the ENG with an amplitude of 1.2 $\pm$ 0.15 mA$_p$. On the other hand, applying 10 and 20 Hz LFAC waveform required lower amplitudes to evoke the burst modulation. The clear nerve modulation on the ENG started at an amplitude of 0.5 $\pm$ 0.06 mA$_p$ for 10 Hz and 0.3 $\pm$ 0.06 mA$_p$ for 20 Hz. These thresholds results suggest that the higher applied LFAC frequency, the lower amplitude required to cause the activation.

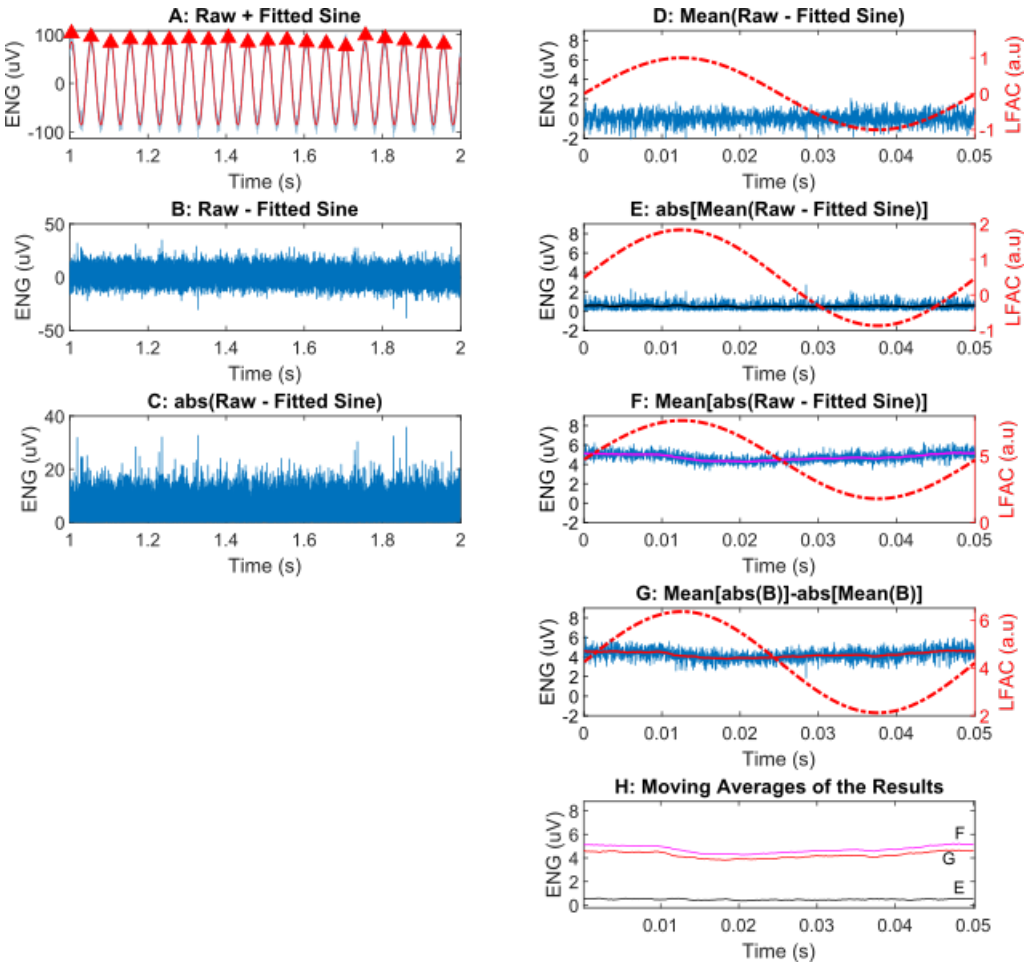

Figure. 2.15. The averaging algorithm results during LFAC activation of **a 2Hr-Post** nerve (stage 2) at **20 Hz 0.3 mA**$_p$. Refer to figure 2.7 for description

2.4 Discussion

The aim of this study was to determine if LFAC could elicit detectable activity in excised peripheral nerve. The analysis of the results revealed the feasibility of the LFAC waveform to evoke the nerve fibers to activate; however, the behavior of this activation was different than the standard pulse activation. As the results show that LFAC applied at 5, 10, and 20 Hz resulted in the appearance of burst nerve activity modulation within the ENG recordings during stage 1. The comparison between stage 1 and stage 2 suggests that the nerve burst modulation was due to the nerve

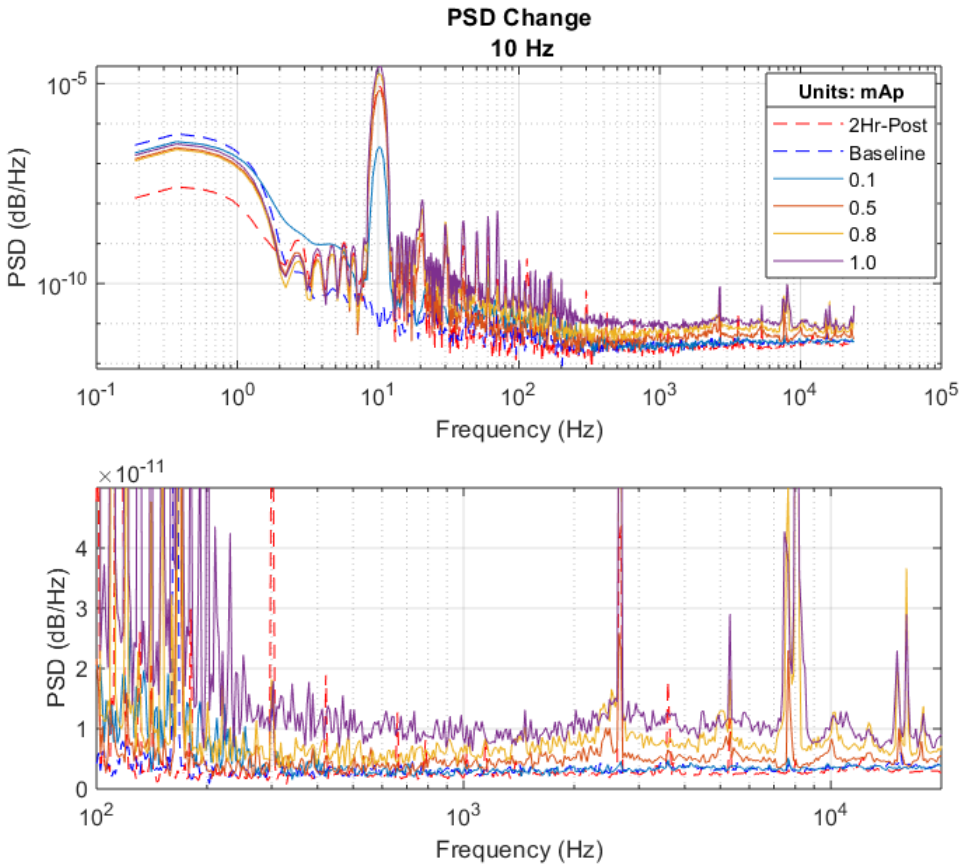

Figure. 2.16. PSD analysis during **10 Hz** LFAC Activation. Upper panel shows the full frequency range the LFAC amplitude increases. The 2Hr-Post nerve result at 1.0 mA_p with the absence of neural activity change. The lower panel shows a zoomed in version in semi-log x-axis scale

activity during stage 1. Furthermore, when comparing the baseline recordings with each stage's results, there was no observed burst modulation, indicating that the modulation of the ENG signal was not due to a random noise from the surrounding devices.

The LFAC amplitude thresholds required to activate the nerve fibers were observed to follow a decreasing trend as the applied LFAC frequency increased. By normalizing the LFAC activation thresholds with the 5 Hz values, the nerve activity modulation using 10 and 20 Hz required ∼50% and ∼25% of amplitude respectively.

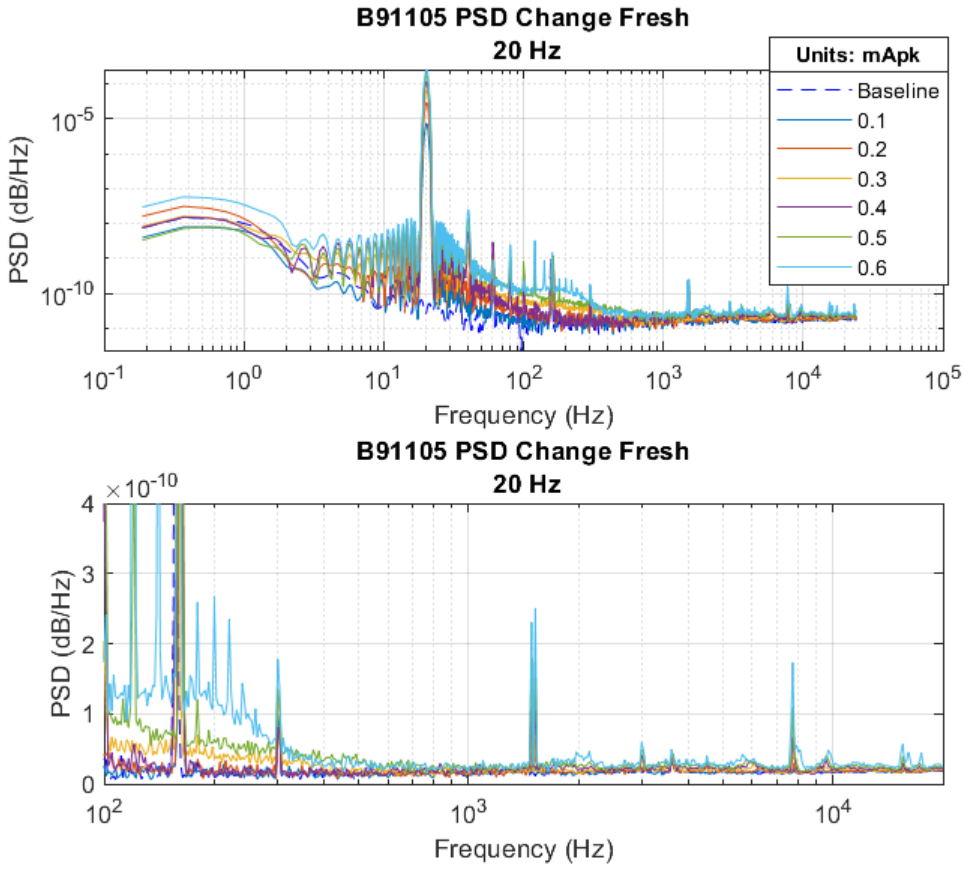

Figure. 2.17. PSD results when applying **20 Hz** LFAC waveform to the **fresh** nerve. Upper panel shows the full frequency range as the LFAC amplitude increased. The lower panel shows a zoomed in view in a semi-log x-axis scale

This behavior suggests a direct dependency of the activation threshold and the applied LFAC frequency. The minimum amplitude determined to cause nerve activation was based on the burst modulation appearances, which is in agreement with the frequency domain analysis and a function of the applied LFAC frequency.

The averaging algorithm revealed that the LFAC activation was random and asynchronous to the stimulus. This is a significant difference between the standard pulse activation and LFAC activation. The CAP was not observed during LFAC activation due to the randomized depolarization of the membrane potential during LFAC

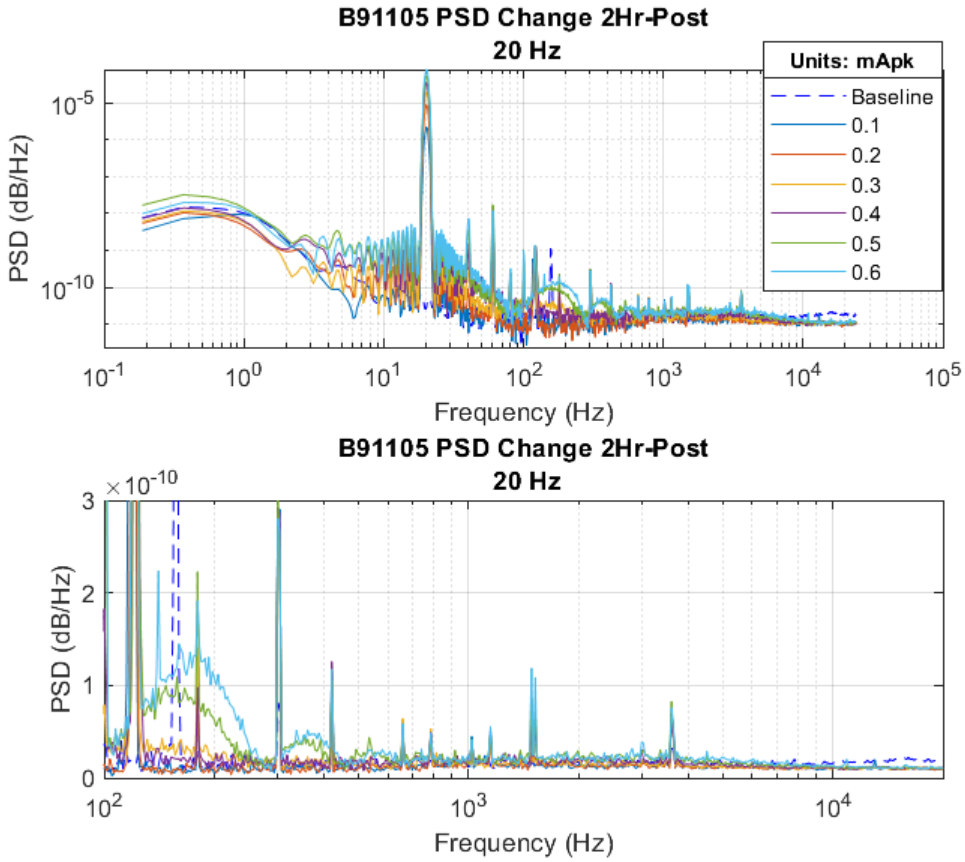

Figure. 2.18. PSD results when applying **20 Hz** LFAC waveform to the **2Hr-Post** nerve. Upper panel shows the full frequency range as the LFAC amplitude increased. The lower panel shows a zoomed in view in a semi-log x-axis scale

activation. By averaging the raw ENG signal in one period window there was no reliable spike detected that could be the CAP due to the spontaneous activity with a zero-mean. As the results show, the burst modulation was significantly reduced in magnitude after averaging, suggesting that the activity evoked by LFAC to be asynchronous to the stimulus and produced in random locations over a single cycle of LFAC. Moreover, closer interpretation of the averaging algorithm results revealed that the overall activity was in phase with the LFAC waveform cycles suggesting the relevantly of the waveform cycle peaks to induce the activation. Averaging the recti-

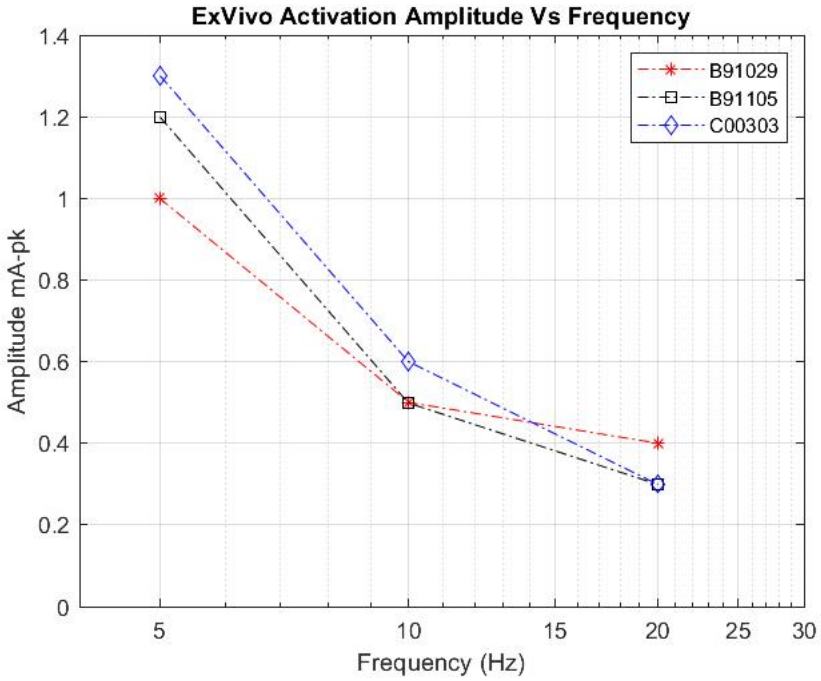

Figure. 2.19. The minimum LFAC amplitude resulted in activation from each experiment as a function of the applied LFAC frequency. The legend refers to the experiments' dates

fication revealed where the overall energy are most likely to occur. Each LFAC cycle produced two burst modulations that are related to the depolarization phase of the LFAC waveform. As the sinusoidal waveform switches polarity between the bipolar electrodes, the cathode depolarizes the membrane driving the activation and as that switches, it resulted in another activation in the other electrode.

The PSD analysis shows a degree of deviation in the ENG signal over the frequency range when applying LFAC with 5, 10, and 20 Hz frequencies at several amplitudes. These findings strongly suggest the presence of the neural activity during stage 1. The neural signal is commonly found in the detail band from 187.5 Hz to 12 kHz [59], but that is subject to several effects due to electrodes types and recording techniques. In this study, it was predicated that the nerve activity would appear around or within that band and therefore, the deviation in the PSD modulation is more likely to be related to the nerve activity induced by the LFAC. In comparison to the single

unit action potential recording using pulse stimulation and intrafascular recording in [59, 60], the PSD level of the nerve activity induced by the LFAC is found to be lower than the normal activity. The results suggest that the population of nerve fibers being activated using LFAC might be less than the pulse stimulation resulting in a lower PSD level. The deviation on the PSD with respect to the LFAC amplitude also suggest that applying higher LFAC amplitude might elect more nerve fibers that could be selectively activated. From the PSD analysis, the noise level induced by the LFAC waveform was cleary larger than the neural activity. In theory, the neural activity is in the scale of microVolt while the applied LFAC amplitude is the in scale of Volt. This is a major issue that limits the PSD analysis to observe a clear deviation in magnitude.

The irregular burst modulation of the 20 Hz LFAC during stage 2 and its corresponding PSD results indicates that the nerve fibers were not completely stopped after 2 hours of extraction. Since the vagus nerve bundle has large population of small C fibers, those types of nerve fibers might last longer in such *ex-vive* environment. As the results suggest, the LFAC activation recruitment order of the nerve fibers might have a frequency-type dependency, which would allow for a selective activation of specific types of the nerve fibers. Since there is no indication of the conduction velocity, nor a triggered CAP, the LFAC activation appear to be more natural in term of the burst modulation. Nevertheless, the PSD shows a variation not only on the PSD level but also on frequency band of the neural activity.

In summary, we explored methods to observe the nerve activity induced by LFAC and the challenges were the loss of nerve activity synchrony to the stimuli and the high level of noise. Activating the autonomic peripheral nerve fibers using 5, 10 and 20 Hz LFAC waveform indicates the suitability of using LFAC waveform to activate peripheral nerve fibers. Additionally, the LFAC activation amplitude was within the water window, which did not cause any irreversible reaction nor damage neither to the electrodes nor the nerve tissue. As the results revealed, the LFAC activation is found to be random and asynchronous to a single point of activation which is

an interesting behavior unlike the historical pulse activation. Moreover, the LFAC activation amplitude is found to be frequency dependent and might be fiber type-size dependent as well. The fiber recruitment order would play a significant role in investigating the selectivity of LFAC activation, which could be a possible aim to explore in future work. Based on the preliminary work done on the rabbit and these results, it is suggested to take the validation study to living animal models – different nerve fibers - to explore the practicability of LFAC activation and to characterize the LFAC activation behavior.

3. APPLICATION OF LFAC ACTIVATION IN-VIVO

Nerve activity could be elicited by applying LFAC to excised peripheral nerve. Chapter 2 suggests that LFACa activates nerve fibers asynchronously to the stimuli and produces two bursts of activity that are correlated to LFAC cycle peaks. Those prior studies suggest different methods to measure the nerve activity induced by LFAC. However, it is not clear if the LFAC generated nerve activity is sufficient to signal and elicit a functional change to the nervous system. In order to determine whether LFAC generated nerve activity can elicit functional changes experiments were conducted and designed to determine whether biomarker function can be modulated using LFAC stimulation. In this chapter, a closer examination of the LFAC activation phenomenon is performed on larger nerve fibers in swine models and smaller bundles on rat models, where the reflexes mediated by autonomic and somatic nerve fibers are analyzed with respect to the LFAC waveform.

3.1 Introduction

The electrical activation of the peripheral nerve fibers provides a substantial understanding of the electrophysiological characteristic of the nerve tissue and its activity. In neuromodulation, interfering with the neural signals is achieved through either enhancing or blocking the nerve activity. The historical use of the standard pulse activation has provided adequate means to induce nerve activity in the intra and extracellular level of nerve stimulation. However, the improvement of selective activation is slowly emerging in the field and would have a significant role in the treatment of nerve injuries and neuroprosthetics design.

The recent work of the LFAC block introduces the possibility of LFAC activation and the preliminary experiment suggested the feasibility of the method in inducing the

peripheral nerve activity. As discussed in chapter 2, applying 5, 10, and 20 Hz LFAC waveform could have elicited nerve activity in the excised cervical vagus nerves. Those results revealed the LFAC activation to be a frequency dependent, which require further investigation to characterize the LFAC activation and verify that dependency. In this chapter, two animal models (swine and rats) were used to investigate the feasibility of LFAC activation to induce biological reflexes that highlight the fiber dependency and the activation mechanism between somatic and autonomic nerve fibers. The Hering-Breuer reflex, Hoffmann reflex and muscle response were investigated in these experiments to provide an experimental observation, within living models, of the possibility of activating different nerve fiber using LFAC.

3.1.1 Hering–Breuer Reflex

The studies of the body reflexes in response to an electrical stimulus is an approach to assess the effectiveness of the electrical stimulation in an experimental setup. The Hering-Breuer reflex (HB) is one of the reflexes mediated by the vagus nerve fibers and its branches. Upon the activation of the sensory and/or motor fibers of the vagus nerve, the breathing rate changes in response to the activity of pulmonary stretch receptors resided in the lung. This reflex naturally occurs with a communication between the CNS and the respiratory center to maintain a normal inspiratory and expiratory mechanism and prevent lung inflation [61–63].

When electrically stimulating the vagus nerve to induce the HB reflex, the breathing rate decreases as a result of alternating the nerve activity carried by the vagus nerve afferent fibers from CNS. However, if the stimulation activates the efferent motor fibers, then the cardiac effects are most likely to elect bradycardia [43]. During HB reflex, the electrical stimulation evokes the nerve activity of myelinated A and B fast fibers and possibly the unmyelinated small C fibers [61, 63].

3.1.2 Hoffmann Reflex and Muscle Response

The PNS electrical stimulation is commonly used to investigate the skeletal muscles contraction strength and as a methodology to assess the functionally of motor neurons. The electrophysiological properties of the skeletal muscle's activation coordinates with PNS through the neuromuscular junction; which have a critical mechanism in transmitting nerve signals into muscle contraction that can be found in [64]. The motor neurons carry information from the CNS to cause muscle contraction, which can be modulated via electrical stimulation to enhance or block those activities. In particular, the Hoffmann reflex is one of the reflexes that can be modulated by electrical stimulation of a somatic nerve bundle to cause muscle contraction. The Hoffmann reflex's pathway starts once the action potential is fired via afferent neurons propagating toward the spinal cord. If the action potential is strong to cause a reflex, the motor neurons propagate AP downward from the spinal cord to the target muscle inducing muscle contraction [65]. However, this reflex has a limited response's strength, which is directly related to the stimuli strength. Once the stimuli strength reaches the motor efferent threshold, the muscle contraction is due to the direct stimulation of the motor neurons known as the muscle response [65].

The electrical pulse stimulation of a somatic nerve bundle to target muscle contraction is interestingly involving different nerve types and size. The recruitment order of the fibers to cause the Hoffmann reflex and muscle responses are found to activate large nerve fibers first (alpha motor fibers) with lower stimuli intensity [65]. After a certain range of stimuli strength, the action potentials propagating through the alpha motor neurons collide resulting in a block of the Hoffmann reflex [65]. However, the muscle response, which is more likely caused by the activation of small motor nerve fibers, reaches a maximum level of contraction that maintains a constant amplitude in the electromyogram (EMG) [65].

3.2 Swine Experiments Methods

3.2.1 Animal Preparation and Euthanasia

All animal uses were done under an approved Laboratory Animal Resource Center and Institutional Animal Care and Use Committee (LARC IACUC) protocol at Indiana University Purdue – University Indianapolis (IUPUI). The first portion of this *in-vivo* validation study was performed on male domestic swine (n=5). The surgeries were conducted following the sedation of the animals using the appropriate dose of sedation drugs (Telazol 100 mg/ml, ketamine 50 mg/ml, xylazine 50 mg/ml) based on each animal's weight. To maintain the animals under anesthesia, vaporized isoflurane anesthesia was administered via endotracheal or tracheostomy intubation. An incision was made to isolate the left vagus nerve in the neck from the surrounding tissues and veins. The environment around the nerve and the electrodes were kept moist by placing parafilm under the nerve and adding sterile saline as needed.

Additionally, another femoral incision was made for an invasive blood pressure monitoring. The intubation was inserted into the femoral artery, secured with sutures, and flushed with sterile saline as needed. Also, three surface electrodes were places on the limbs of the animal for a single lead electrocardiogram (ECG) monitoring though the experiments. Furthermore, an IR SpO_2 sensor was clipped to the animal's ear to monitor the oxygen level during the experiments. Also, about one-meter fabric blood pressure cuff was wrapped around the animal chest to transduce the breathing rate as the chest rises. At the end of the experiments, the animals were euthanized under deep anesthesia via the application of 9.0 Volt battery to the heart, which induces heart fibrillation resulting in the death of the animal.

3.2.2 Experimental Setup and Electrode Configuration

Following the surgical isolation of the vagus nerve, three bipolar cuff electrodes were placed on the nerve as shown in figure 3.1. The LFAC activation waveform

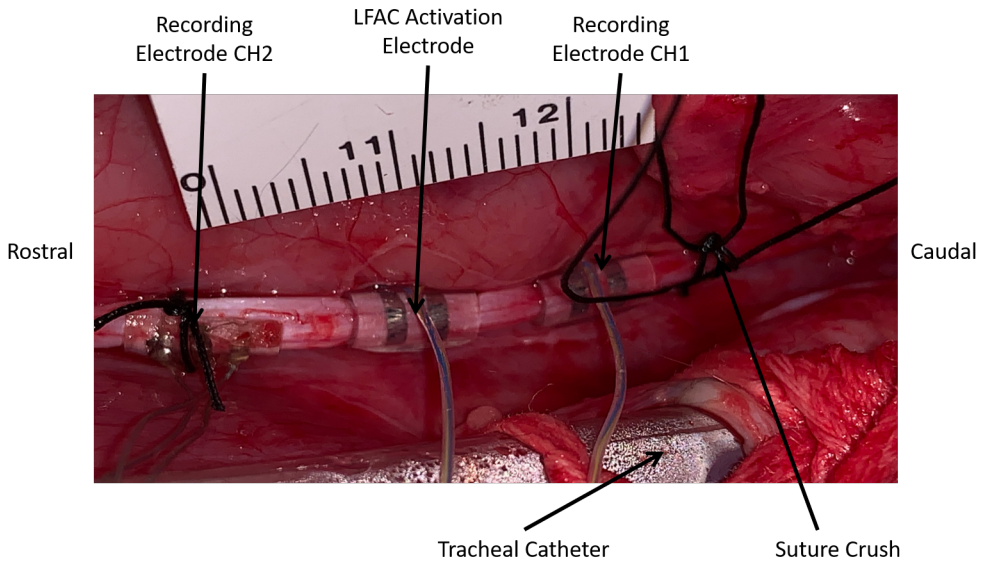

Figure. 3.1. The electrode setup of one of the swine experiments. The middle electrode was used to apply the LFAC waveform, and the side electrodes were used to record the ENG signals. The suture crush was performed to prevent the cardiac response during the LFAC simulation

was applied though the middle electrode (2.0 mm inner diameter, CorTec cuff). The ENG recording electrode CH1 was also a 2.0 mm CorTec cuff, and the ENG recording electrode CH2 was a custom-made cuff electrode with platinum contacts, 2-3 mm inner diameter. The LFAC waveform was generated and tuned using the Analog Discovery 2 (Digilent, USA) waveform generator, which was controlled by a tuning application written in LabVIEW® (K. Yoshida, 2019). In only one experiment, the function generator (DG5072, Rigol) was used to apply higher LFAC frequencies. The signal was then aided through an isolated voltage controlled current source (CS580, SRS: Stanford Research Systems) before connecting to the tissue with a constant gain of 1 mA per Volt-peak. Both channels of the ENG were passed through a differential amplifier with an exchangeable gain between 100x-5kx, and high pass filter at 300 Hz (CyberAmp 320, Axon Instruments).

3.2.3 LFAC Activation Protocol

The LFAC stimulation protocol was conducted in all swine experiments with a minimum amplitude as low as possible to prevent any damage to the nerve tissue or the electrode and maintain the potential to be within the water window. The LFAC waveform was applied using three different frequencies: 5, 10, and 20 Hz. Each frequency was applied with a gradual increasing of the amplitude until the HB reflex was observed. In one experiment, the LFAC frequency was increased to 100 and 500 Hz. The breathing rate was observed to change as a biomarker of the HB reflex. Between each increment of the LFAC amplitudes, a zero amplitude LFAC was applied for few seconds to allow the animal to recover after the episode of non-breathing. Once the HB reflex was observed with a complete non-breathing case, the amplitude of LFAC was reduced gradually until the normal breathing was resumed. This allowed to identify the minimum LFAC amplitudes as a function of frequency.

3.2.4 Data Acquisition and Signal Processing

The LFAC waveform, both channels of ENG signals, and the breathing rate change were recorded digitally at a sampling rate of 48 kHz using F8 MultiTrack Field Recorder (ZOOM corporation, Tokyo, Japan). Since the LFAC waveform and the breathing signal were less than 100 Hz, those signals were frequency modulated with a carrier frequency of 5.55 kHz before recording using Vetter FM recording adapter (A.R. Vetter Co., Rebersburg, Pa).

Breathing Rate Analysis (HB Reflex)

The recorded breathing signals were processed digitally using a custom MATLAB script (Version: R2018b, The MathWorks). The analysis was performed with respect to the applied LFAC frequency and amplitude to calculate the change of the breathing

rate in time per minuets. This allowed for a clear comparison in determining the activation threshold with respect to the LFAC amplitude and frequency.

Table 3.1.
The theoretical bandwidths (Hz) of the ten-level decomposition used with in SWT analysis with respect to the sampling rate of 48 kHz

	Bandwidth (Hz)
D1	12000-24000
D2	6000-12000
D3	3000-6000
D4	1500-3000
D5	750-1500
D6	375-750
D7	187.5-375
D8	93.75-187.5
D9	46.875-93.75
D10	23.4375-46.875
A10	0-23.4375

Stationary Wavelet Transform (SWT) and Averaging

The recorded ENG signals were interfered by a large hormonic line noise coupled with the LFAC waveform. The continuous recordings of the ENG signal were segmented based on the applied LFAC frequency and amplitude. Due to the higher degree of the noise and its correlation with the ENG signal, a stationary wavelet transform of the ENG signal was performed using the Neuralyzer (V1.0, S. Qiao and T. Lian, Bioelectronics Lab, IUPUI, 2013). The Neuralyzer performs a ten-levels SWT decomposition of the signal and based on the mother wavelet, the subband-signals are reconstructed by the inverse Stationary Wavelet Transform (iSWT) with respect

to the frequency ranges shown in table 3.1 with respect to the used sampling rate of 48 kHz.

The Daubechies 10 mother wavelet was used in this analysis due to its best matching characteristic of identifying the signal components of the nerve activity if any was presented in the ENG raw signal [59]. Following the decomposition of ENG signal using the Neuralyzer, the change on the reconstructed ENG due to the nerve activity was averaged with respect to the applied LFAC cycle in order to observe how relevant the nerve activity and the LFAC waveform are. The reconstructed ENG signal was phased locked with the applied LFAC cycles, and averaged in one period window with respect to each applied frequency. Furthermore, the rectified version of the ENG recording was calculated to show the LFAC peaks influence on the ENG.

PSD and Fast Fourier Transform (FFT)

In order to observe the frequency components of the nerve activity buried in the ENG signal and the embedded noise, the PSD and the fast fourier transform were performed with respect to each applied LFAC frequency and amplitude. This frequency domain analysis characterizes the change in the spectrum of each buried signal within the ENG. This was done with respect to the applied LFAC frequency and amplitude in terms of signal power estimation and amplitude of their corresponding frequency content, which would clarify indicating the presents of any nerve activity.

3.3 Rat Experiments Methods

3.3.1 Animal Preparation and Euthanasia

All animal uses were done under an approved Science Animal Resource Center and Institutional Animal Care and Use Committee (SARC IACUC) protocol at Indiana University Purdue – University Indianapolis (IUPUI). The second portion of this *in-vivo* validation study was performed over male adult Sprague Dawley rats (n=4).

The animal was deeply anesthetized after placing it in a sealed induction chamber for 5-8 mins containing vaporized anesthetic Isoflurane. To maintain the animals under anesthesia, vaporized Isoflurane anesthesia was administrated via a mask covering the nose and mouth. Following the anesthesia, the animal was securely laid down on the prone position over a heating pad (infrared warming pad) to maintain the body temperature after shaving the hind limb. A rectal thermometer was used to monitor the core body temperature and a tail blood pressure (BP) cuff was placed around the tail to continuously monitor the BP (CODA monitor, Kent Scientific). Also, an IR SpO_2 oximeter (8500M, Nonin Medical, Inc, USA) was clipped onto the animal's front paw to monitor the oxygen level during the experiments and the heart rate.

Surgeries were conducted to expose the left sciatic nerve and its branches. A lateral or medial incision was made to access the sciatic nerve between sciatic notch and the popliteal fossa or between the knee joint and the ischial tuberosity. Following the superficial dissection of separating the muscle and connective tissue, the sciatic nerve and its branches were isolated under the microscope. During the dissection, ligature of blood vessels was performed to avoid extreme bleeding. After placing the electrodes on the nerve bundle, the incision was closed with sutures and staples, and filled with adequate amount of sterile saline.

Following the closure of the incision, the animal was moved to the experimental station, where the left leg was attached to a foot pedal, while still on the prone position, to measure the force. Additionally, in two experiments, a physical crush by clamping the nerve tissue proximal to the activating electrode was performed. This required reopening the incision and staple again. At the end of the experiments, the animal was euthanized under deep anesthesia via overdose of pentobarbital though intravenous injection.

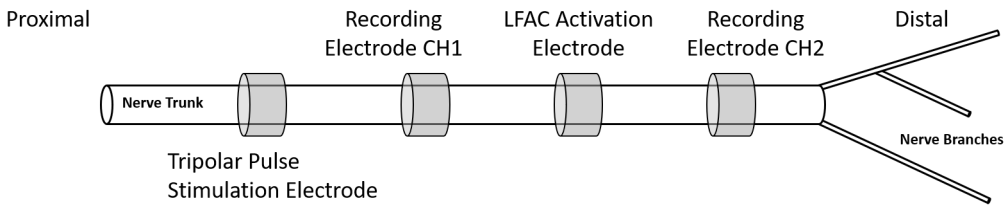

Figure. 3.2. A schematic illustration of the cuff electrode configuration relative to the sciatic nerve trunk and its branches

3.3.2 Experimental Setup and Electrode Configuration

Following the surgical isolation of the sciatic nerve, four custom-made cuff electrodes with platinum contacts, 0.5-0.65 mm inner radius were placed over the sciatic nerve trunk in the following order as shown in figure 3.2: tripolar pulse stimulation electrode was placed most proximal followed by a bipolar recording electrode CH1 to record the ENG. Following that, the LFAC activation electrode and CH2 recording electrode were cascaded, which also were bipolar cuffs. In some experiments, the recording electrode CH2 was placed on one of the nerve branches due to the limited area of the isolated nerve trunk. The EMG recording was performed using stainless steel wires placed within the gluteus maximus muscles. The left foot of the animal was securely attached to the lever arm of the lever system (300C, Aurora Scientific, Aurora, ON, Canada) in order to measure the force induced by the foot movement.

The LFAC waveform was generated and tuned using the Analog Discovery 2 (Digilent, USA) waveform generator, controlled by a tuning application written in LabVIEW® (K. Yoshida, 2019). The signal was then aided through a custom-made isolated voltage controlled current source with a constant gain of 1 mA per 1 Volt-peak. In some experiments, the mode of activation was changed from a current mode to a voltage mode due to few offset issues, but the LFAC current was maintained to be within the water window. Both channels of the ENG were passed through a differential amplifier with an exchangeable gain of 100x-5kx and high pass filter at 300

Hz (CyberAmp 320, Axon Instruments). The EMG signal was amplified with 1000x gain using a custom-made Biopotential amplifier (Aalborg University, K. Yoshida).

3.3.3 LFAC Activation Protocols

The LFAC waveform was applied using four different frequencies:1, 5, 10, and 20 Hz. Each frequency was applied with a gradual increasing of the amplitude until the muscle twitches were observed. The main frame of the protocol was similar to the swine experiment, but the reflex of interest was the observation of the muscle contraction as a sign of either the Hoffmann reflex or the muscle response. The activation of the somatic nerve was expected to induce force change in form of muscle contraction seen by continuous twitching. Furthermore, to examine the nerve fibers dependency of the LFAC activation in two rat experiments, the nerve trunks were crushed proximally, and the LFAC activation protocol was repeated with the same frequencies. Moreover, to compare the LFAC activation's effect on the muscle responses, the standard pulse activation was performed for further exploration at the end of the experiments with a pulse duration of 40-50 μsecond and pulse amplitude of 0.45-0.5 mA (DS3 Isolated Current Stimulator, Digitimer, UK) at a stimulation frequency of one pulse per second (1 Hz).

3.3.4 Data Acquisition and Signal Processing

The LFAC waveform, both channels of ENG, force, and EMG signals were recorded digitally at a sampling rate of 48 kHz using F8 MultiTrack Field Recorder (ZOOM corporation, Tokyo, Japan). Since the LFAC waveform and the force signal were in the range less than 100 Hz, those signals were frequency modulated with a carrier frequency of 5.55 kHz before recording using Vetter FM recording adapter (A.R. Vetter Co., Rebersburg, Pa). All the signals were processed digitally in a custom MATLAB script (Version: R2018b, The MathWorks).

Force and EMG (H-reflex)

The analysis of the EMG and the induced force was performed with respect to the applied LFAC frequency and amplitude. The EMG signal was zero-mean, rectified, and digitally filtered with a 4^{th} order bandpass filter (Butterworth, high pass at 50 Hz and low pass at 1 kHz). The force signal was also filtered with a 3^{rd} order low pass filter (Butterworth at 100 Hz). The EMG and force were plotted with respect to the applied LFAC frequency and amplitude that allowed for determining the activation threshold as function of the LFAC parameters along with the ENG modulation.

ENG Filtering and PSD

The ENG signal was zero-mean and digitally filter with a Butterworth 6^{th} order bandpass filter between 300 and 6 kHz. The filter was capable of eliminating the underlying noise and the LFAC waveform from the raw ENG. In order to observe the frequency components of the embedded noise and neural activity buried in the ENG signal, the PSD was estimated with respect to each applied LFAC frequency and amplitude. The frequency domain analysis characterizes the change in the spectrum of each buried signal with respect to the applied LFAC frequency and amplitude which clarify identifying the neural signal from the muscle activity.

Crushed Vs. Uncrushed Nerve Activation

The LFAC activation mechanism is hypothesized to have fiber type and size dependency. The activation of the somatic nerve fibers also mediates H-reflex. Thus, by crushing the afferent fibers projecting to the spinal cord, the LFAC activation was explored in the same analysis settings to provide preliminary observations of its ability to activate the motor fibers and ensure the muscle twitches was due to the LFAC activation not the H-reflex. This analysis was an attempt to investigate the

LFAC activation fiber type dependency (afferent versus efferent), if any, as a function of frequency.

3.4 Results of Swine Experiments

The breathing rate analysis showed a clear activation of the vagus nerve fibers that was able to evoke HB reflex. The results in figures 3.3, 3.4, and 3.5 show representative continuous recordings of the breathing change during the application of 5, 10, and 20 Hz LFAC waveforms respectively. The lower traces of each of those figures show the calculated breathing rate per minutes based of the time intervals between each adjacent peak. As the 5Hz LFAC waveform (figure 3.3) amplitude increases, the breathing rate decreases further until reaching a point of non-breathing at an amplitude of 1.5 mA_p. The recovery time between each LFAC increment was observed to resume the normal breathing as shown in the calculated breathing rate. As expected, the HB-reflex resulted in a larger time interval between the breathings, and further increments of LFAC amplitude resulted in a non-breathing situation. Similarly, the application of 10 (figure 3.4) and 20 Hz (figure 3.5) LFAC waveforms induced the HB-reflex as a result of activating the vagus nerve fibers; however, the LFAC amplitude threshold required to induce the HB-reflex was much less than the 5 Hz.

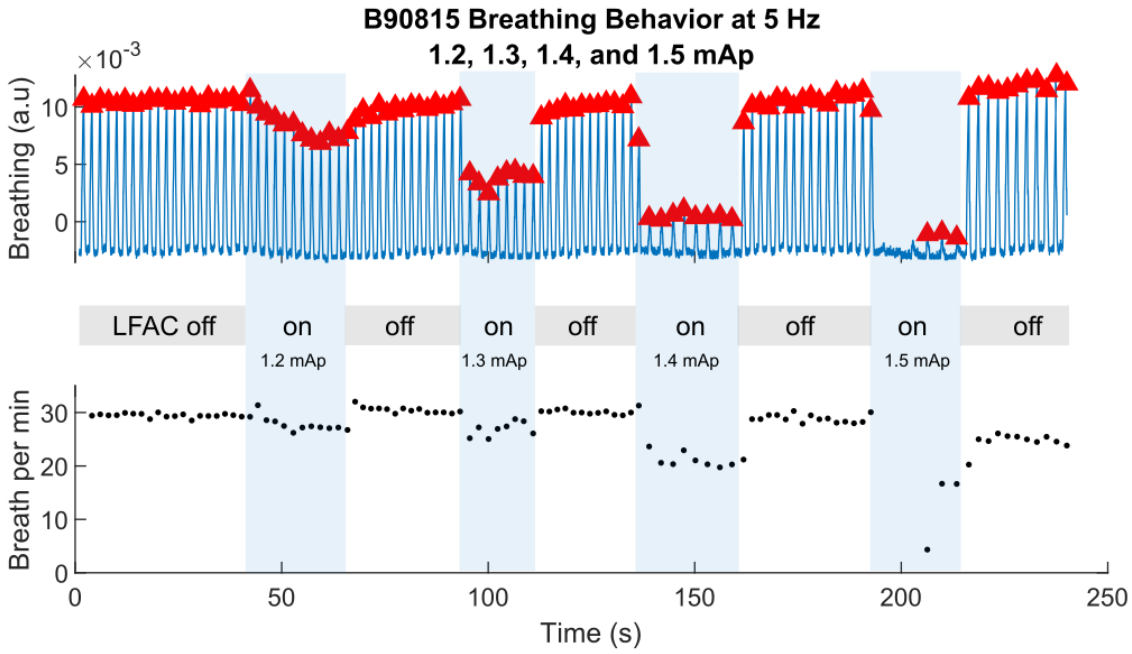

Figure. 3.3. Breathing behavior during **5 Hz** LFAC activation with **1.2, 1.3, 1.4, and 1.5 mA**$_p$ in the swine experiment. Upper panel shows the raw breathing peaks used in calculating the breathing rate. Lower panel shows the breathing rate change as the LFAC amplitude changes in breath per min. The breathing unit is arbitrary

The SWT analysis revealed the nerve activity change in a higher frequency band due to the high level of in-band noise interfering with ENG signals. Only two experiments had valid ENG recordings, the others were either clipped due to a high gain of amplification (n=2), or not recorded (n=1). The burst modulation on the ENG appeared in the frequency band between 12k to 24 kHz, which is assumed to be a possible nerve activity induced by the LFAC. Figure 3.6 shows the subbands-reconstructed signals produced by the Neurlyzer during the application of 0.4 mA$_p$, 5 Hz LFAC waveform. The decomposition of the raw signal into 10 levels allowed to graphically observe the burst modulation, applied LFAC waveform, and different type of noise signals that were embedded within the ENG signal.

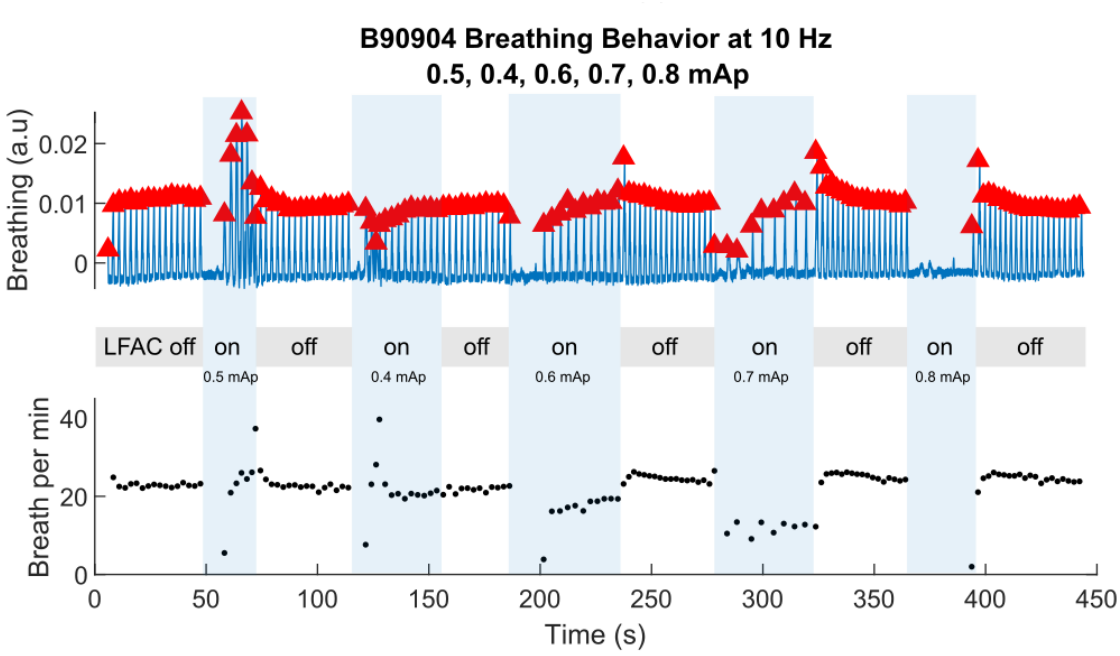

Figure. 3.4. Breathing behavior during **10 Hz** LFAC activation with **0.4, 0.5, 0.6, 0.7, and 0.8 mA**$_p$ in a swine experiment. Refer to Figure 3.3 for description

To verify that the burst modulation in D1 could be the neural activity, the lower 5 Hz LFAC amplitude at 0.1 mA$_p$ did not show the burst modulation as shown in figure 3.7. Additionally, the reconstructed subband signal from the SWT analysis was traced and phased locked with LFAC waveform and averaged against one period. The results shown in figure 3.8 reveled that the modulation is related to the LFAC cycles peaks, which is in agreement with previous findings from the *ex-vive* experiment. The rectified and averaged signal also suggest that the bust modulation was due to the nerve activation via LFAC. The SWT analysis of the non-activating amplitudes of the LFAC showed no change in the D1 reconstructed signals implying that the burst modulation was due to the nerve fibers activity. Since the signal was decomposed, the magnitude of the signal was very low and the phase of the burst modulation was shifted.

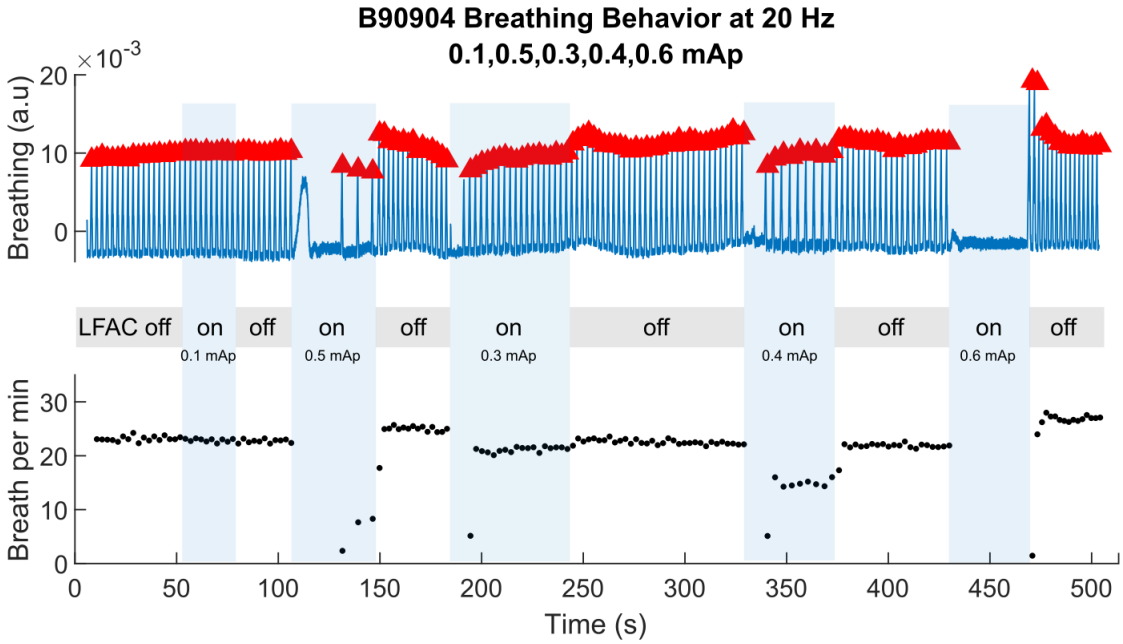

Figure. 3.5. Breathing behavior during **20 Hz** LFAC activation with **0.1, 0.3, 0.4, 0.5, and 0.6 mA**$_p$ in a swine experiment. Refer to Figure 3.3 for description

On the other hand, the application of 1.0 mA$_p$ 10 Hz LFAC and 0.6 mA$_p$ 20 Hz LFAC showed microlevel changes on the reconstructed ENG signals as shown in D1 of figures 3.9 and 3.10. By averaging those reconstructed signals, the results did not reveal any burst modulation as shown in figure 3.11 panel A and B. With the fact that applying 1.0 mA$_p$ 10 Hz and 0.6 mA$_p$ 20 Hz LFAC induced the HB reflex, the dispersion of the burst modulation might due to two possible reasons. First, the reconstructed signals were extremely low in amplitude due to the decomposition of SWT. Second, the SRS noise was very high and correlated with the signal which led to its corruption.

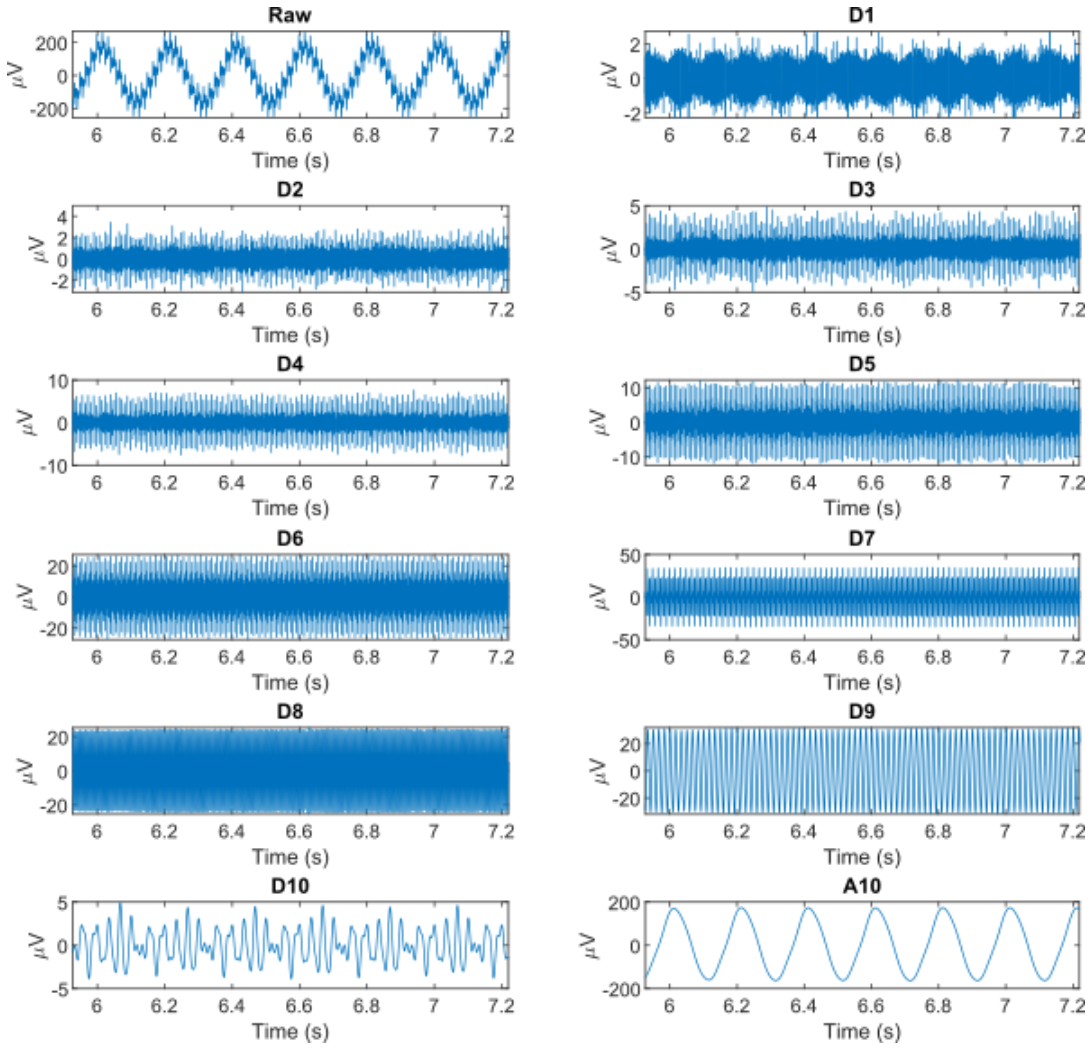

Figure. 3.6. The reconstructed subbands signals produced by the Neurlyzer during **5 Hz, 0.4 mA**$_p$ LFAC activation. The burst modulation is shown in D1 level

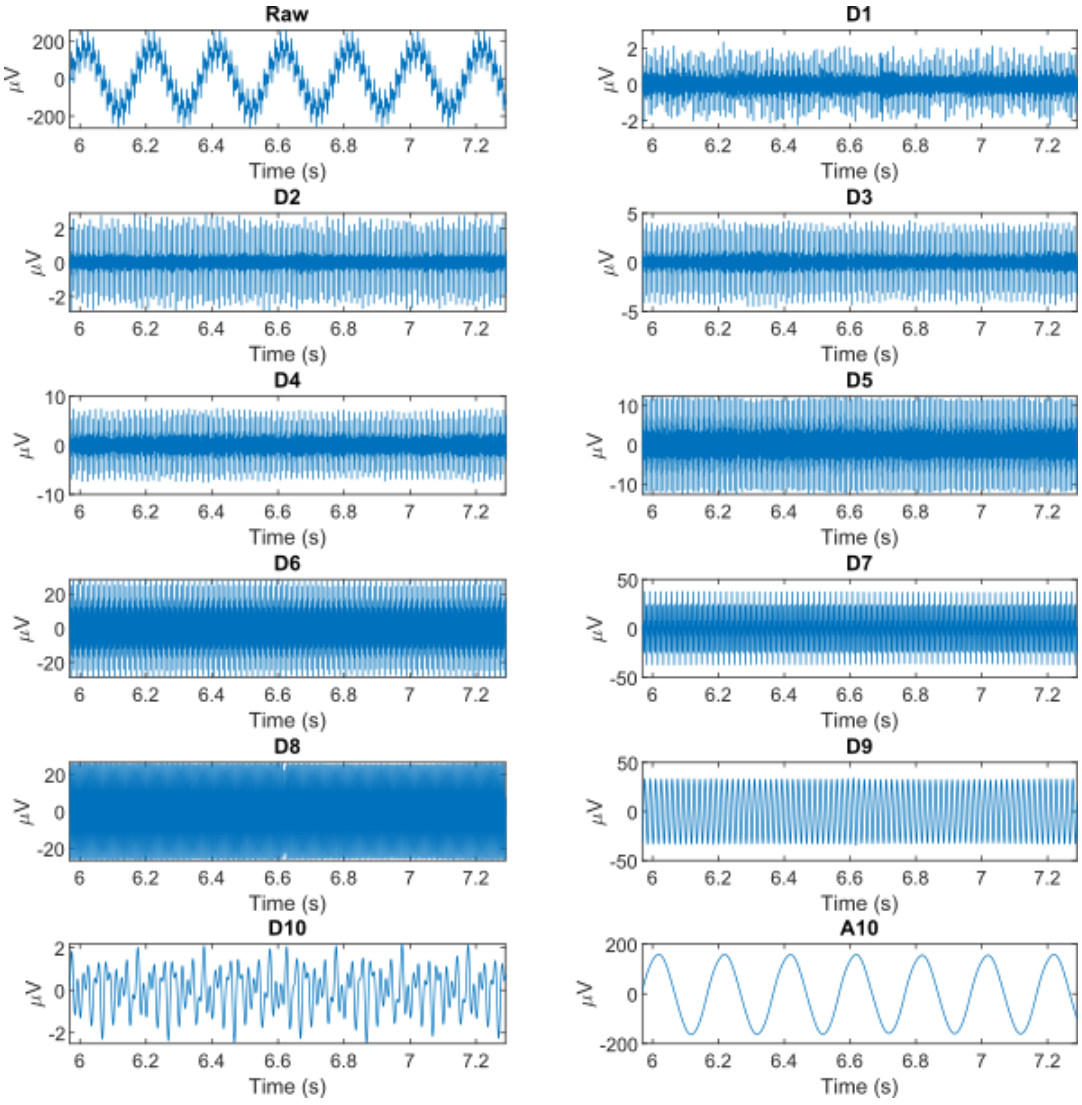

Figure. 3.7. The reconstructed subbands signals produced by the Neurlyzer during **5 Hz, 0.1 mA**$_p$LFAC activation. The burst modulation did not appear in D1 level

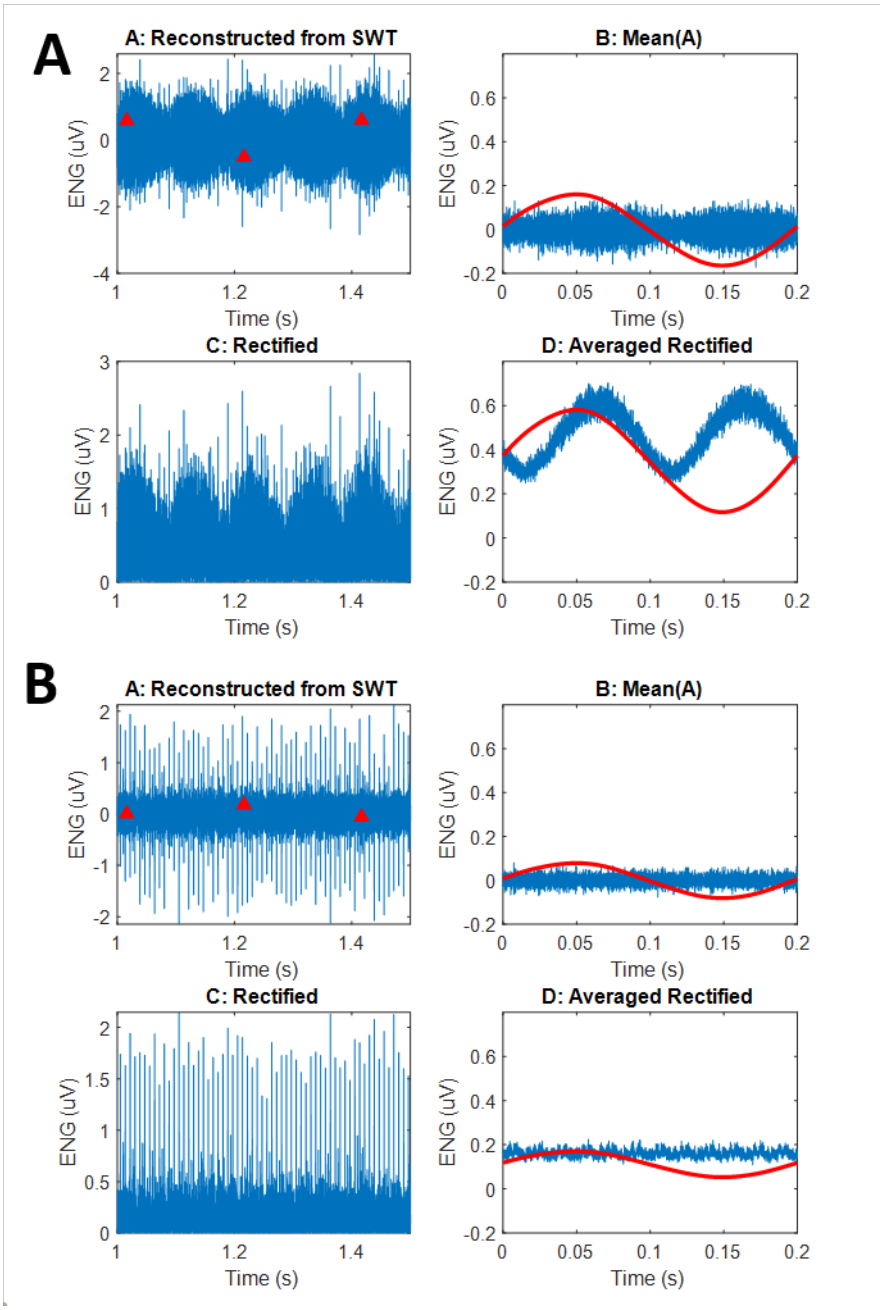

Figure. 3.8. The neural activity revealed from the reconstructed sub-bands signal during the application of **5 Hz** LFAC waveform. Panel A shows the results from **0.4 mA**$_p$. Panel B shows the results from **0.1 mA**$_p$. In each panel, A: the reconstructed signal. B: the averaged reconstructed signal. C: the rectified version of the reconstructed signal. D: the average of the rectified version. The red LFAC waveform is an arbitrary unit to reflect the phase of the applied LFAC waveform

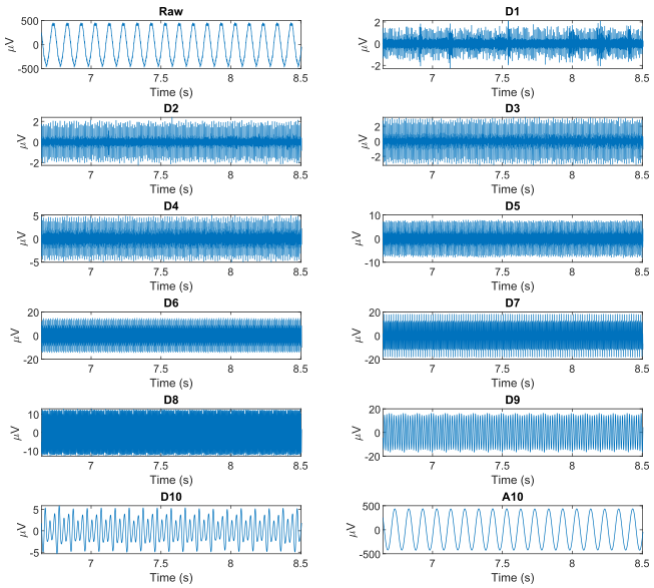

Figure. 3.9. The reconstructed subbands signals produced by the Neurlyzer during the application of **10 Hz, 1.0 mA**$_p$ LFAC waveform

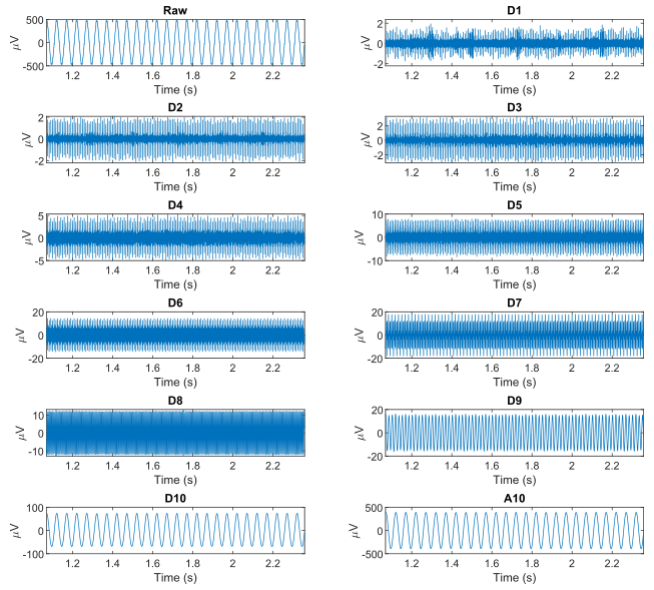

Figure. 3.10. The reconstructed subbands signals produced by the Neurlyzer during the application of **20 Hz, 0.6 mA**$_p$ LFAC waveform. The burst modulation did not appear in D1 level

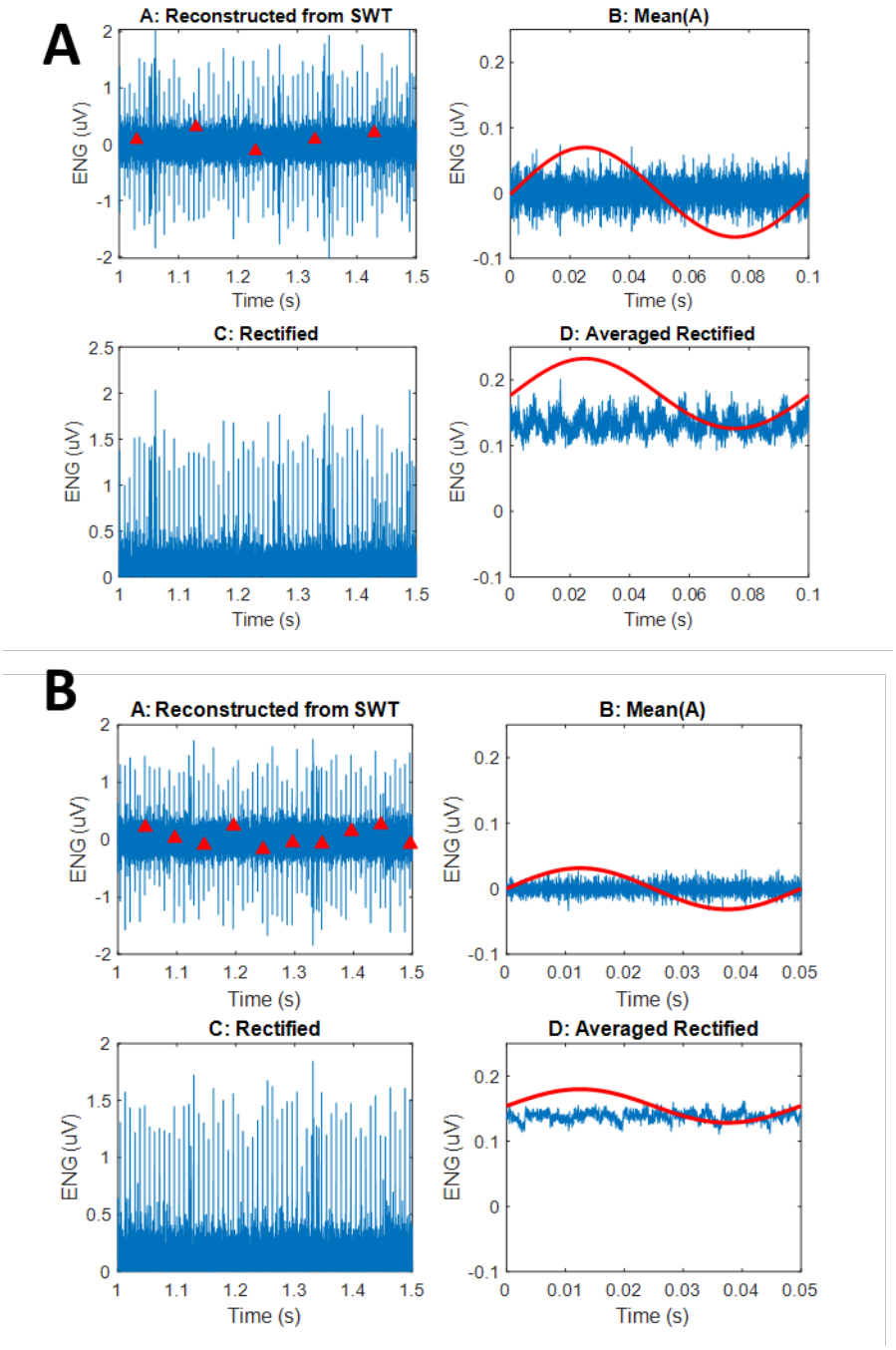

Figure. 3.11. Example of averaging the reconstructed subbands signal. Panel A: the results during **10 Hz, 1.0 mA**$_p$ LFAC activation. Panel B: the results during **20 Hz, 0.6 mA**$_p$ LFAC activation

The PSD analysis of the ENG signal shows a high magnitude of the embedded noise comparing to the expected nerve activity. As shown in figure 3.12, as the applied LFAC amplitude increases, the large peak at 5 Hz influences the PSD to increase and deflect slightly from the baseline. Although it is not clear, the change in the magnitude is an indication of the presence of nerve activity. For better observation of the frequency components contained within the ENG, the FFT of the raw ENG signal was computed as shown in figure 3.13 A and B. The applied 5 Hz LFAC waveform appeared to increase in amplitude and induce an increase in amplitude of the adjacent frequency components. The common noise peaks overlap with its identical components in both active ENG and the baseline. The amplitude change started to deviate in the higher frequency band, above 100 Hz.

As shown in the breathing rate results, the transient response of the nerve to the LFAC caused an instantaneous drop in the breathing rate which was not considered in finding the minimum threshold to induce the HB-reflex. Following that, the breathing rate reached a plateau of decreased breathing rate. Figure 3.14 shows the LFAC amplitude threshold required to induce HB-reflex as a function of the LFAC waveform. These experimental threshold curves were constructed based on the minimum LFAC amplitude that was capable to induce a steady HB-reflex. The results suggest that the LFAC amplitude threshold to activate the autonomic nerve fibers follows the same trend as the *ex-vivo*, where the higher the LFAC frequency is, low current intensity is required.

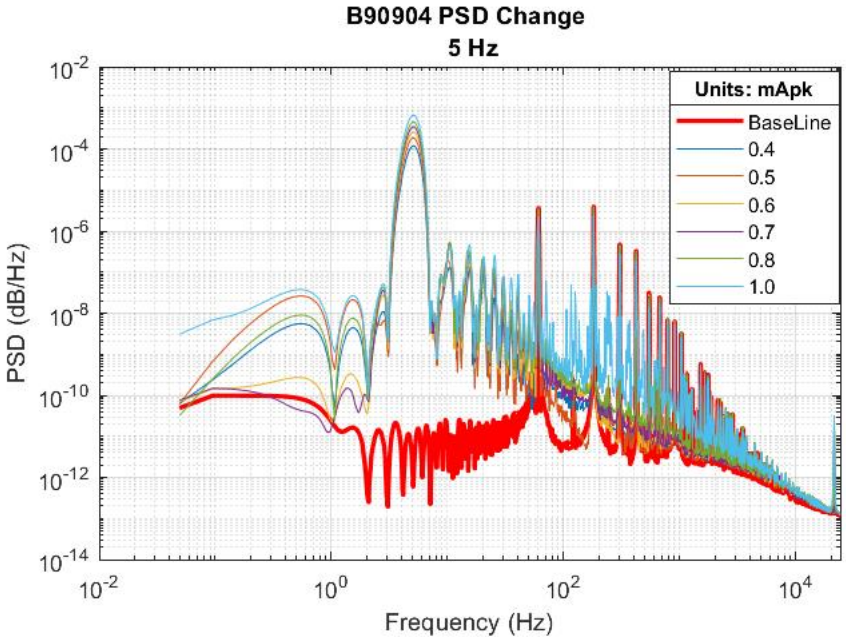

Figure. 3.12. The PSD results during the application of **5 Hz** and amplitudes of **0.4, 0.5, 0.6, 0.7, 0.8, and 1.0 mA**$_p$

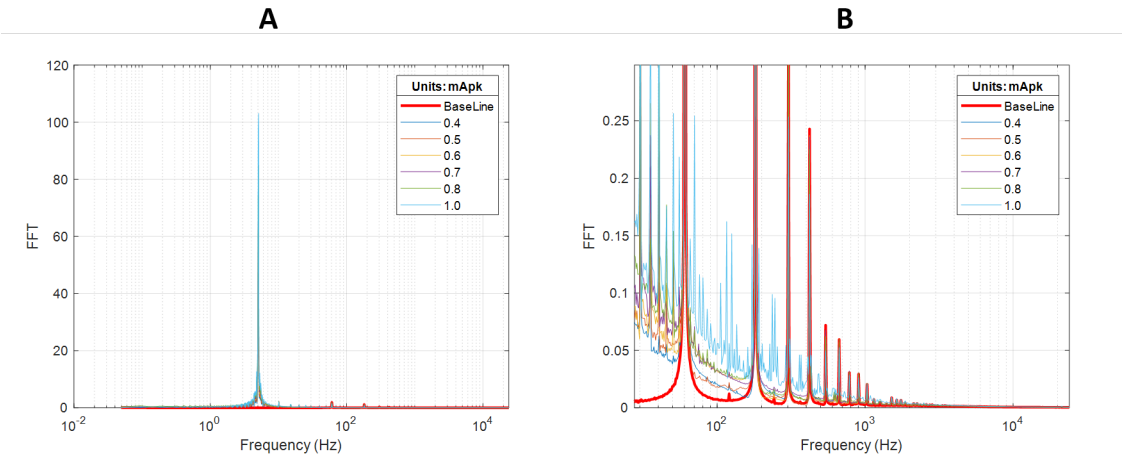

Figure. 3.13. The fast Fourier transform (FFT) result of the raw ENG during the application of **5 Hz** and amplitudes of **0.4, 0.5, 0.6, 0.7, 0.8, and 1.0 mA**$_p$. Panel A shows the full scale over the range of frequency and Panel B shows a zoomed in view

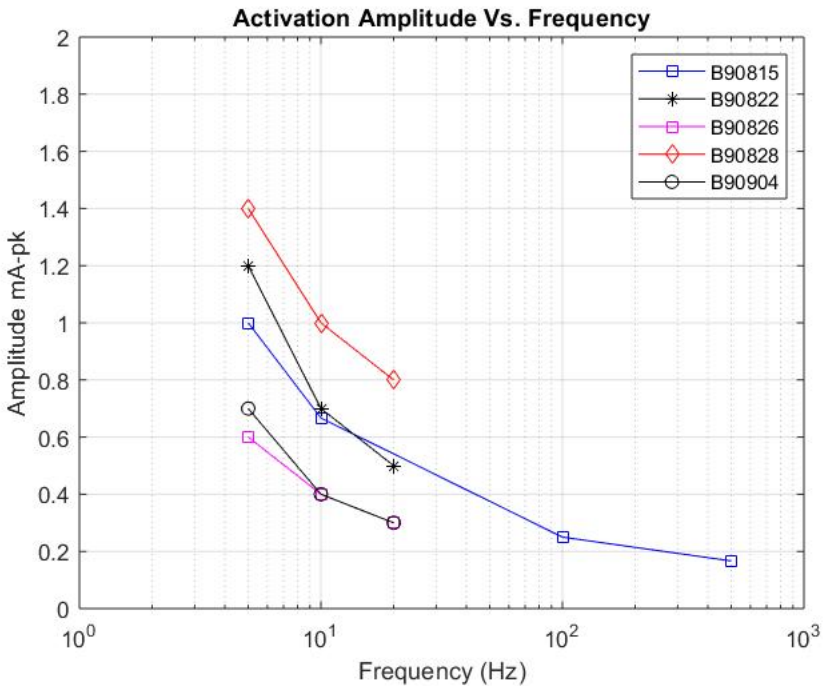

Figure. 3.14. The resulted LFAC threshold curves as function of frequency to induces HB-reflex. Legend represents the experiment date

3.5 Results of Rat Experiments

The LFAC activation of the sciatic nerve was evaluated based on the nerve burst modulation, the muscle contraction and the change on the force induced by muscle twitches before and after crushing the nerve. Figure 3.15A shows a representative continuous recording during the 5 Hz LFAC activation (baseline, 28.0, 55.9, 122.1, 163.3, 210.1, 233.6, and 262.0 μA_p) that includes the ENG, EMG, force, and the applied LFAC waveform signals before crushing the nerve. The EMG showed no firing of muscle activity during the baseline nor during the lower LFAC amplitudes ($<$210.1 μA_p), as shown in figure 3.15B. As the amplitude increased, the muscle activity started to emerge and the force deviated from the baseline state. The strong muscle activity occurred at higher LFAC amplitude ($>$233.6 μA_p) caused the animal foot to produce some movements as shown in figure 3.15C. The muscle activity was not synchronized with the LFAC cycles that indicates the randomization of the LFAC

activation. The EMG activity firing was in response to the ENG burst modulation. Giving the fact that the induced nerve activity by the LFAC was not producing a sustained action potential firing to track, the muscle activity could be a result from the H-reflex, or the muscles response.

To investigate that, the crushed nerve in two experiments (n=2) was reactivated using the same LFAC frequency and amplitudes. The results of the activation after crushing the nerve are shown in figure 3.16 during the application of 5 Hz LFAC waveforms. The muscle activity showed clear twitching with a lower firing rate. The induced force also showed a slight change in parallel with the EMG after crushing the nerve. By comparing the two results, it is possible that the LFAC activation induced the muscle's response with less amplitude in the absence of the H-reflex, which was different in magnitude before the elimination of the H-reflex.

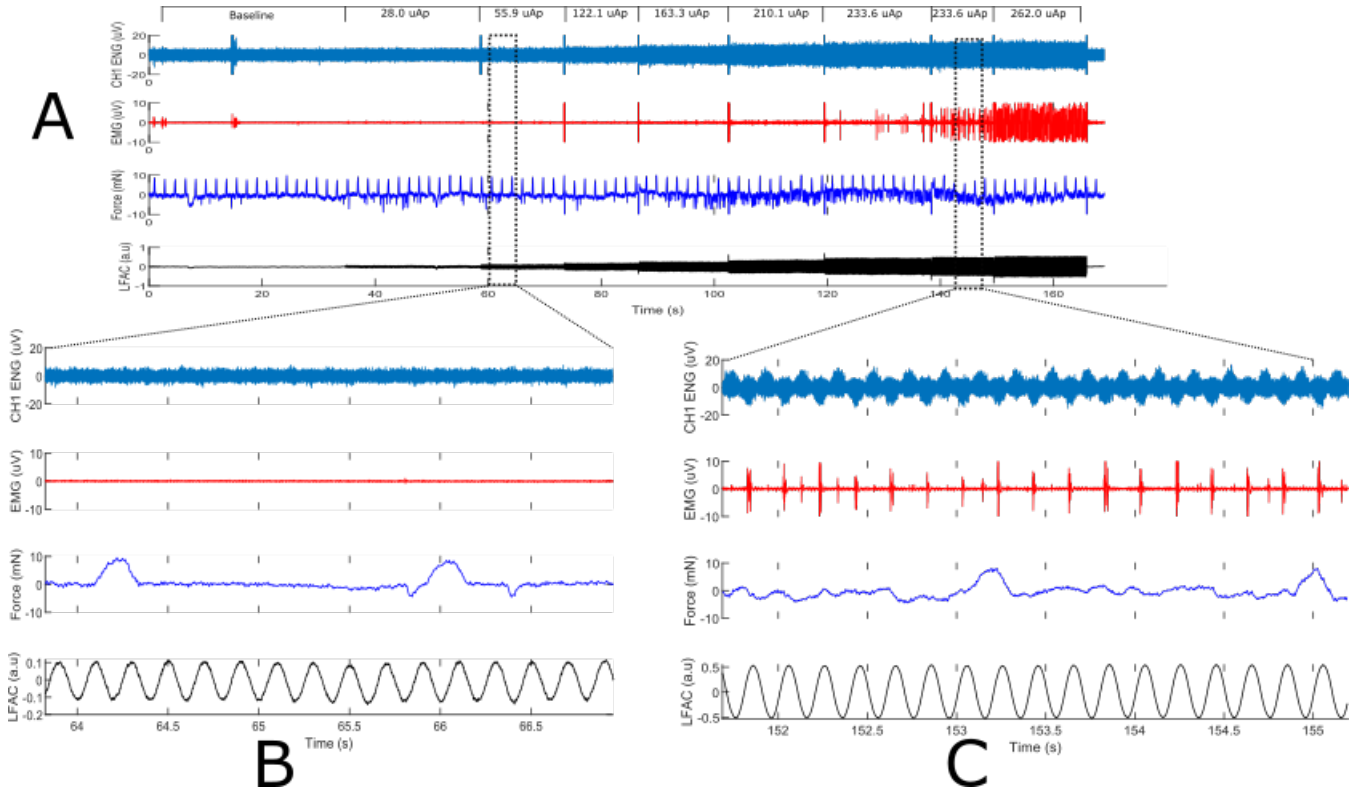

Figure. 3.15. An example of the results **BEFORE** crushing the nerve showing the ENG, EMG, force and the corresponding **5 Hz** LFAC waveform at different amplitudes. A: show the continuous recording. B: shows a 3-seconds window when no activation was observed at **5 Hz, 55.8** $\mu\mathbf{A}_p$. C: shows a 3-seconds window when LFAC activation was observed at **5 Hz, 233.6** $\mu\mathbf{A}_p$

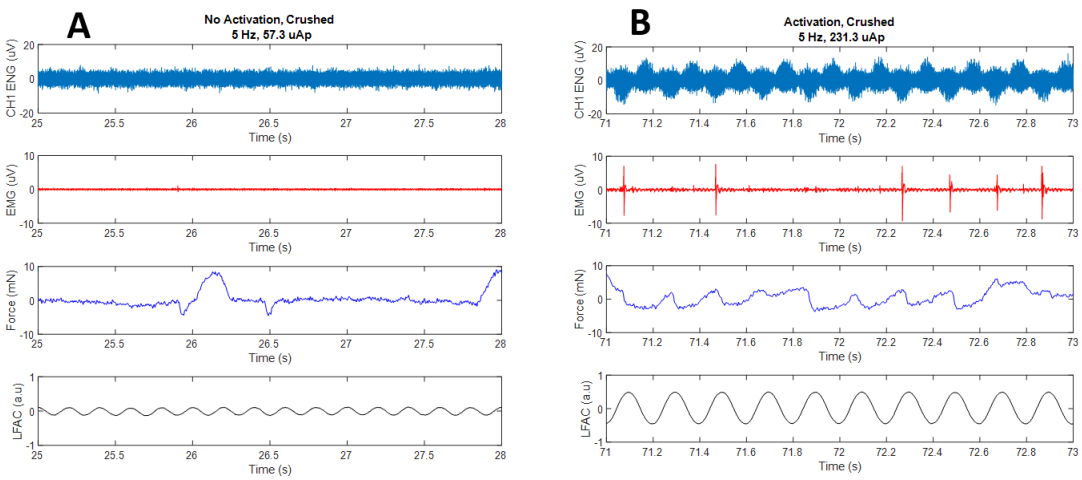

Figure. 3.16. The results of **5 Hz** LFAC activation **AFTER** crushing the nerve. A: no activation was observed at **5 Hz, 57.3** $\mu\mathbf{A}_p$. B: activation was observed at **5 Hz, 231.3** $\mu\mathbf{A}_p$ amplitude

The activation was also observed during the 10 and 20 Hz LFAC application before and after crushing the nerve. Figure 3.17 and figure 3.18 shows the changes on the ENG, EMG, and force during the application of 10 Hz LFAC waveform before and after eliminating H-reflex. Similarly, figure 3.19 and figure 3.20 show the results of applying 20 Hz LFAC waveform. From those results, the ENG showed the burst modulation in response the high LFAC amplitudes. However, the EMG activity were observed to be lower than those during 5 Hz LFAC application in both magnitude and frequency.

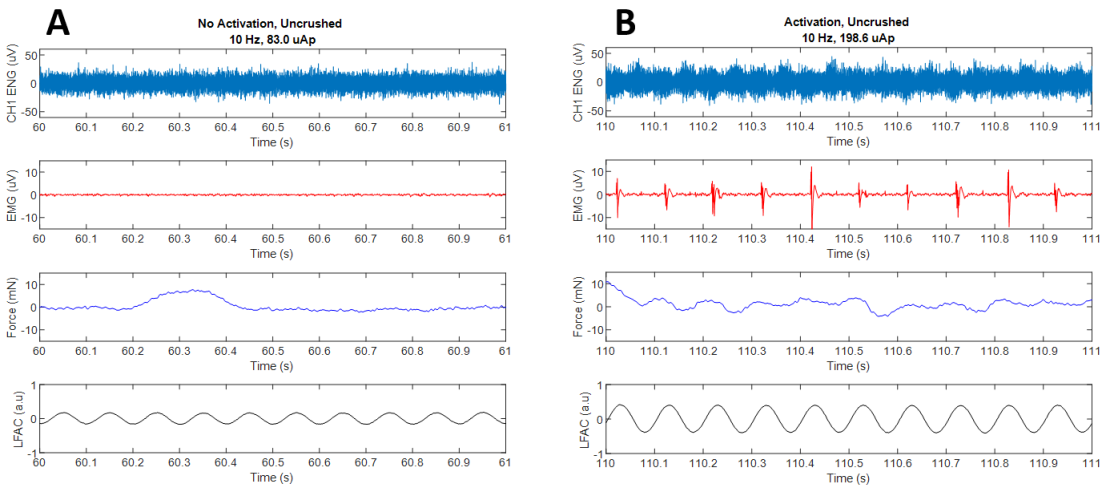

Figure. 3.17. The results of **10 Hz** LFAC activation **BEFORE** crushing the nerve. A: no activation was observed at **10 Hz, 83.0** $\mu\mathbf{A}_p$. B: activation was observed at **10 Hz, 198.6** $\mu\mathbf{A}_p$ amplitude

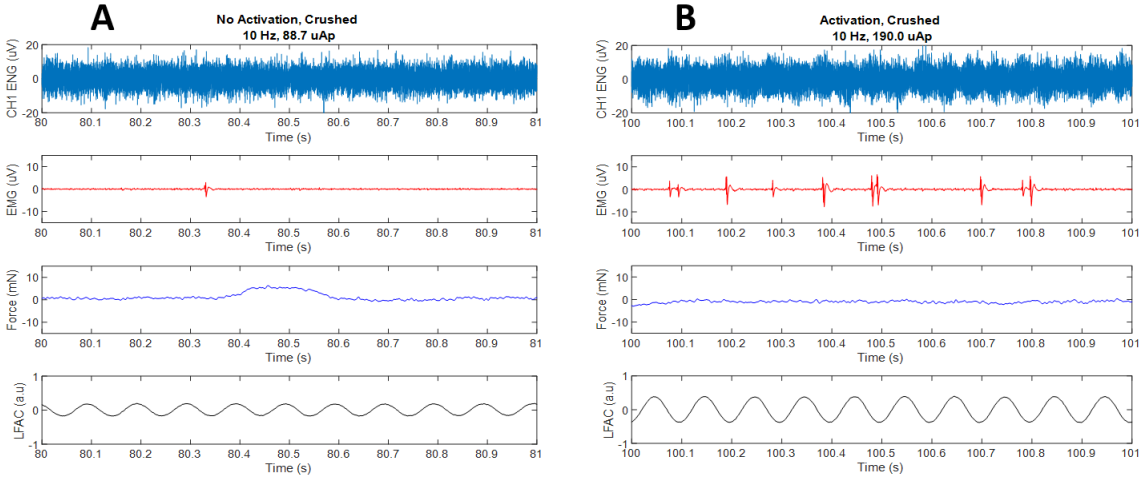

Figure. 3.18. The results of **10 Hz** LFAC activation **AFTER** crushing the nerve. A: no activation was observed at **10 Hz, 83.0** $\mu\mathbf{A}_p$. B: activation was observed at **10 Hz, 198.6** $\mu\mathbf{A}_p$ amplitude

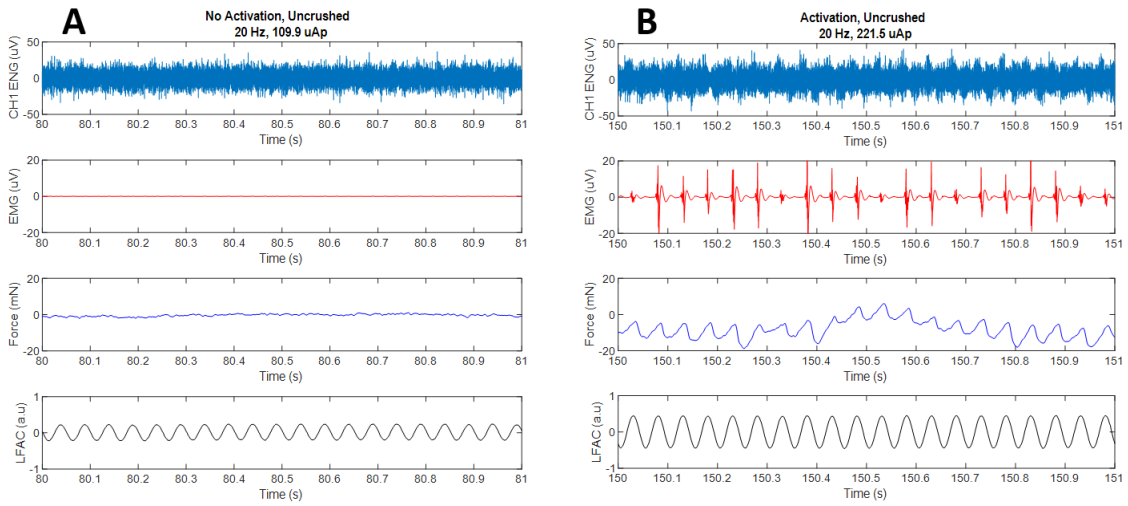

Figure. 3.19. The results of **20 Hz** LFAC activation **BEFORE** crushing the nerve. A: no activation was observed at **20 Hz, 109.9** $\mu\mathbf{A}_p$. B: activation was observed at **20 Hz, 221.5** $\mu\mathbf{A}_p$ amplitude

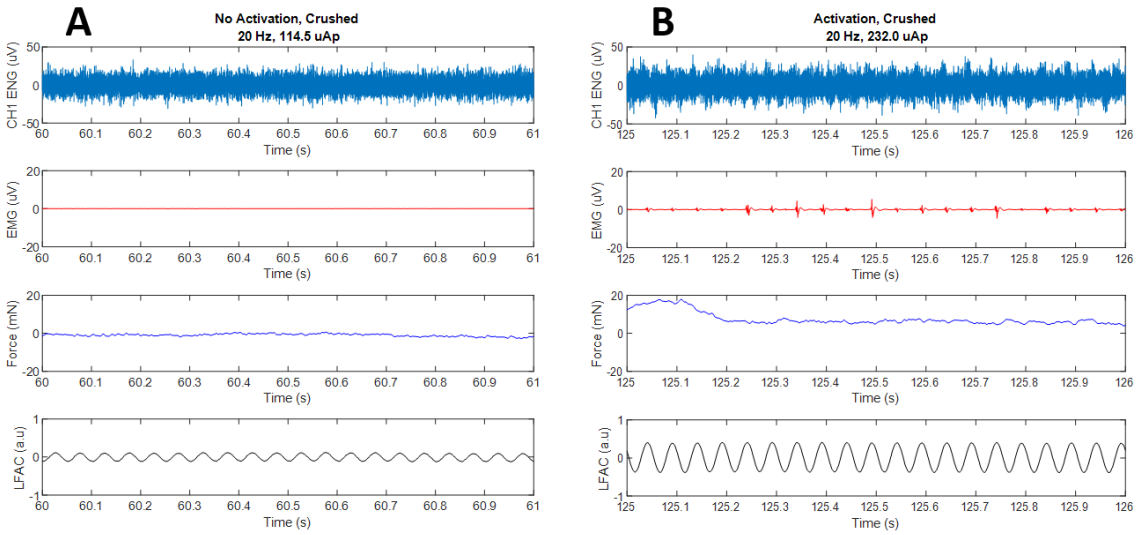

Figure. 3.20. The results of **20 Hz** LFAC activation **AFTER** crushing the nerve. A: no activation was observed at **20 Hz, 114.5** $\mu\mathbf{A}_p$. B: activation was observed at **20 Hz, 232.0** $\mu\mathbf{A}_p$ amplitude

The frequency components of the ENG showed a clear presence of the EMG and the nerve activity within the ENG signal. As shown in figure 3.21, the 5 Hz LFAC waveform and the muscle activity dominate the PSD curve as the LFAC amplitude increases. The muscle activity usually has frequency components in the frequency band from 100 to 1000 Hz, which might overlap with the nerve activity signal. However, the variation in peaks distribution beyond 1 kHz is most likely representing the nerve activity. Comparing the baseline and during the activation, the lower LFAC amplitudes did not induce muscle's nor nerve activity; which superimpose the baseline curve. The same results were confirmed during the application of 10 and 20 Hz LFAC waveform as shown in figure 3.22. However, during the activation at 20 Hz, the ENG signals showed large hormonic signal in the frequency band less than 3kHz, which is most likely to be a hormonic noise.

The minimal LFAC amplitude required to induced the muscle twitches was a function of the LFAC frequency. As shown in figure 3.23, the threshold of each experiment deviates in magnitude, but they follow the same trend as the *ex-vivo* and the swine results. As the LFAC frequency increases, the amplitude threshold decreases. These amplitude thresholds were constructed based on the burst nerve activity modulation appearance on the ENG, where all the animals required less than 1.0 mA_p in order to induce muscle activity.

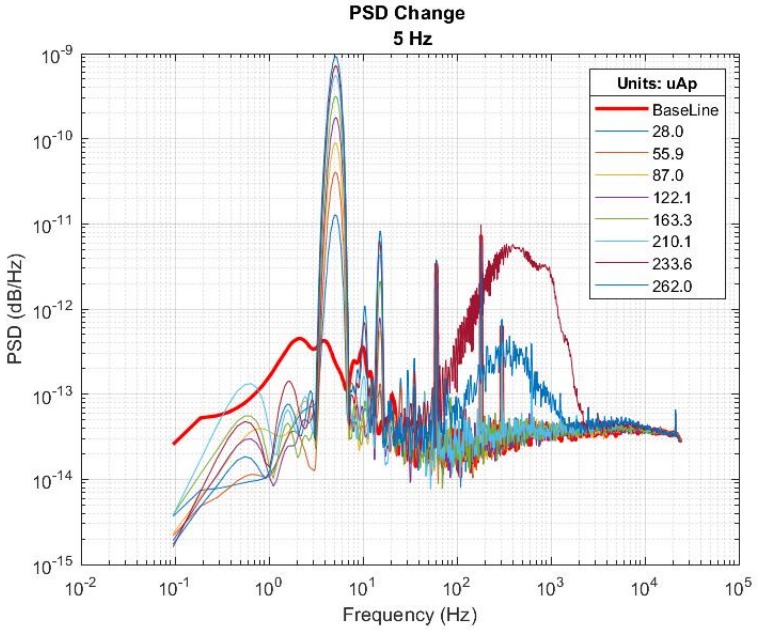

Figure. 3.21. PSD results during the application of **5 Hz LFAC** waveform

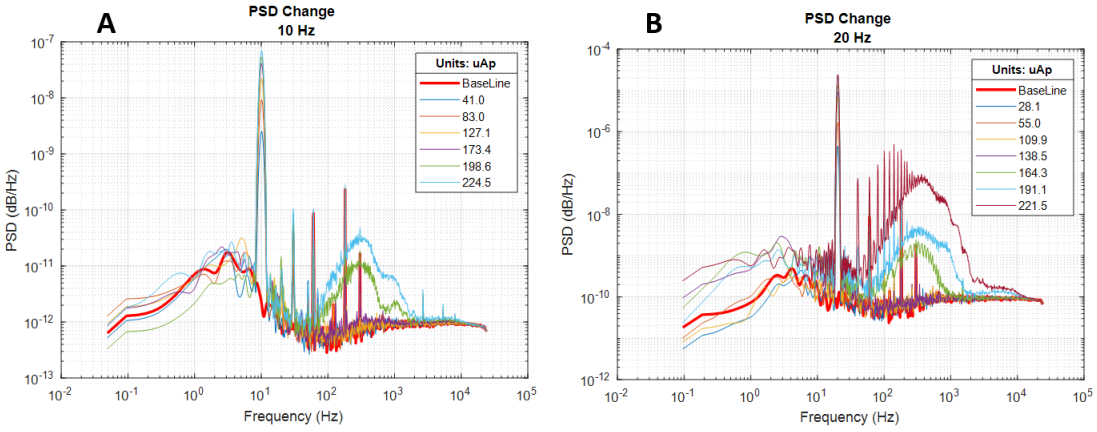

Figure. 3.22. PSD results during the application of A: **10 Hz LFAC** B: **20 Hz LFAC** waveforms

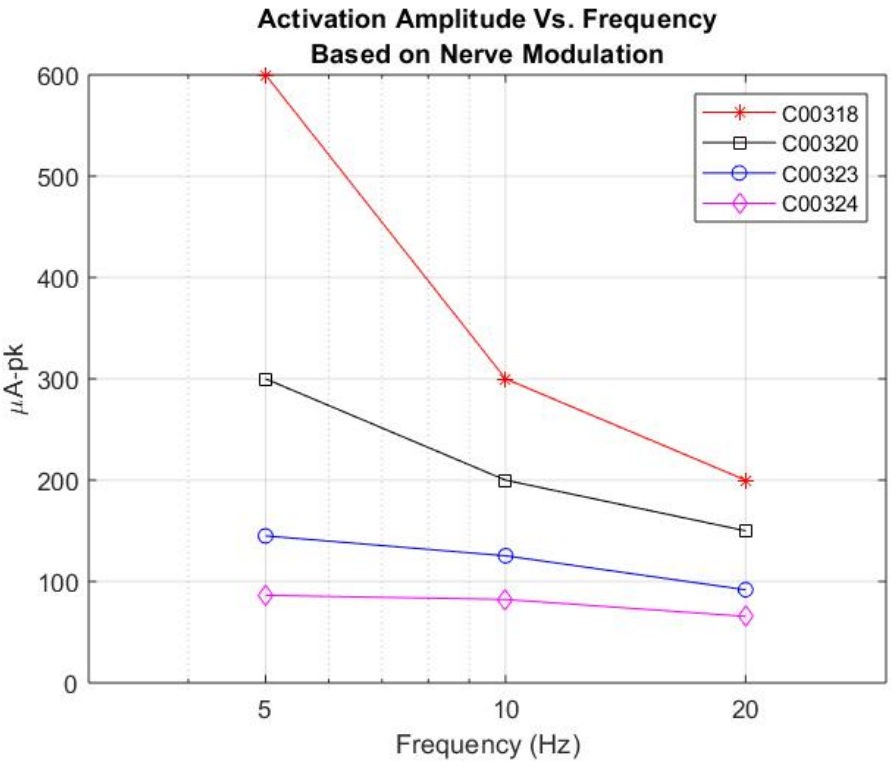

Figure. 3.23. The resulted LFAC threshold curves as function of frequency to induce muscle activity. 1 Hz activation was beyond the water window and did not result in activation. Legend represents the experiments date

3.6 Discussion

In both swine and rat experiments, the LFAC waveform was able to activate the targeted nerve fibers to produce the intended reflex. The nerve activity was captured in most cases during the application of 5, 10, and 20 Hz. The burst modulation was the common parameter to investigate in both experiments, which revealed that the LFAC activation has a random mechanism in activating nerve fibers. By averaging the nerve activity against the LFAC waveform cycles, the results showed a relationship between the modulation and the peak's time. However, there was not a single point of activation. The rectification of those activities also suggested uncorrelation behavior between the LFAC cycles and the burst modulation.

In the swine experiments, the burst nerve modulation was found in a higher frequency band as the SWT results suggested. However, the PSD and FFT analysis showed that the nerve activity variation was more likely to be in the frequency band less than 10 kHz. This inconsistency was observed only with the swine data, which had a high level of noise, sourced from the SRS device and appeared to correlate harmonically with the ENG signal. The neural signal could be shifted to a different frequency band and that would occur if that recording electrodes' impedance was changed as a function of frequency. Since there was not a single frequency component, the electrode's phase shifting could have influenced the recorded ENG signal. However, the breathing rate (HB-reflex) analysis revealed more reasonable results as a biomarker for the validity of LFAC activation. The activation of the vagus nerve bundle using LFAC evoked the nerve fibers projected to the spinal cord to activate. Once the threshold is reached, the HB-reflex AP was propagated toward the respiratory system to stop inhalation. Experimentally, the breathing rate change confirms the successful activation of the afferent fibers, most likely to be fast B fibers [61–63]. The direction of activation was assumed to be toward the spinal cord as the efferent fibers were crushed. These findings allowed to pronounce the feasibility of the LFAC waveform activation in the autonomic nerve fibers.

The rats' experiments also yielded more details on the LFAC activation mechanism with respect to the motor nerve fibers activation. As the somatic nerve fibers activate, the muscle filaments recruitment produces the overall twitching. During the LFAC activation, the twitches were observed to be regulated with the LFAC waveform but not synchronized. This is a remarkable finding to characterize the LFAC activation to not produce fatigable contraction. By comparing the LFAC activation results before and after crushing the nerve, it was revealed that the LFAC waveform is capable of inducing the motor nerve fibers activation. It was assumed that physical crushing on the nerve would eliminate the Hoffmann reflex and the muscle activity would be due the motor fibers activation. As the results show in figures 3.15 to figure 3.20,

applying 5, 10 and 20 Hz LFAC waveforms to the sciatic nerve induced the burst nerve modulation along with muscles contraction.

As the LFAC amplitude increases, more motor fibers are recruited resulting in a faster and strong muscle twitches. The force induced by the muscles was not correlated with the LFAC waveform, which is another possible indication of the unsynchronized activation of the LFAC waveform despite the applied frequency level. Although the force change was interfered with breathing peaks, the inner interval between the breathing peaks shows a variation from the baseline and during the muscle activation.

In summary, activating the autonomic and somatic nerve fibers using 5, 10 and 20 Hz LFAC waveform indicates the practicability of using LFAC waveform to activate peripheral nerve fibers without causing any damages to the nerve tissues. The LFAC activation was found to be random and asynchronous to a single point of activation which is in agreement with the preliminary work of the lab and the *ex-vivo* findings and provides a means to the natural-like activation mechanism produced under the normal physiological conditions. The use of biomarkers supported the validation study to observed and quantify the change due to the LFAC activation. Moreover, the LFAC activation amplitude was a frequency and most-likely to be fiber-type dependent. The differences in the revealed thresholds suggests that the current intensity required to achieve the autonomic nerve fibers is higher that the somatic nerve fibers. These findings pronounce that fiber-size dependency and might be the recruitment order of the LFAC activation. Moreover, the muscle activation via LFAC was normal and can be seen as unfused tetanus contraction from the force and the EMG results. This remarks that the LFAC activation feature is a safe electrical stimulation that does not alter the muscle contraction mechanism.

4. DISCUSSION AND FUTURE DIRECTIONS

In this chapter, the general features of the LFAC activation mechanism revealed from the experiments are discussed based on the analysis methods explored. The overall discussion is aimed also to provide an insight into the LFAC activation mechanism with respect to the autonomic and somatic nerve fibers.

4.1 Overall Discussion

The experimental findings demonstrated the feasibility of the LFAC activation method to induce peripheral nerve fibers activation. The resulted burst nerve modulation suggests the relationship between the LFAC waveform and the nerve activity. The correlation between the LFAC cycles and the burst modulation indicates that the LFAC waveform is able to induce nerve fibers activation in a stochastic manner that is not synchronized to a single point of activation. This activation as suggested by the preliminary work on the rabbit experiment was observed to occur on small nerve fiber first. This is also in agreement with the findings from the rat experiments. As the Hoffmann reflex was assumed to be eliminated, the LFAC waveform was able to reactivate the motor nerve fibers. This activation is most likely to be activating the small nerve fibers to induce muscle contraction. Furthermore, the HB-reflex in the swine experiments was mostly related to a large population of small C fibers and afferent fibers, most likely to be fast B fibers [61–63] and the LFAC waveform induced HB-reflex with several amplitudes. By looking into the recruitment order of this activation to induce HB-reflex, the low current intensity caused a slow breathing changing, indicating the start of HB-reflex and by increasing the LFAC amplitude the complete non-breathing situation accrued. These findings suggest the activation of small C, and B fibers first, followed by large nerve fibers.

From the swine results, the decomposition of the ENG signals revealed the frequency components associate with the burst modulation. The frequency band of the induced nerve activity was not consistent with all conducted experiments. From the canine *ex-vivo* and the rat *in-vivo* experiments, the ENG signals reveled the neural activity existence in the band from 100 to 10 kHz. These finding are in the normal neural activity range discussed in [59]. However, the frequency components of the nerve activity from the swine experiments were found to reside in a high frequency band (>12 kHz). There are two possible reasons for that to occur. First, the ENG signal was interfered with a large amount of hormonic noise that was correlating with signal. This noise issue could be minimized by the SWT decomposition that resulted in the apparency of the burst modulation in higher subband ranges. The decomposition of the signal could have altered the signal frequency components during the noise subtraction and that might have shifted the neural signal frequency components to the higher bands. Secondly and most likely, the recording electrodes' impedance was changed as a function of LFAC frequency and the correlated harmonic noise frequency. As the electrodes have a capacitive-like properties, the phase shift of the neural signal could occur.

4.1.1 Threshold Determination

Determining the thresholds of activation was accomplished by tracking the applied LFAC waveform current amplitude. In the canine *ex-vivo* experiments, the burst modulation on the ENG recording was the indication of the nerve activity. Although there were two channels of ENG recording, only one channel was considered in the analysis. Unless there was a gain issue associated with the recordings, both channels were showing exactly the same behavior. However, in the *in-vivo* experiments, the biomarkers activation was the main parameter to indicate the activation using LFAC.

As the results show, the minimal LFAC amplitudes required to induce nerve fibers activation were clearly frequency and fiber size dependent with the higher the fre-

quency, the lower LFAC amplitude. The autonomic and somatic nerve fibers responded to the LFAC waveform differently. During the activation of the vagus nerve, the required LFAC amplitude to induce HB-reflex at 5 Hz ranged from 0.6 to 1.6 mA_p, whereas during the LFAC activation of the sciatic nerves, it required 0.09 to 0.6 mA_p. The difference in these ranges suggests the dependency of the LFAC activation on nerve size. On the other hand, during the activation of the sciatic nerve, figure 3.23 shows a clear variation between the experiment's thresholds. The differences in the ranges of activation suggested the possibility of the variation in the induced muscles activity. This could be a result from the activation of large fibers first, the age of the animals, or both; however, in all the experiments, the decreasing trend of the thresholds as a function of the LFAC frequency was consistent as shown in figures 2.19, 3.14, and 3.23.

4.1.2 Sciatic Nerve Activation Using Standard Pulse and LFAC

The LFAC activation phenomenon is a new technique that could provide a safe stimulation method that would improve the field of neuromodulation. Although the standard pulse activation is an effective method to activate the peripheral nerve fibers, the onset issues associated with the artifact in recordings, reverse recruitment order, the possible interference with bipotential field, and the extra caution taken for charge imbalance limit its applications in some research settings. The key features of the LFAC activation, as seen from the results in chapter 2 and 3, are the absence of the artifact, the waveform cycles symmetry provides a zero-charge imbalance, and the ability to induce non-fatigable muscle contraction.

Comparing the results of activating the rat's sciatic nerve using pulse stimulation and 5Hz LFAC waveform revealed the absence of the CAP from the nerve activity during the LFAC activation. Figure 4.1 shows the results of using the standard pulse activation (duration 50 μsec, amplitude of 0.45 mA_p, 1 Hz) while figure 4.2 shows the results of 5 Hz LFAC activation with an amplitude of 233.6 μA_p. By

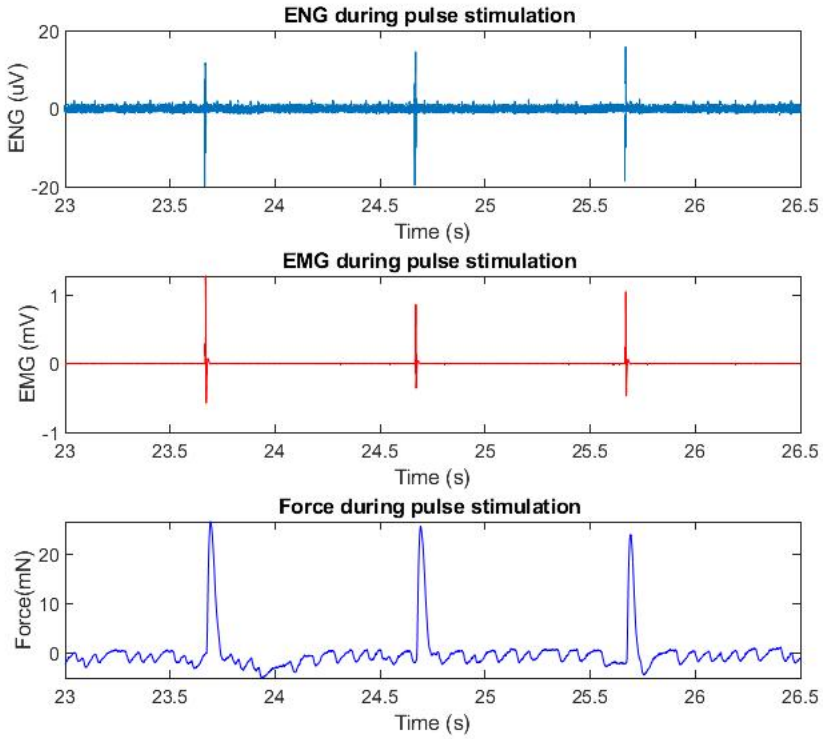

Figure. 4.1. Results of standard pulse activation (duration 50 μsecond, amplitude of 0.45 mA_p, 1 Hz) in inducing the rat sciatic nerve fiber activation

detecting, aligning, and averaging the ENG signal from the pulse activation the CAP was observed, as shown in figure 4.4. The EMG and the force associated with that activation are shown in the lower traces of figures 4.3 and 4.4. As can be seen, the pulse artifacts appeared in every second of the ENG recording and the activation of the muscles is synchronous to the stimuli. As shown in the EMG trace, a large amount of muscle activity was produced following the artifact. This muscle activity produced an increase in the recorded force that followed the muscle twitching. The force could be reaching a fused tetanus rather than single twitches. On the other hand, the 5 Hz LFAC activation results shown in figure 4.2 display the burst modulation on the ENG and by averaging that against one period cycles a dispersion to the burst modulation occurred. This is a key difference between the pulse activation and LFAC

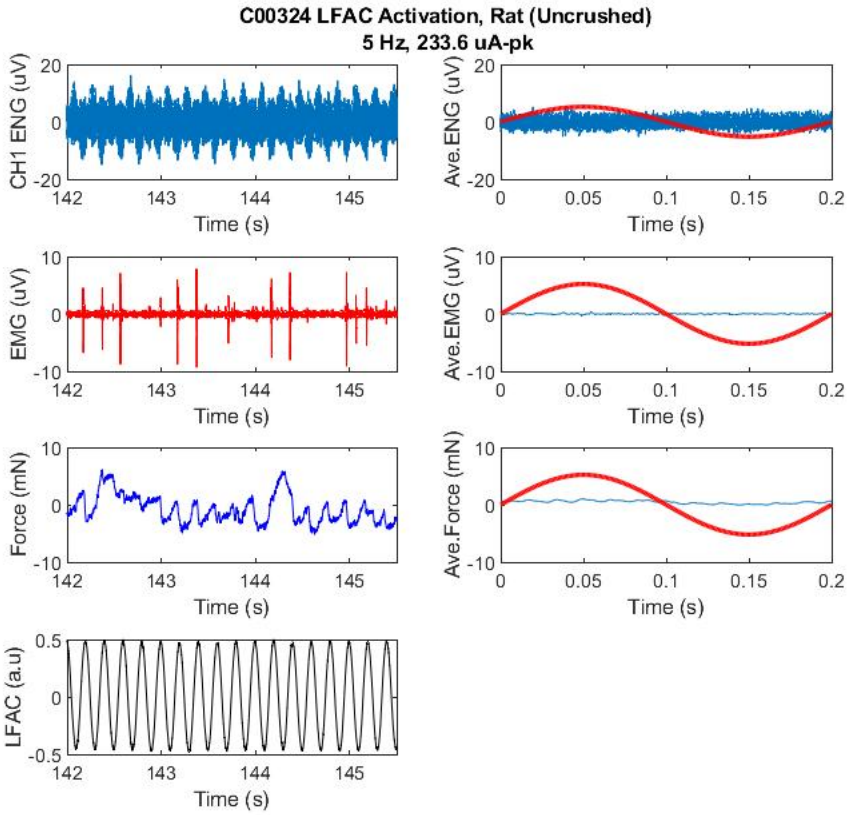

Figure. 4.2. The results of **5 Hz** LFAC activation of the rat sciatic nerve with an amplitude of **233.6** $\mu\mathbf{A}_p$

activation that verifies LFAC stochastic mechanism and the ability to induce muscle contraction. The EMG and force traces also show the muscle activation. However, by averaging the EMG and the force with respect to a single LFAC cycle the results show a clear dispersion of the activity due to the random nature of the LFAC and non-synchronized activation.

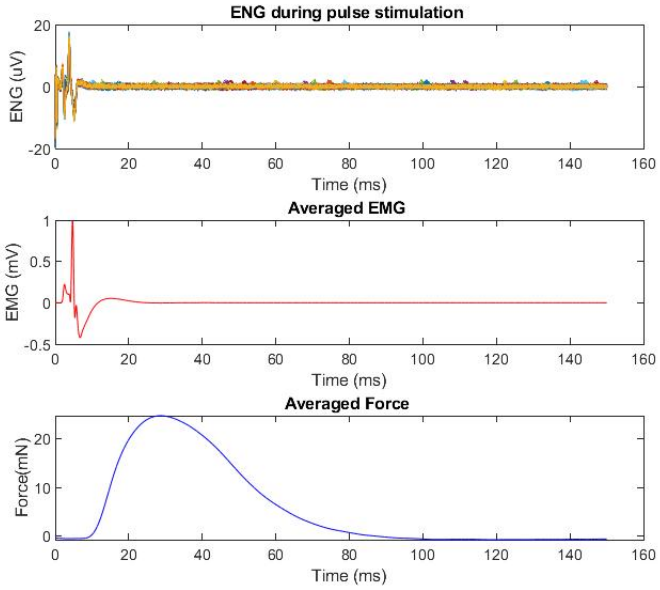

Figure. 4.3. The results of averaging the ENG, EMG, and force signals from the pulse activation. The timeline shows the muscle activity preceded by the neural activity and followed by the increase in force

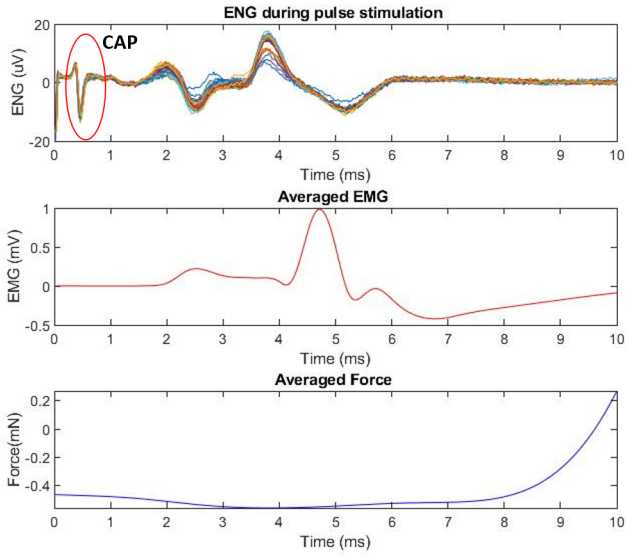

Figure. 4.4. A 10-millisecond window of the pulse activation results showing the compound action potential (CAP) resulting from pulse stimulation at t=0 in the top panel. Middle and lower panels show the corresponding EMG and force induced by that activation respectively

4.2 Thesis Aim 1

Provide Experimental Evidence of the Possibility of Activating Peripheral Nerve Fibers Using the LFAC Waveform

The preliminary results from the rabbit experiment suggested the possibility of activating the peripheral nerve fibers using LFAC. The investigation of this hypothesis in *ex-vivo* (chapter 2) setups revealed that the activation using 5, 10, and 20 Hz LFAC waveforms could elect the nerve activity in an unusual manner. The canine *ex-vivo* results shown in figure 2.2 and 2.3 suggests the efficiency of 5 Hz LFAC waveform in inducing the vagus nerve activity as a burst modulation shown in the ENG recordings. The 10 and 20 Hz LFAC waveform also displayed the same behavior as shown in figures 2.10 and 2.11. By examining the activation during two stages, fresh and 2Hr-Post nerve fibers, the results suggested that the burst modulation on the ENG signal was due to the nerve activity during the LFAC application. Furthermore, the frequency analysis of the ENG signal with respect to the LFAC application revealed that the PSD level deviated to the neural frequency band with respect to the LFAC amplitude with a slight change on the PSD level. As another control, the ENG baseline recordings did not show any sign of burst modulation in the absence of the LFAC waveform that indicates the burst modulation appearance was due to the activation of the nerve fibers by the LFAC.

Examining the hypothesis using *in-vivo* (chapter 3), the animal models allowed for more reliable results to prove the LFAC activation feasibility. The biological reflexes mediated by the autonomic and somatic nerve fibers enhanced the experimental studies to test the LFAC activation hypothesis. From the swine experiments, the HB-reflex was the major factor of interest that demonstrated the LFAC activation. The 5, 10, and 20 Hz LFAC activation of the vagus nerve fibers projected the spinal cord induced the HB-reflex and the breathing rate was dropped in response to the nerve fibers activation. The results shown in figures 3.3, 3.4, and 3.5 highlights the change

in the animal breathing rate with respect to the applied LFAC frequency and amplitude. As the intensity of the LFAC waveform increases, a complete non-breathing incident occurred and reversibly resumed to normal breathing upon the discharge of the LFAC waveform. This evidence allowed for further investigation on the ENG signal as the results show in figure 3.6 and figure 3.7. The burst modulation was presented as a sign of the nerve activity during 5 Hz LFAC activation. The application of 10 and 20 Hz also showed the same behavior as shown in figures 3.9, 3.10, and 3.11. Furthermore, the frequency domain analysis of the ENG signal provides an analytical proof of the neural activity existence due to the LFAC activation.

The rat model experiments also support the studies and provide more descriptive indicators for the reliability of LFAC activation in different nerve fibers. The LFAC activation of the sciatic nerve fibers produced muscle twitches similar to those observed accidentally in the rabbit experiment. The results shown in figure 3.15 and figure 3.16 suggest the nerve activation induced by 5 Hz LFAC waveform. Similar to the canine and swine results, the rats ENG signal displayed the burst modulation in response to the LFAC application. The EMG and the muscle force were also responding to the sciatic nerve activation by the LFAC waveform. The remarkable observation from these rat studies is that the twitching behavior did not cause muscle fatigue and was not correlated spatially or temporally to the LFAC cycles. The capability of the LFAC waveform to induce the Hoffmann reflex and the muscle responses is directly related to the activation of sciatic nerve fibers, which highlights the feasibility of the LFAC activation method.

From the conducted experiments, the characteristics of the LFAC activation were consistent even with different nerve fibers. First, the induced neural activity using the LFAC waveform did not show the CAP, which is different than the standard pulse activation as shown in figure 4.1, 4.3, and 4.4. This feature highly suggests the stochastic nature of the neural activity produced by the LFAC waveform. The burst modulation appeared to be correlated with the LFAC cycle, but quantitatively averaging those modulations resulted in a complete or partial dispersion of the burst

modulation. Nevertheless, the averaging did not reveal a synchronized point of activation that provides suggests that the LFAC activation occurs in an analogous mechanism of natural nerve activity and is somehow similar to those induced by chemical activation [38, 39]. The second feature of the LFAC activation was revealed from the induced muscle's activity. The LFAC activation of the sciatic nerve fibers caused the muscles to respond, which suggests the possibility to activate the muscle motor fibers for a longer period of time without casing tissue damages. Lastly, the mechanism of the LFAC activation is hypothesized to activate small nerve fibers first then large nerve fibers. This recruitment order is different than the pulse activation, especially the motor fibers where it either activates larger nerve fibers first or all the fibers at the same time resulting in fatigable twitches based on the current intensity. However, the LFAC activation of the sciatic nerve might activate in the normal order. After eliminating the H-reflex, the muscle contraction was produced suggesting that LFAC can elect motor fibers. This could be a possible selective activation technique and strongly suggests for the feasibility of using LFAC activation.

4.3 Thesis Aim 2

Determine Whether There is a Frequency Dependence for LFAC Activation in Peripheral Nerves

The LFAC activation phenomenon is a novel method in the field of neuromodulation and this thesis is aimed to establish its initial characteristics while exploring methods to evaluate that activation. Beside the activation oservations and suggestions discussed above, the LFAC activation of different nerve fibers bundles were found to be frequency and fiber-size dependent. The minimum required LFAC amplitude to achieve peripheral nerve activation in the autonomic and somatic nerve fibers followed the same decreasing trend as a function of the LFAC waveform frequency. As the LFAC frequency increases, the amplitude to achieve activation decreases. The

window of activation appeared to change also with respect to the nerve fiber type and size. The activation of the autonomic nerve fibers tends to require higher amplitudes while the somatic fibers require less intensity. Based on that, the experimental established thresholds results from the *ex-vivo* and *in-vivo* experiments provide a foundation for the future investigations of LFAC activation.

4.4 Future Directions and Improvements

The LFAC activation feasibility is newly discovered and several investigations have to be conducted before reaching to the clinical applications. During the work of this thesis, several complications were faced, and need to be improved for better results along with other technical considerations.However, this hypothesis is proven to be a promising technique for safe and possibly selective activation. From a signal processing standpoint, the ENG, EMG, breathing, and force signals showed a substantial amount of noise that might be the reason for the deviation from the optimal results. As an example, the need of using the SWT was mainly due to the SRS correlated noise that resulted in the neural activity to deport the normal neural frequency band. The in-band noise issue was common among all the nerve recordings, which impacted the PSD analysis. The magnitude of the LFAC stimulus was in the Volt range that masked the microVolts neural signal limiting the frequency separation method. From a technical standpoint, there were some offset and noise issues associated with the voltage-current isolators used, which could impact the results in unsafe manner that could also damage the nerve tissue.

The positive and negative control issues faced during these experiments limited the definitive proof of the nerve activity. In all settings, the electrodes placements were mostly symmetrical to the LFAC electrode, which prevented the measurement and observation of the conducted nerve activity. Although the living animal models showed changes in the neural-based reflexes, the ENG analysis required further investigation for better characterisation of the nerve activity. An alternative experi-

mental paradigm can assess measuring the nerve conduction. By placing two cascaded recording electrodes to the stimulation electrode, the traveling nerve activity between can be used to observe and evaluate the induced nerve activity when applying LFAC.

The electrodes design and characteristics impacts were not considered during this work, which would have significant effects on the results and the feasibility of LFAC activation. It is one of the main factors that should be considered for future work and to investigate their influence. Changing the electrodes type from extrafascicular to intrafascicular might and most likely to play a major role in the LFAC activation performance and might have an influence on the threshold and the selectivity of activation. Additionally, characterizing the LFAC activation spatial mechanism might reveal the relationship between block and activation, which would provide a solid background for electrodes and implementable devices design that could have selective waveforms to block and activate nerve fibers at the same time. Lastly, tuning and characterizing the LFAC waveform for the activation purpose needs to be considered to prevent any overshooting or transient responses that may damage the target nerve tissues.

LIST OF REFERENCES

LIST OF REFERENCES

[1] R. G. Northcutt, "Changing views of brain evolution," *Brain Research Bulletin*, vol. 55, no. 6, pp. 663–674, 2001. [Online]. Available: http://www.sciencedirect.com/science/article/pii/S0361923001005603

[2] J. Feher, *The Action Potential and Organization of the Nervous System.* Boston: Academic Press, 2012, pp. 215–418. [Online]. Available: http://www.sciencedirect.com/science/article/pii/B9780123821638000335

[3] D. Purves, *Voltage-Dependent Membrane Permeability*, 6th ed. New York: Oxford University Press, 2018, pp. 49–63.

[4] A. L. Hodgkin, A. F. Huxley, and B. Katz, "Measurement of current-voltage relations in the membrane of the giant axon of loligo," *The Journal of physiology*, vol. 116, no. 4, pp. 424–448, 1952. [Online]. Available: https://www.ncbi.nlm.nih.gov/pubmed/14946712 https://www.ncbi.nlm.nih.gov/pmc/PMC1392219/

[5] D. Purves, *Electrical Signals of Nerve Cells*, 6th ed. New York: Oxford University Press, 2018, pp. 33–48.

[6] A. L. Hodgkin and A. F. Huxley, "A quantitative description of membrane current and its application to conduction and excitation in nerve," *The Journal of physiology*, vol. 117, no. 4, pp. 500–544, 1952. [Online]. Available: https://pubmed.ncbi.nlm.nih.gov/12991237 https://www.ncbi.nlm.nih.gov/pmc/articles/PMC1392413/

[7] M. W. Barnett and P. M. Larkman, "The action potential," *Practical Neurology*, vol. 7, no. 3, p. 192, 2007. [Online]. Available: http://pn.bmj.com/content/7/3/192.abstract https://pn.bmj.com/content/7/3/192.long

[8] B. Roth, *The Electrical Conductivity of Tissues.* CRC, 01 2000, book section 21, pp. 1–13.

[9] J. L. Parker, N. H. Shariati, and D. M. Karantonis, "Electrically evoked compound action potential recording in peripheral nerves," *Bioelectronics in Medicine*, vol. 1, no. 1, pp. 71–83, 2018. [Online]. Available: https://www.futuremedicine.com/doi/abs/10.2217/bem-2017-0005

[10] K. Chakravarthy, A. Nava, P. J. Christo, and K. Williams, "Review of recent advances in peripheral nerve stimulation (pns)," *Current Pain and Headache Reports*, vol. 20, no. 11, p. 60, 2016. [Online]. Available: https://doi.org/10.1007/s11916-016-0590-8

[11] K. Hennings, L. Arendt-Nielsen, and O. K. Andersen, "Orderly activation of human motor neurons using electrical ramp prepulses," *Clin Neurophysiol*, vol. 116, no. 3, pp. 597–604, 2005.

[12] F. Rattay, "Analysis of models for external stimulation of axons," *IEEE Transactions on Biomedical Engineering*, vol. BME-33, no. 10, pp. 974–977, 1986.

[13] 1988.

[14] J. Malmivuo and R. Plonsey, *Bioelectromagnetism - Principles and Applications of Bioelectric and Biomagnetic Fields*. Oxford University Press, New York, 01 1995.

[15] K. Yoshida and J. Struijk, *The Theory of Peripheral Nerve Recordings*. River Edge, NJ: World Scientific, 2004, book section 2.2, pp. 342–426.

[16] S. Nag and N. V. Thakor, "Implantable neurotechnologies: electrical stimulation and applications," *Medical & Biological Engineering & Computing*, vol. 54, no. 1, pp. 63–76, 2016. [Online]. Available: https://doi.org/10.1007/s11517-015-1442-0

[17] D. R. Merrill, M. Bikson, and J. G. R. Jefferys, "Electrical stimulation of excitable tissue: design of efficacious and safe protocols," *Journal of Neuroscience Methods*, vol. 141, no. 2, pp. 171–198, 2005. [Online]. Available: http://www.sciencedirect.com/science/article/pii/S0165027004003826

[18] W. M. Grill and J. T. Mortimer, "Stimulus waveforms for selective neural stimulation," *IEEE Engineering in Medicine and Biology Magazine*, vol. 14, no. 4, pp. 375–385, 1995.

[19] K. E. I. Deurloo, J. Holsheimer, and P. Bergveld, "The effect of subthreshold prepulses on the recruitment order in a nerve trunk analyzed in a simple and a realistic volume conductor model," *Biological Cybernetics*, vol. 85, no. 4, pp. 281–291, 2001. [Online]. Available: https://doi.org/10.1007/s004220100253

[20] E. A. Blair and J. Erlanger, "A comparison of the characteristics of axons through their individual electrical responses," *American Journal of Physiology-Legacy Content*, vol. 106, no. 3, pp. 524–564, 1933. [Online]. Available: https://journals.physiology.org/doi/abs/10.1152/ajplegacy.1933.106.3.524

[21] Z. Fang and J. T. Mortimer, "Selective activation of small motor axons by quasitrapezoidal current pulses," *IEEE Transactions on Biomedical Engineering*, vol. 38, no. 2, pp. 168–174, 1991.

[22] W. M. Grill and J. T. Mortimer, "Selective activation of distant nerve fibers," in *Proceedings of the 15th Annual International Conference of the IEEE Engineering in Medicine and Biology Societ*, 1993, pp. 1249–1250.

[23] M. Sassen and M. Zimmermann, "Differential blocking of myelinated nerve fibres by transient depolarization," *Pflügers Archiv*, vol. 341, no. 3, pp. 179–195, 1973. [Online]. Available: https://doi.org/10.1007/BF00592788

[24] K. Hennings, L. Arendt-Nielsen, S. S. Christensen, K. Andersen, and O. K. Andersen, "Selective activation of small-diameter motor fibres using exponentially rising waveforms: a theoretical study," *Medical & Biological Engineering & Computing*, vol. 43, no. 4, pp. 493–500, 2005.

[25] H. Bostock, M. Baker, P. Grafe, and G. Reid, "Changes in excitability and accommodation of human motor axons following brief periods of ischaemia," *The Journal of physiology*, vol. 441, no. 1, pp. 513–535, 1991.

[26] H. Bostock and M. Baker, "Evidence for two types of potassium channel in human motor axons in vivo," *Brain Research*, vol. 462, no. 2, pp. 354–358, 1988. [Online]. Available: http://www.sciencedirect.com/science/article/pii/0006899388905641

[27] M. Baker and H. Bostock, "Depolarization changes the mechanism of accommodation in rat and human motor axons," *J Physiol*, vol. 411, pp. 545–61, 1989.

[28] H. Bostock, K. Cikurel, and D. Burke, "Threshold tracking techniques in the study of human peripheral nerve," *Muscle & Nerve*, vol. 21, no. 2, pp. 137–158, 1998.

[29] K. Hennings, L. Arendt-Nielsen, and O. K. Andersen, "Breakdown of accommodation in nerve: a possible role for persistent sodium current," *Theoretical biology & medical modelling*, vol. 2, pp. 16–16, 2005. [Online]. Available: https://pubmed.ncbi.nlm.nih.gov/15826303 https://www.ncbi.nlm.nih.gov/pmc/articles/PMC1090618/

[30] J. Howells, H. Bostock, and D. Burke, "Accommodation to hyperpolarization of human axons assessed in the frequency domain," *Journal of neurophysiology*, vol. 116, no. 2, pp. 322–335, 2016. [Online]. Available: https://pubmed.ncbi.nlm.nih.gov/27098023 https://www.ncbi.nlm.nih.gov/pmc/articles/PMC4969388/

[31] E. Henneman, G. Somjen, and D. O. Carpenter, "Functional significance of cell size in spinal motoneurons," *Journal of Neurophysiology*, vol. 28, no. 3, pp. 560–580, 1965, pMID: 14328454. [Online]. Available: https://doi.org/10.1152/jn.1965.28.3.560

[32] J. Wells, P. Konrad, C. Kao, E. D. Jansen, and A. Mahadevan-Jansen, "Pulsed laser versus electrical energy for peripheral nerve stimulation," *Journal of neuroscience methods*, vol. 163, no. 2, pp. 326–337, 2007. [Online]. Available: https://pubmed.ncbi.nlm.nih.gov/17537515 https://www.ncbi.nlm.nih.gov/pmc/articles/PMC2993156/

[33] K. Luedtke, A. Rushton, C. Wright, T. P. Juergens, G. Mueller, and A. May, "Effectiveness of anodal transcranial direct current stimulation in patients with chronic low back pain: design, method and protocol for a randomised controlled trial," *BMC Musculoskelet Disord*, vol. 12, p. 290, 2011.

[34] G. B. Hughes, M. B. Bottomy, C. G. Jackson, M. E. Glasscock, and A. Sismanis, "Myelin and axon degeneration following direct current peripheral nerve stimulation: A prospective controlled experimental study," *Otolaryngology–Head and Neck Surgery*, vol. 89, no. 5, pp. 767–775, 1981. [Online]. Available: https://journals.sagepub.com/doi/abs/10.1177/019459988108900515

[35] G. B. Hughes, M. B. Bottomy, J. R. E. Dickins, C. G. Jackson, A. Sismanis, and M. E. Glasscock, "A comparative study of neuropathologic changes following pulsed and direct current stimulation of the mouse sciatic nerve," *American Journal of Otolaryngology*, vol. 1, no. 5, pp. 378–384, 1980. [Online]. Available: http://www.sciencedirect.com/science/article/pii/S0196070980800184

[36] G. Y. Fridman and C. C. Della Santina, "Safe direct current stimulation to expand capabilities of neural prostheses," *IEEE transactions on neural systems and rehabilitation engineering : a publication of the IEEE Engineering in Medicine and Biology Society*, vol. 21, no. 2, pp. 319–328, 2013. [Online]. Available: https://pubmed.ncbi.nlm.nih.gov/23476007 https://www.ncbi.nlm.nih.gov/pmc/articles/PMC4050981/

[37] R. D. Miller, L. I. Eriksson, L. A. Fleisher, J. P. Wiener-Kronish, and W. L. Young, *Anesthesia E-Book*. Elsevier Health Sciences, 2009.

[38] Y. Uchida and S. Murao, "Acid-induced excitation of afferent cardiac sympathetic nerve fibers," *American Journal of Physiology-Legacy Content*, vol. 228, no. 1, pp. 27–33, 1975. [Online]. Available: https://journals.physiology.org/doi/abs/10.1152/ajplegacy.1975.228.1.27

[39] ——, "Potassium-induced excitation of afferent cardiac sympathetic nerve fibers," *American Journal of Physiology-Legacy Content*, vol. 226, no. 3, pp. 603–607, 1974. [Online]. Available: https://journals.physiology.org/doi/abs/10.1152/ajplegacy.1974.226.3.603

[40] F. J. Brink, D. Bronk, and M. Larrabee, "Chemical excitation of nerve," *Annals of the New York Academy of Sciences*, vol. 47, no. 4, pp. 457–485, 1946. [Online]. Available: https://nyaspubs.onlinelibrary.wiley.com/doi/abs/10.1111/j.1749-6632.1946.tb49547.x

[41] W. W. Dawson, "Chemical stimulation of the peripheral trigeminal nerve," *Nature*, vol. 196, no. 4852, pp. 341–345, 1962. [Online]. Available: https://doi.org/10.1038/196341a0

[42] M. R. Horn, C. Ahmed, and K. Yoshida, "Low frequency alternating current block - a new method to stop or slow conduction of action potentials*," in *2019 9th International IEEE/EMBS Conference on Neural Engineering (NER)*, 2019, pp. 787–790.

[43] L. M. Mintch, I. Muzquiz, M. R. Horn, M. Carr, J. H. Schild, and K. Yoshida, "Reversible conduction block in peripheral mammalian nerve using low frequency alternating current*," in *2019 9th International IEEE/EMBS Conference on Neural Engineering (NER)*, 2019, pp. 823–824.

[44] C. Tai, J. R. Roppolo, and W. C. de Groat, "Analysis of nerve conduction block induced by direct current," *Journal of computational neuroscience*, vol. 27, no. 2, pp. 201–210, 2009.

[45] K. Yoshida and M. R. Horn, "Methods and systems for blocking nerve activity propagation in nerve fibers," U.S Patent US16/606,301, April, 2020.

[46] A. Rosenblueth, J. Reboul, and A. Grass, "The action of alternating currents upon the spike-potential magnitude, conduction velocity and polarization of nerve," *American Journal of Physiology-Legacy Content*, vol. 130, no. 3, pp. 527–538, 1940.

[47] M. Langille, J. A. Gonzalez-Cueto, and S. Sundar, "Analysis of the selective nature of sensory nerve stimulation using different sinusoidal frequencies," *International Journal of Neuroscience*, vol. 118, no. 8, pp. 1131–1144, 2008.

[48] K. Koga, H. Furue, M. H. Rashid, A. Takaki, T. Katafuchi, and M. Yoshimura, "Selective activation of primary afferent fibers evaluated by sine-wave electrical stimulation," *Molecular Pain*, vol. 1, no. 1, p. 13, 2005.

[49] K. L. Kilgore and N. Bhadra, "Nerve conduction block utilising high-frequency alternating current," *Medical and Biological Engineering and Computing*, vol. 42, no. 3, pp. 394–406, 2004.

[50] B. Wodlinger, S. Rashid, and D. M. Durand, "Block of peripheral pain response by high-frequency sinusoidal stimulation," *Neuromodulation: Technology at the Neural Interface*, vol. 16, no. 4, pp. 312–317, 2013.

[51] K. L. Kilgore and N. Bhadra, "Reversible nerve conduction block using kilohertz frequency alternating current," *Neuromodulation : journal of the International Neuromodulation Society*, vol. 17, no. 3, pp. 242–255, 2014. [Online]. Available: https://pubmed.ncbi.nlm.nih.gov/23924075 https://www.ncbi.nlm.nih.gov/pmc/articles/PMC3834124/

[52] M. I. Muzquiz, "Quantification of low frequency alternating current conduction block applied to mammalian autonomic peripheral nerves," Thesis, Purdue University, 2020.

[53] M. I. Muzquiz and al et, "A reversible low frequency alternating current nerve conduction block in mammalian autonomic nerves," 2020, unpublished.

[54] ——, "Reversible low frequency alternating current nerve conduction block in large caliber mammalian autonomic nerves," 2020, unpublished.

[55] G. D. Baquis, W. F. Brown, J. T. Capell, V. Chaudhry, D. Cros, B. R. Drexinger, J. B. Gelblum, J. M. Gilchrist, A. J. Gitter, and A. J. Haig, "Technology review: the neurometer® current perception threshold (cpt)," *Muscle and Nerve*, vol. 22, no. 4, pp. 523–531, 1999.

[56] F. J. Rodri guez, D. Ceballos, M. Schu ttler, A. Valero, E. Valderrama, T. Stieglitz, and X. Navarro, "Polyimide cuff electrodes for peripheral nerve stimulation," *Journal of Neuroscience Methods*, vol. 98, no. 2, pp. 105–118, 2000. [Online]. Available: http://www.sciencedirect.com/science/article/pii/S0165027000001928

[57] H. O. Parrack, "Excitability of the excised and circulated frog's sciatic nerve," *American Journal of Physiology-Legacy Content*, vol. 130, no. 3, pp. 481–495, 1940.

[58] J. Rossmeisl, A. Logadottir, and J. K. Nørskov, "Electrolysis of water on (oxidized) metal surfaces," *Chemical physics*, vol. 319, no. 1-3, pp. 178–184, 2005.

[59] S. Qiao, M. Torkamani-Azar, P. Salama, and K. Yoshida, "Stationary wavelet transform and higher order statistical analyses of intrafascicular nerve recordings," *Journal of neural engineering*, vol. 9, no. 5, p. 056014, 2012.

[60] S. Qiao and K. Yoshida, "Influence of unit distance and conduction velocity on the spectra of extracellular action potentials recorded with intrafascicular electrodes," *Medical engineering & physics*, vol. 35, no. 1, pp. 116–124, 2013.

[61] R. M. McAllen, A. D. Shafton, B. O. Bratton, D. Trevaks, and J. B. Furness, "Calibration of thresholds for functional engagement of vagal a, b and c fiber groups in vivo," *Bioelectronics in Medicine*, vol. 1, no. 1, pp. 21–27, 2018.

[62] J. Feher, *Control of Ventilation*. Boston: Academic Press, 2012, pp. 602–610. [Online]. Available: http://www.sciencedirect.com/science/article/pii/B9780123821638000335

[63] C. Iber, P. Simon, J. B. Skatrud, M. W. Mahowald, and J. A. Dempsey, "The breuer-hering reflex in humans. effects of pulmonary denervation and hypocapnia," *American journal of respiratory and critical care medicine*, vol. 152, no. 1, pp. 217–224, 1995.

[64] J. Feher, *The Neuromuscular Junction and Excitation-Contraction Coupling*. Boston: Academic Press, 2012, pp. 259–269. [Online]. Available: http://www.sciencedirect.com/science/article/pii/B9780123821638000335

[65] R. M. Palmieri, C. D. Ingersoll, and M. A. Hoffman, "The hoffmann reflex: methodologic considerations and applications for use in sports medicine and athletic training research," *Journal of athletic training*, vol. 39, no. 3, pp. 268–277, 2004. [Online]. Available: https://pubmed.ncbi.nlm.nih.gov/16558683 https://www.ncbi.nlm.nih.gov/pmc/articles/PMC522151/